Lateral-Torsional-Axial coupled vibration for a geared system

In the vibration study of a single rotor system, the lateral, torsional, and axial vibrations are typically decoupled and can be studied separately in general. However, for a geared rotor system with multiple rotors, the lateral, torsional, and axial vibration are coupled through the gear mesh and/or rider ring (sometimes called thrust collar ring), as illustrated in Figure 1. The rider ring is commonly used in turbomachinery applications, such compressors and expanders, to transfer the thrust load from high speed pinions to the low speed gear to reduce the mechanical friction loss and eliminate thrust bearings in the high speed pinions, as shown in Figure 2. The rider ring is more commonly used in high speed and low power small machines where the mechanical frictional power loss is critical to the entire machine and the cost is also competitive in the market.

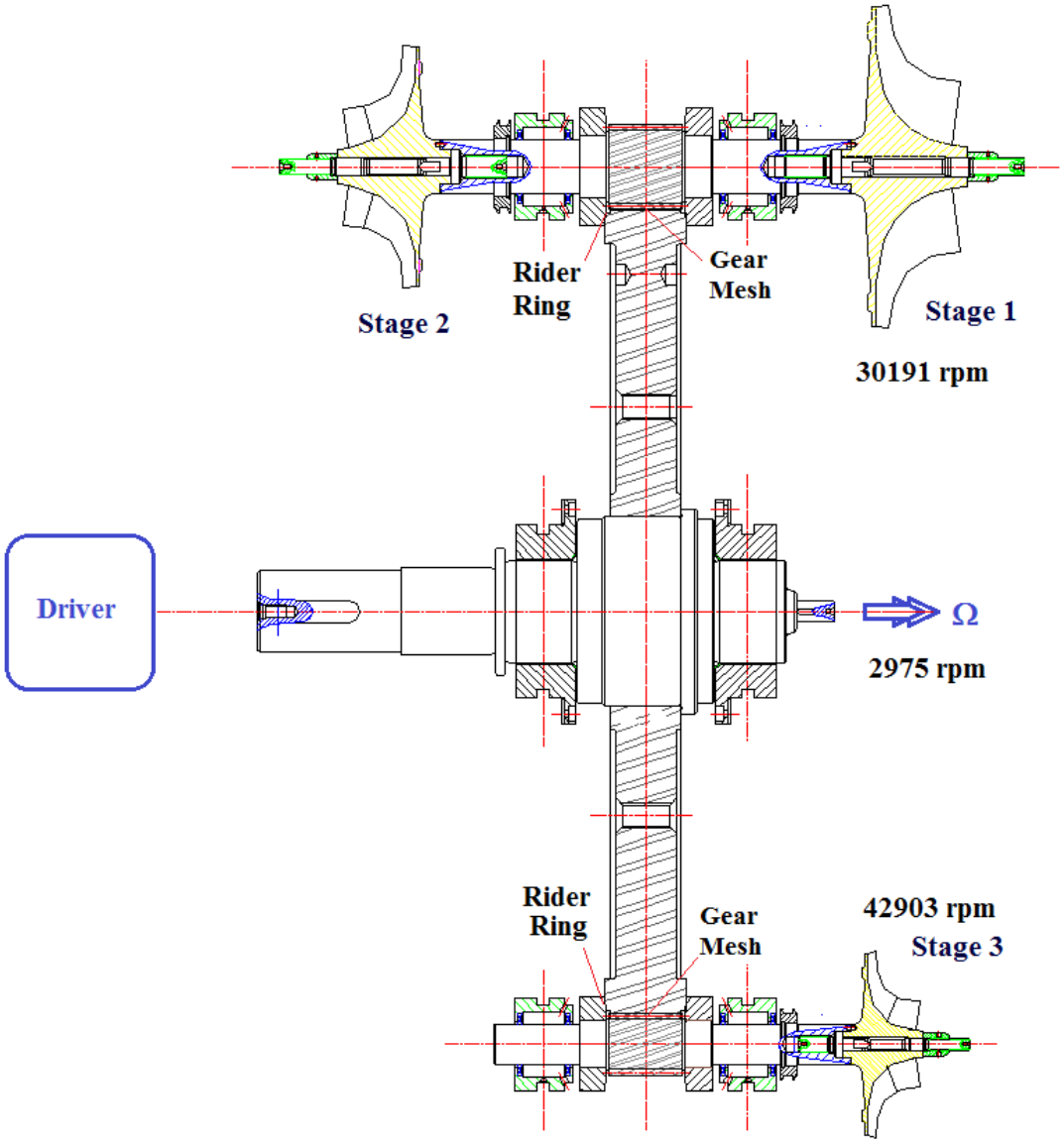

Figure 1 Geared system with rider ring

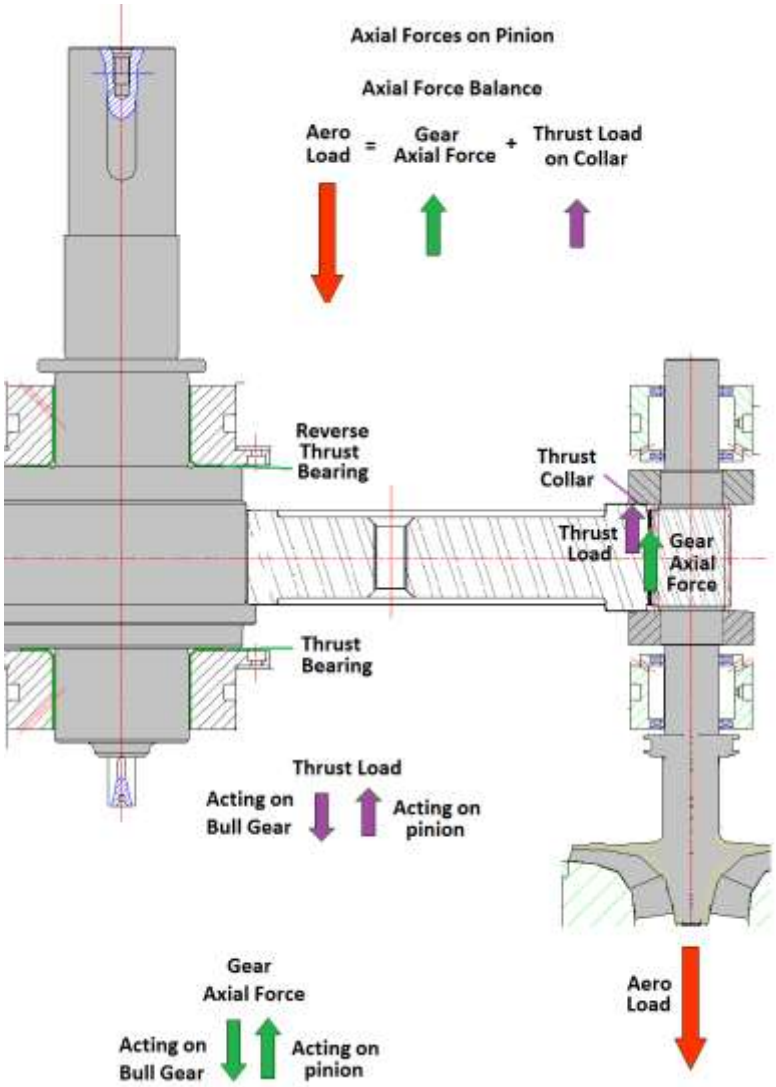

Figure 2 Rider ring for thrust balance

Consider a gear-paired system, as shown in Figure 3, gear 1 is used as a reference gear where the gear 2 angular position, γ, is specified with respect to the gear 1. Gear 1 can be either a driving or driven shaft and rotates CCW or CW. The (X,Y,Z) coordinate system is a fixed Cartesian coordinate system with Z axis in line with the spinning axis and X and Y in the transverse directions perpendicular to the Z axis, following the right hand rule. The motion for each finite element station along the rotor (including the gear center) is described by 6 degrees-of-freedom: three (3) translational displacements (x,y,z) along (X,Y,Z) axes and three (3) rotational displacements ($\theta_x,\theta_y,\theta_z$) about (X,Y,Z) axes. For lateral vibration, the motion of each finite element station is described by two translational displacements (x,y) in the X and Y directions respectively, and two rotational (angular) displacements (θ_x,θ_y) about the X and Y axes respectively. For torsional vibration, the motion of each finite element station is described by a rotational displacement (θ_z) about the spinning axis (Z). For axial vibration, the motion of each finite element station is described by a translational displacement (z) along the spinning axis (Z).

Therefore, the motions at a typical finite element station are described by the following displacement vectors:

Complete motion: $\boldsymbol{q}_{(6X1)} = \{x,\ y,\ z,\ \theta_x,\ \theta_y,\ \theta_z\}^T$ (1a)

Lateral vibration: $\boldsymbol{q}_L = \{x,\ y,\ \theta_x,\ \theta_y\}^T$ (1b)

Torsional vibration: $\boldsymbol{q}_T = \{\theta_z\}$ (1c)

Axial vibration: $\boldsymbol{q}_A = \{z\}$ (1d)

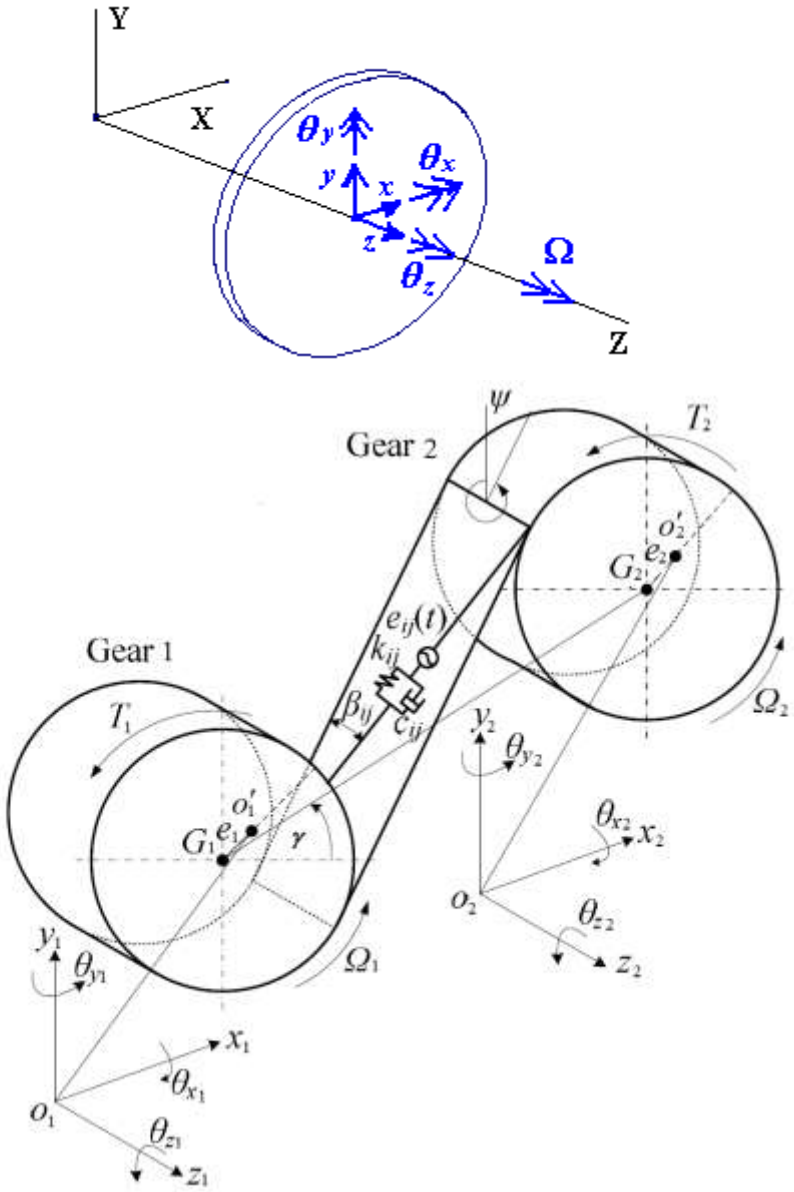

Figure 3 A typical gear set

Note that the spinning direction of the rotor is commonly defined as CCW along the positive Z axis (+Z) for a single rotor system. However, for a geared multiple rotor system, some rotors will rotate CW in the negative Z direction (-Z). Therefore, caution must be taken when defining the forward and backward precessions of the lateral orbit motion. The detailed explanation of the orbit motion has been documented in Chen and Gunter (2005), some highlights and cautions for the geared system are addressed here.

The lateral rotor motion at each finite element station is either forward or backward precession in relation to the direction of rotation (spin) of the rotor and not the direction of the Z axis, as shown in Figure 4. The whirling motion is defined as a *forward precession* if it is whirling in the same direction as the rotor spinning direction, and as a *backward precession* if it is whirling opposite to the rotor spinning direction. A straight line motion is a degeneration of a whirling orbit and a transition between the forward and backward precessions without the whirling motion.

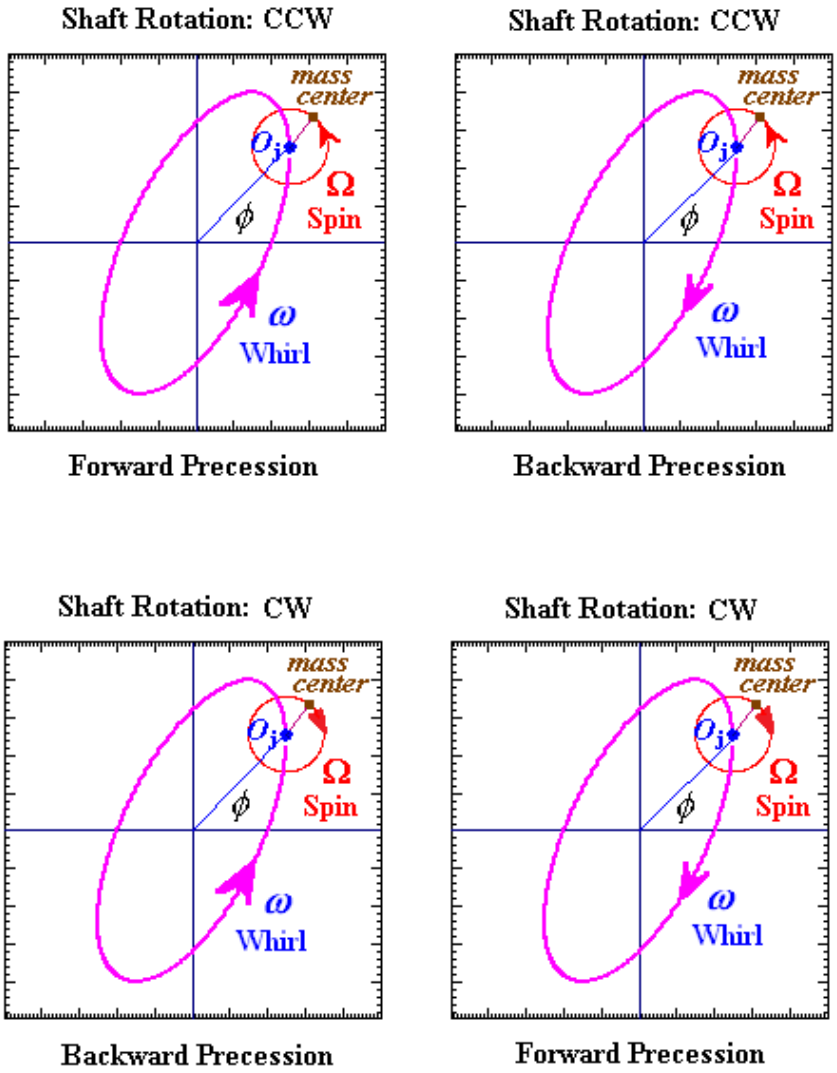

Figure 4 Whirling orbits

The direction of precession, or a whirling direction, of a lateral vibration orbit is defined by the rate of precession angle in the (X,Y) plane. The precessional angle is defined as:

$$\phi(t) = \arctan \frac{y(t)}{x(t)} \tag{2}$$

The direction of precession (whirling) is determined by the rate of precessional angle

$$sign\left(\dot{\phi}\right) \tag{3}$$

When $\dot{\phi}$ is a positive value (CCW) and the rotor is spinning in the positive Z direction (CCW), the orbit motion is a *forward whirl* (precession). When $\dot{\phi}$ is a negative value (CW) and the rotor is spinning in the positive Z direction (CCW), the orbit motion is a *backward whirl* (precession). When $\dot{\phi}$ is zero the orbit motion degenerates into a *straight-line* path without whirling. However, when the rotor is spinning in the negative Z direction (CW), then a positive $\dot{\phi}$ (CCW) indicates a *backward whirl* and a negative $\dot{\phi}$ (CW) indicates a *forward whirl*. For a single rotor system, this confusion can be avoided by modeling the rotor with positive Z is the spinning direction. For a multiple rotor geared system, the spinning direction of a rotor can be either in the positive or negative Z axis. Therefore, it is convenient to define the rotor speed Ω as a vector with direction. That is, if the rotor is spinning in the positive Z direction, the rotor rotational speed Ω is positive and vice versa. Then the forward and backward whirl is defined by the product of $\dot{\phi}$ and Ω:

Forward whirl (precession):	$\Omega\dot{\phi} > 0$	$sign\left(\Omega\dot{\phi}\right)$ is positive	(4a)
Backward whirl (precession):	$\Omega\dot{\phi} < 0$	$sign\left(\Omega\dot{\phi}\right)$ is negative	(4b)
Straight line motion:	$\Omega\dot{\phi} = 0$		(4c)

Another caution is that almost all the calculated bearing coefficients, including the so-called aerodynamic cross-coupling terms $\left(k_{xy} = Q,\ k_{yx} = -Q\right)$ where Q is a positive value, are obtained with the assumption that the spinning direction is in the positive Z direction (CCW). With the opposite spinning direction, i.e., spinning in the (-Z) direction, all the cross-coupled stiffness and damping coefficients (k_{xy}, k_{yx}, $k_{\theta_x}, k_{\theta_y}$, c_{xy}, c_{yx}, $c_{\theta_x}, c_{\theta_y}$) must change sign to accommodate the negative spinning direction. Since the shaft (rotor) properties is isotropic for a circular cross-section, therefore the rotor governing equation and related matrices are not affected by this spinning direction, with the exception on the sign of the gyroscopic matrix and related forcing vectors.

For a purely torsional vibration, it is commonly describe the torsional vibration rotational displacement $\left(\theta_z^*\right)$ in the same direction as the spinning direction. For a geared system, this could lead to some confusions since the directions of rotor rotation are opposite for a mating gear set. In this context, for consistency, we will use the definition in Eq. (1) for the rotor vibration

displacements. That is, the torsional displacement (θ_z) is defined along the positive Z axis, regardless the spinning direction. Therefore for a positive Ω, $\theta_z^* = \theta_z$, and for a negative Ω, $\theta_z^* = -\theta_z$.

In summary, when analyzing the geared rotor system and the motion at each finite element station is defined in Eq, (1), then the following cautions must be taken:

1. Treat the rotor rotational speed Ω as a vector, positive if it rotates in the positive Z direction (CCW for a right hand ruled Cartesian coordinate system as used in Eq, (1)) and negative if it rotates in the negative Z direction (CW). This will take care of the gyroscopic matrix and related forcing function involved rotational speed.

2. Change the cross-coupled bearing stiffness and damping coefficients *if necessary* when the rotor speed is negative, since almost all the bearing coefficients are obtained by assuming the rotor speed is positive in the positive Z direction. This is particularly important when performing the stability analysis since cross-coupled stiffness coefficients, including the aerodynamic cross-coupling term, significantly affect the system stability.

3. When viewing the results for lateral motion, the direction of whirling needs to take into account the rotor speed. That is, the forward and backward whirl is defined by the product of $\dot{\phi}$ and Ω, not just $\dot{\phi}$ as used for a single rotor system.

Example 1: A dual rotor system

A dual rotor system, as shown in Figure 1-1, is utilized here to demonstrate the effects of rotor direction of rotation on the system dynamics. For multiple rotor systems, if all the shafts are in the same axis and connected through couplings with the same rotational speed and direction of rotation, then they can really be treated or modeled as a single rotor system and all the discussions on the single rotor system are valid. However, for system as demonstrated in this dual rotor system and geared systems (which will be discussed later), the rotors are having their own rotational speed and direction of rotation. Then, the results will not be easily comprehended and deserve some discussions. This dual rotor system has been presented by many publications by Nelson, etc. and the system details are analyzed and documented in Chen & Gunter (2005) with the same direction of rotation. Since rotors are supported by isotropic bearings with constant stiffness and damping coefficients, the effects of rotational speed (magnitude and direction) on the system dynamics are discussed here. Only the lateral vibrations are considered and torsional and axial vibrations are neglected in this example.

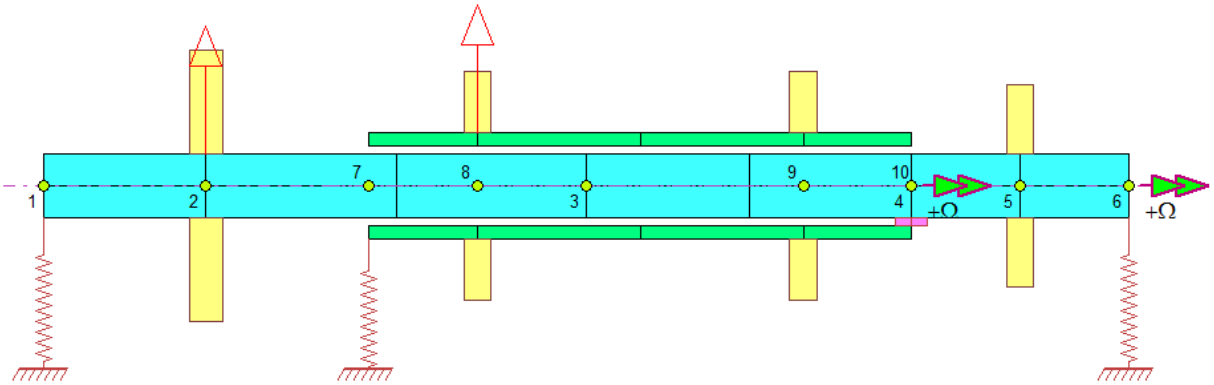

Figure 1-1 Dual rotor system

Case 1: $\Omega_2 = 1.5\,\Omega_1$**,** Ω_1**:** CCW and Ω_2**:** CCW

Let us review our previous discussion in Chen & Gunter with $\Omega_2 = 1.5\,\Omega_1$. That is, the rotor 2 rotates in the same direction of rotation with rotor 1 in a speed ratio of 1.5. The speed relationship is entered in the Shaft Elements tab. A positive value indicates a CCW rotation and a negative value indicates a CW rotation. To display the direction of rotation, the check box in the Model Graphic Settings must be checked.

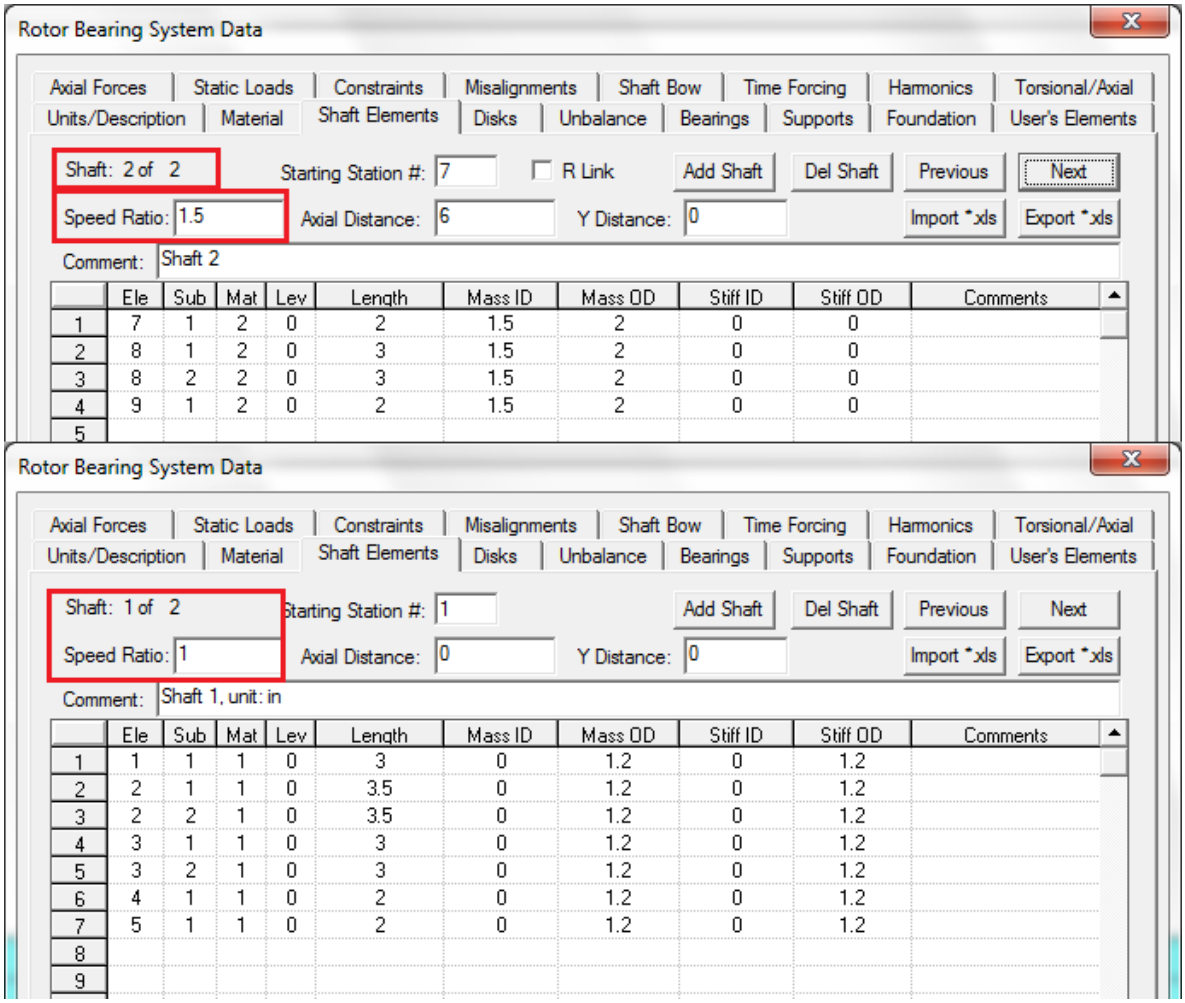
Rotor Bearing System Data
Axial Forces
Static Loads
Constraints
Misalignments
Shaft Bow
Time Forcing
Harmonics
Torsional/Axial
Units/Description
Material
Shaft Elements
Disks
Unbalance
Bearings
Supports
Foundation
User's Elements
Shaft: 2 of 2
Starting Station #: 7
R Link
Add Shaft
Del Shaft
Previous
Next
Speed Ratio: 1.5
Axial Distance: 6
Y Distance: 0
Import *.xls
Export *.xls
Comment: Shaft 2
Ele Sub Mat Lev Length Mass ID Mass OD Stiff ID Stiff OD Comments
1 7 1 2 0 2 1.5 2 0 0
2 8 1 2 0 3 1.5 2 0 0
3 8 2 2 0 3 1.5 2 0 0
4 9 1 2 0 2 1.5 2 0 0
5
Rotor Bearing System Data
Axial Forces
Static Loads
Constraints
Misalignments
Shaft Bow
Time Forcing
Harmonics
Torsional/Axial
Units/Description
Material
Shaft Elements
Disks
Unbalance
Bearings
Supports
Foundation
User's Elements
Shaft: 1 of 2
Starting Station #: 1
Add Shaft
Del Shaft
Previous
Next
Speed Ratio: 1
Axial Distance: 0
Y Distance: 0
Import *.xls
Export *.xls
Comment: Shaft 1, unit: in
Ele Sub Mat Lev Length Mass ID Mass OD Stiff ID Stiff OD Comments
1 1 1 1 0 3 0 1.2 0 1.2
2 2 1 1 0 3.5 0 1.2 0 1.2
3 2 2 1 0 3.5 0 1.2 0 1.2
4 3 1 1 0 3 0 1.2 0 1.2
5 3 2 1 0 3 0 1.2 0 1.2
6 4 1 1 0 2 0 1.2 0 1.2
7 5 1 1 0 2 0 1.2 0 1.2
8
9

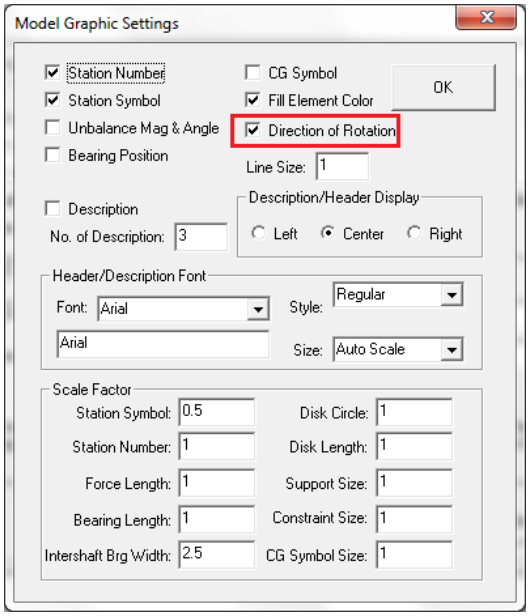
Model Graphic Settings
Station Number
Station Symbol
Unbalance Mag & Angle
Bearing Position
CG Symbol
Fill Element Color
Direction of Rotation
OK
Line Size: 1
Description
No. of Description: 3
Description/Header Display
Left
Center
Right
Header/Description Font
Font: Arial
Style: Regular
Arial
Size: Auto Scale
Scale Factor
Station Symbol: 0.5
Station Number: 1
Force Length: 1
Bearing Length: 1
Intershaft Brg Width: 2.5
Disk Circle: 1
Disk Length: 1
Support Size: 1
Constraint Size: 1
CG Symbol Size: 1

Assuming the both rotors rotate CCW in the positive Z direction in this first case. Figure 1-2, whirl speed map, shows the first 4 system damped natural frequencies verse the rotor speeds with the synchronous excitation lines overlapped in the maps. It is noted that these two graphs are identical with the exception of the scale in the X-axis (speed axis), where one labeled with the rotor 1 speed and the other labeled with rotor 2 speed. These four frequencies (modes) are labeled as ($\omega_1, \omega_2, \omega_3, \omega_4$) for identification purpose. Also noted that in addition to the using of the forward and backward precession labels (***F***, ***B***), the (CCW+) and (CW-) are also used to represent the direction of whirling of the mode. So, the first and third modes whirl in the CW (-Z) direction and the second and fourth modes whirl in the CCW (+Z) direction. Since both rotors rotate CCW (+Z) direction, so, modes 1 and 3 are backward precession modes for both rotors, and modes 2 and 4 are forward precession modes for both rotors. At zero speed, modes (1, 2) and (3, 4) are essentially the planar modes with the same frequency, one in X direction and the other in Y direction, and they form two circular whirling modes, one forward and the other backward, due to gyroscopic effects as the speed increases in this example. The gyroscopic effect stiffens the forward precession modes (increases the associated frequencies) and softens the backward precession modes (decreases the associated frequencies).

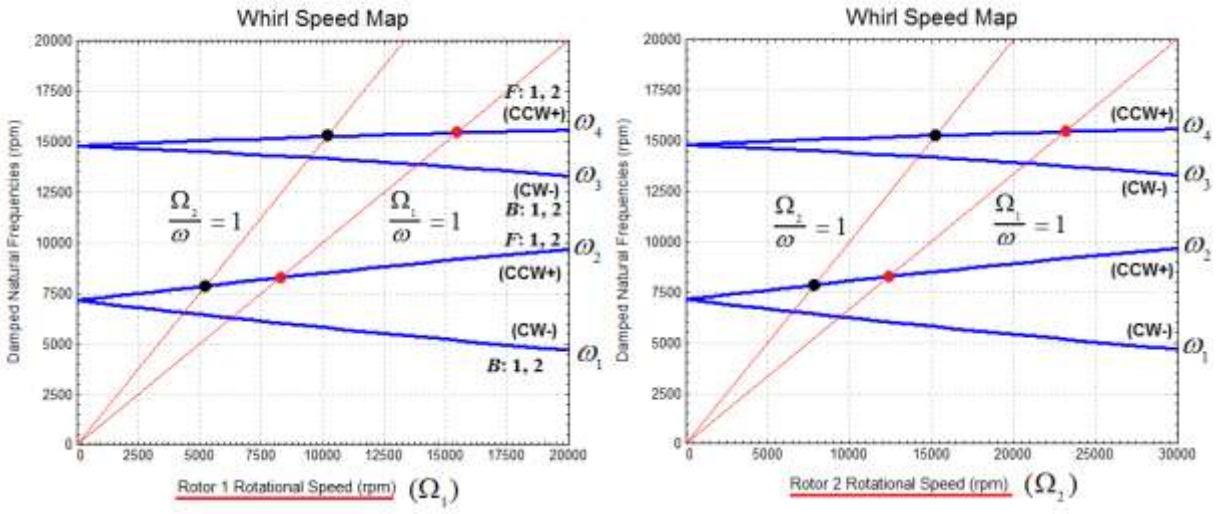

Figure 1-2 Whirl speed map for $\Omega_2 = 1.5\,\Omega_1$

The associated mode shapes with whirling directions for the rotor speeds of $(\Omega_1, \Omega_2) = (10000, 15000)$ rpm are shown in Figure 1-3. Again, the mode shapes for the first and second modes are very similar and mode shapes for the third and fourth modes are very similar. For the first and third modes, both rotors are whirling in the CW direction with a whirl frequency of 5825 and 14189 cpm, respectively. For the second and fourth modes, both rotors are whirling in the CCW direction with a whirl frequency of 8504 and 15260 cpm, respectively. Since both rotors rotate CCW, therefore, the second and fourth modes are classified as the *forward precessional modes*, and the first and third modes are referred to as the *backward precessional modes*. For the isotropic systems, the mass unbalance excites the forward modes only. Therefore, the critical speeds are the intersections of frequency curves of modes 2 and 4 and the excitation lines in the whirl speed map.

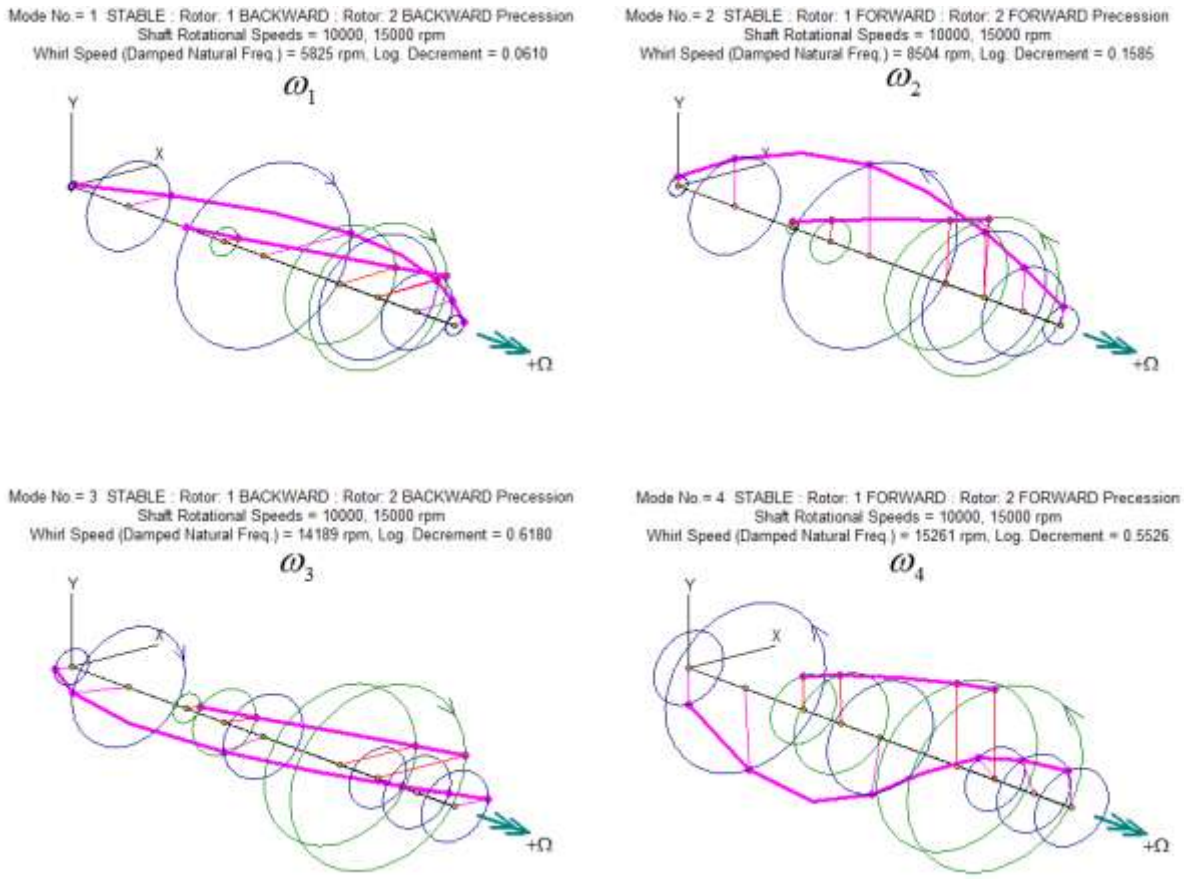

Figure 1-3 Precessional mode shapes at speed of Ω_1=10000, Ω_2=15000 rpm

After knowing the mode precessional direction, we can go back to examine the whirl speed maps and to identify the critical speeds due to shaft mass unbalance. The damped critical speeds are the intersection points between the system natural frequencies and the synchronous excitation line in the whirl speed map. The first two critical speeds due to rotor 1 mass unbalance occur at rotor speeds of about (Ω_1=8250, Ω_2=12375 rpm) and (Ω_1=15292, Ω_2=22938 rpm) with the whirling frequencies of 8250 and 15292 cpm, respectively. That is, the critical speeds due to rotor 1 mass unbalance are identified by the excitation line with the spin(1)/whirl ratio of 1, i.e., ($\frac{\Omega_1}{\omega}=1$, $\frac{\Omega_2}{\omega}=1.5$). And the first two critical speeds due to rotor 2 mass unbalance occur at rotor speeds of about (Ω_1=5233, Ω_2=7849 rpm) and (Ω_1=10062, Ω_2=15093 rpm) with the whirling frequencies of 7849 and 15093 cpm, respectively. That is, the critical speeds due to rotor 2 mass unbalance are identified by the spin(2)/whirl ratio of 1, i.e., ($\frac{\Omega_2}{\omega}=1, \frac{\Omega_1}{\omega}=\frac{1}{1.5}=0.66667$). Therefore, the first forward mode (ω_2) will be excited by the rotor 2 mass unbalance at rotor speed about (Ω_1=5233, Ω_2=7849 rpm) and again be excited by the rotor 1 mass unbalance at rotor speed about (Ω_1=8250, Ω_2=12375 rpm) during the startup. The second forward mode (ω_4) will be excited by the rotor 2 mass unbalance at rotor speed about (Ω_1=10062, Ω_2=15093 rpm) and again be excited by the rotor 1 mass unbalance at rotor speed about (Ω_1=15292, Ω_2=22938 rpm) during the startup. Each forward mode is excited twice by

the mass unbalance during startup in this case, the first one is by rotor 2 mass unbalance due to higher speed ratio and the other is by rotor 1 mass unbalance. The backward modes (ω_1, ω_3) are not excited by the mass unbalance in this isotropic system.

Since this system is an isotropic system with speed independent (constant) bearing coefficients, the critical speeds can also be estimated using the critical speed analysis. The critical speeds due to rotor 1 mass unbalance are obtained by assigning the spin(1)/whirl ratio = 1, i.e. $\frac{\Omega_1}{\omega} = 1$ and $\frac{\Omega_2}{\omega} = 1.5$. And the critical speeds due to rotor 2 mass unbalance are obtained by assigning the spin(2)/whirl ratio = 1, i.e. $\frac{\Omega_1}{\omega} = \frac{1}{1.5} = 0.66667$ and $\frac{\Omega_2}{\omega} = 1$. The associated mode shapes are shown in Figure 1-4.

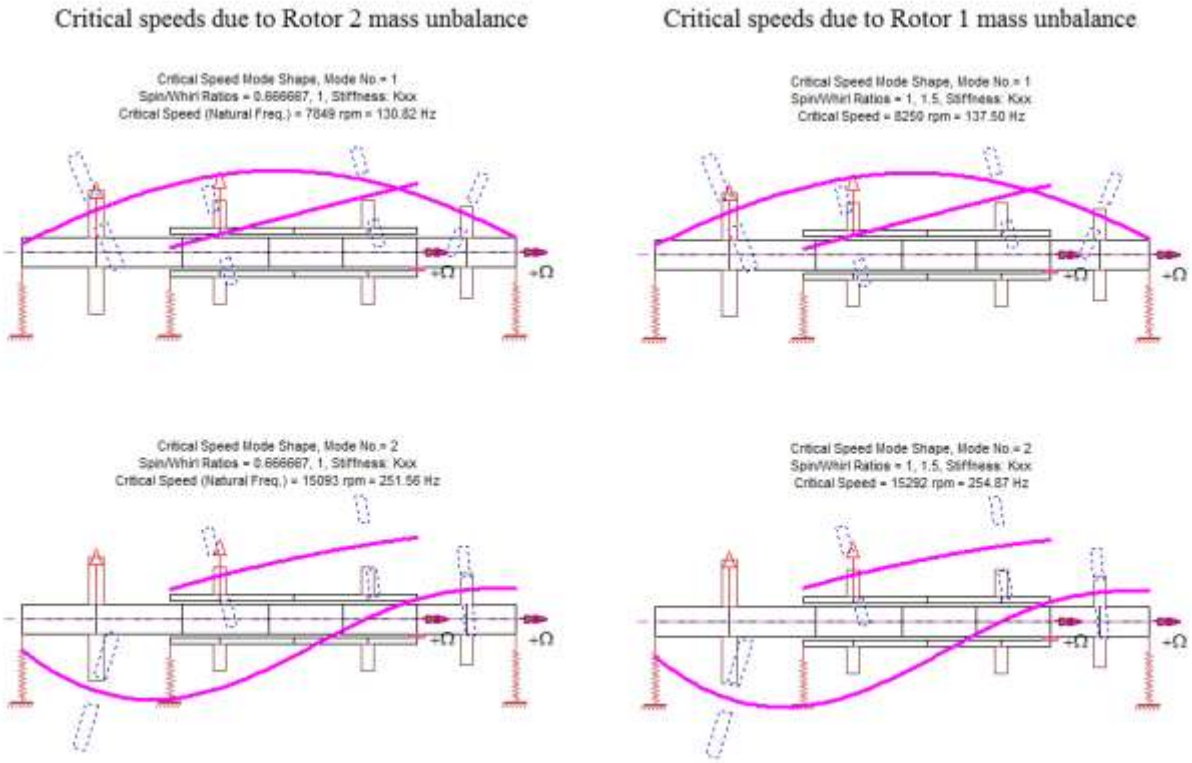

Figure 1-4 Critical speed mode shapes for $\Omega_2 = 1.5\,\Omega_1$

The rotor steady state responses at station 2 (rotor 1) and station 9 (rotor 2) are shown in Figure 1-5. As expected, the peak responses due to rotor 1 mass unbalance occur around (Ω_1=8250, Ω_2=12375 rpm) and (Ω_1=15292, Ω_2=22938 rpm) and the peak responses due to rotor 2 mass unbalance occur around (Ω_1=5233, Ω_2=7849 rpm) and (Ω_1=10062, Ω_2=15093 rpm). To fully understand the rotor motion with both mass unbalances, a transient analysis is performed at the rotor speed of $\Omega_1 = 10,000$ and $\Omega_2 = 15,000$ rpm with both the mass unbalance forces from

rotors 1 and 2 included. The steady state results are presented in Figure 1-6. Both rotors are whirling in the CCW direction, which is the same as the rotor direction of rotation, with two whirl frequencies of 10,000 and 15,000 rpm, which are caused by the rotor mass unbalances. The steady state motion is not a single harmonic vibration with simple elliptical orbit, it is the sum of two harmonics and the whirling direction is the same as the rotor rotational direction, as shown in Figure 1-6.

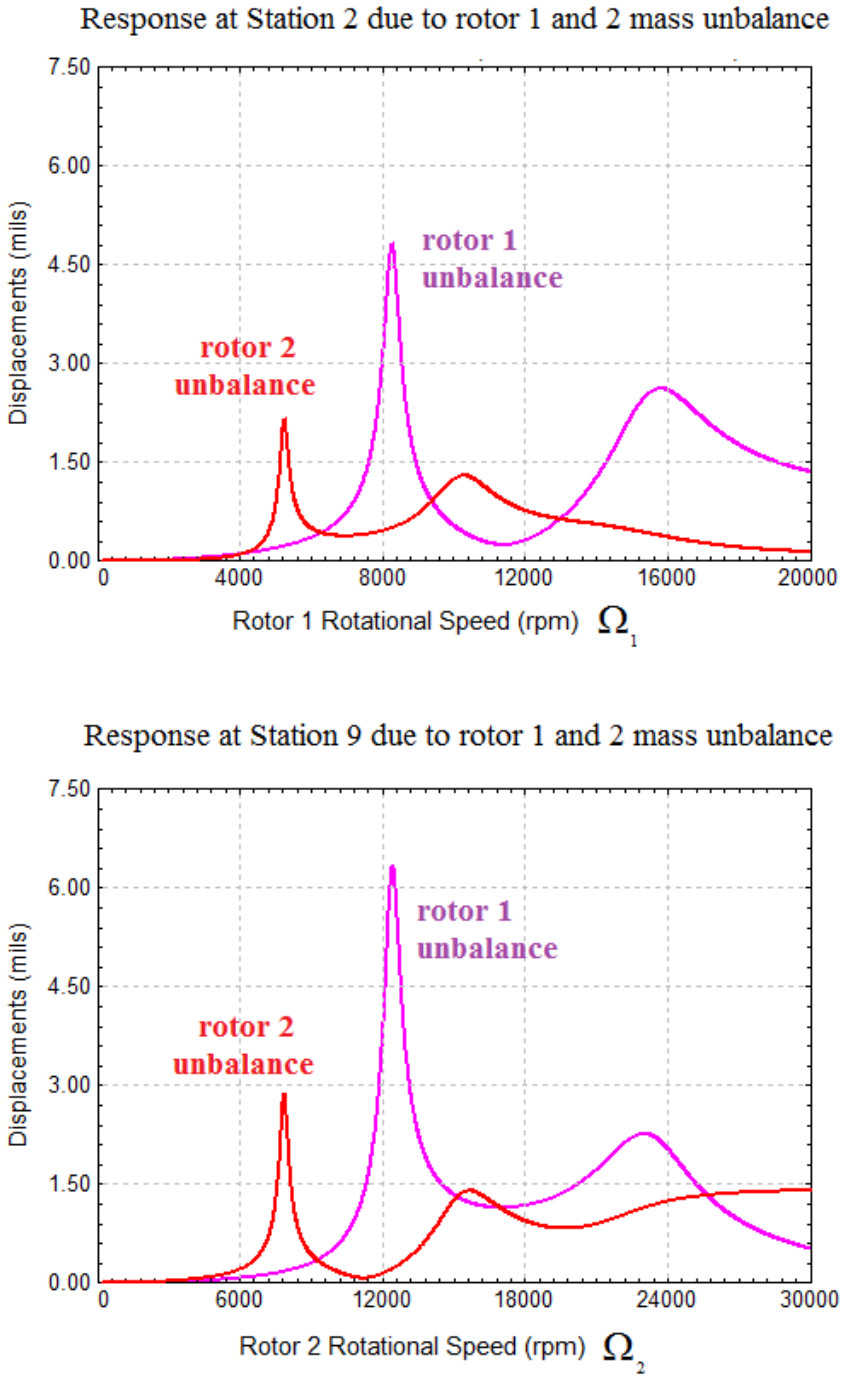

Figure 1-5 Rotor responses for $\Omega_2 = 1.5\,\Omega_1$

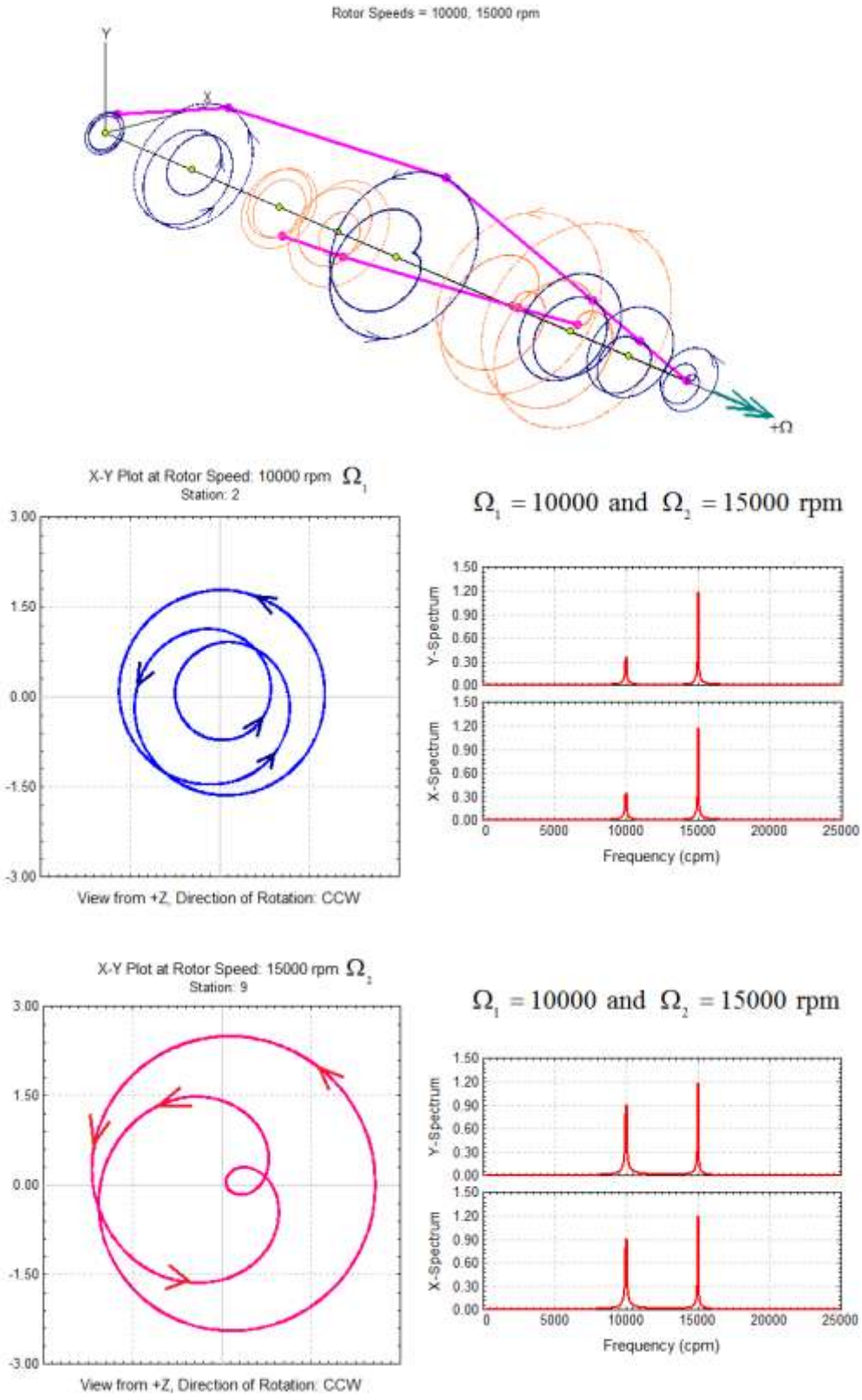

Figure 1-6 Rotor responses at speed Ω_1=10000 and Ω_2=15000 rpm

Case 2: $\Omega_2 = -1.5\,\Omega_1$**,** Ω_1**:** CCW and Ω_2**:** CW

Let us consider the rotor 2 is counter-rotation of rotor 1, that is, rotor 1 rotates CCW and rotor 2 rotates CW, as shown in Figure 1-7. The resulted first 4 natural frequencies ($\Omega_2 = -1.5\,\Omega_1$) are overlapped with the original first 4 natural frequencies ($\Omega_2 = +1.5\,\Omega_1$) shown in Figure 1-8. The associated 4 mode shapes at speed of Ω_1=10000, Ω_2=-15000 rpm shown in Figure 1-9. Note that the first and third modes, as shown in Figure 1-9, are whirling CW in the negative Z axis, which are backward precessions for rotor 1, however, are forward precessions for rotor 2. And the second and fourth modes are whirling CCW in the positive Z axis, which are forward precessions for rotor 1 and backward precessions for rotor 2. Since the rotor 2 rotates CW which has the opposite gyroscopic effect from rotor 1, therefore, the two modes (ω_1', ω_2') and (ω_3', ω_4') split less than that in Case1 with the same direction of rotation. The gyroscopic effect from rotor 1 stiffens the second and fourth modes since they are forward precessions for rotor 1. However these two modes are softened by the gyroscopic effect from rotor 2 since they are backward precessions for rotor 2. Same discussions apply for the other two modes. Again, for the isotropic systems, the mass unbalance excites the forward modes, which whirl in the same direction as the rotor direction of rotation. Therefore, the mass unbalance of rotor 1 excites the modes (ω_2', ω_4') with CCW whirling direction and the mass unbalance of rotor 2 excites the modes (ω_1', ω_3') with CW whirling direction. So, each mode will be excited once during rotor startup in this case, which is different from Case 1.

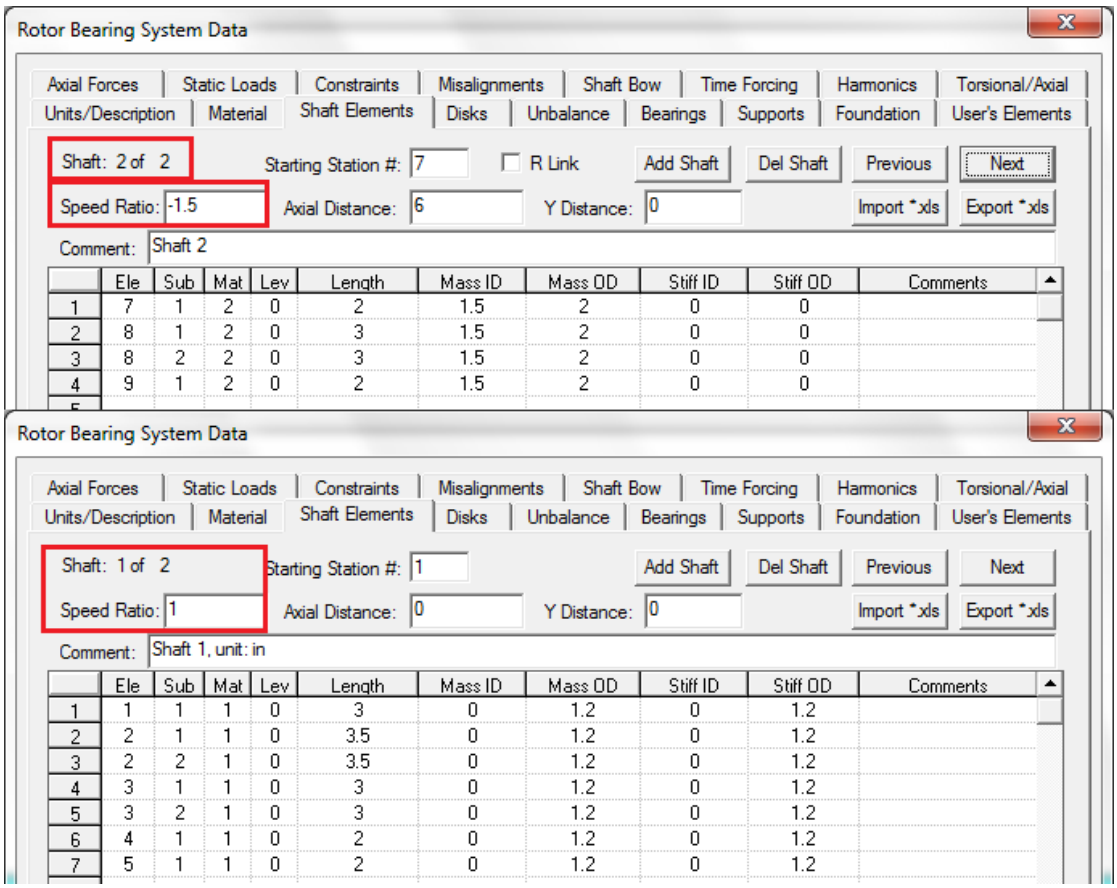

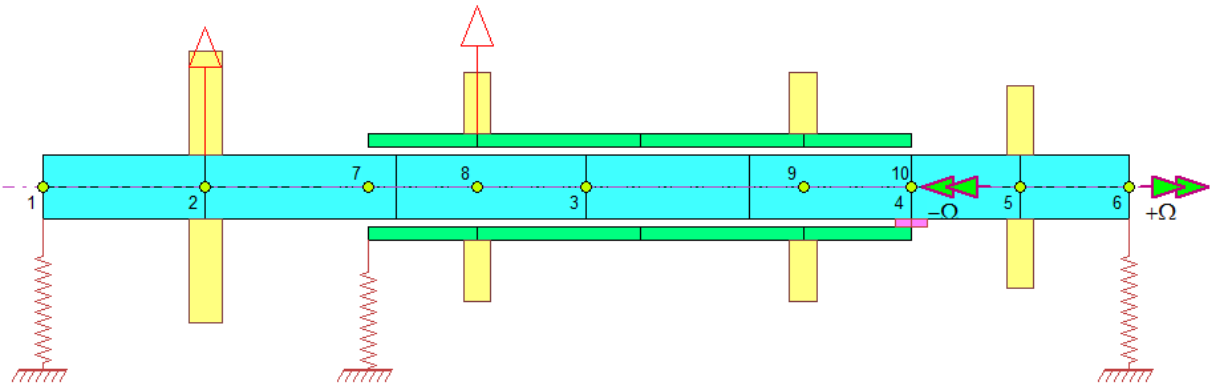

Figure 1-7 Dual rotor system, $\Omega_2 = -1.5\,\Omega_1$, Ω_1: CCW and Ω_2: CW

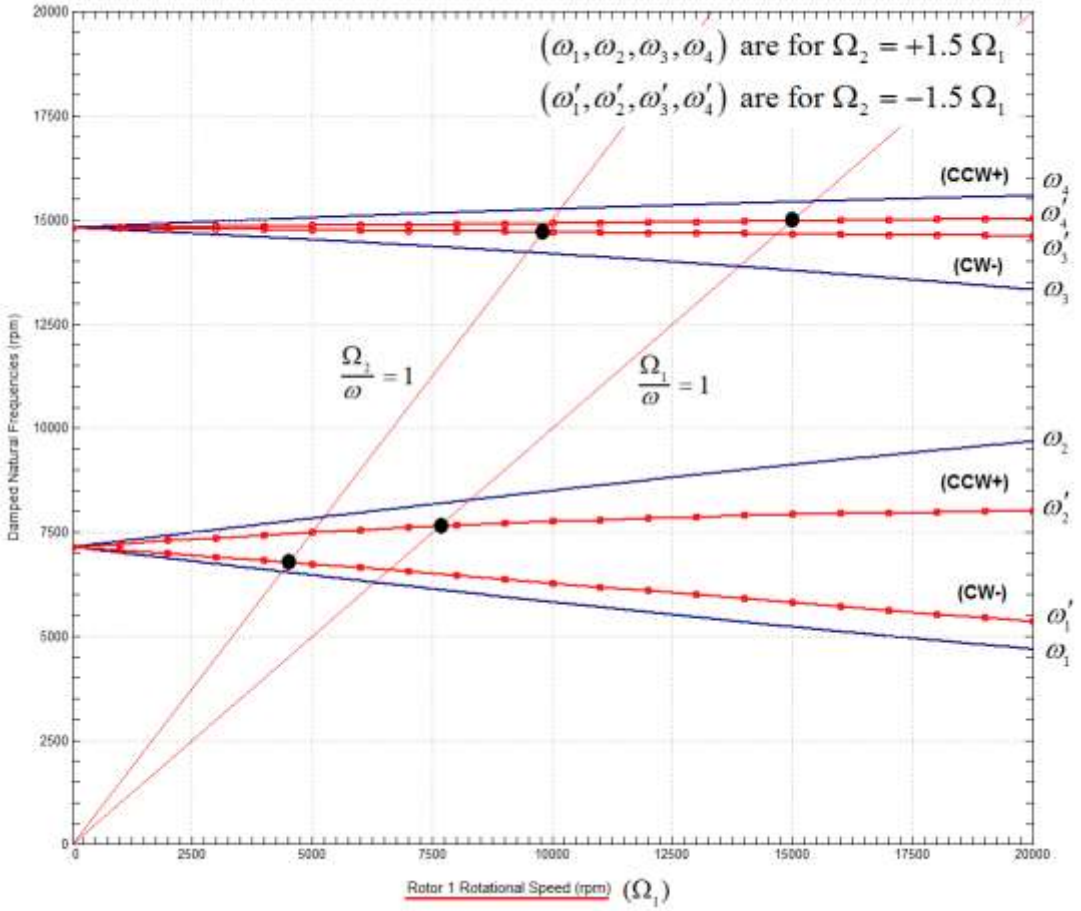

Figure 1-8 Whirl speed map for $\Omega_2 = -1.5\,\Omega_1$ and $\Omega_2 = 1.5\,\Omega_1$

The critical speeds due to rotor 1 mass unbalance are obtained by assigning the spin(1)/whirl ratio = 1, i.e. $\frac{\Omega_1}{\omega} = 1$ and $\frac{\Omega_2}{\omega} = -1.5$. And the critical speeds due to rotor 2 mass unbalance are

obtained by assigning the spin(2)/whirl ratio = 1, i.e. $\frac{\Omega_2}{\omega}=1$ and $\frac{\Omega_1}{\omega}=\frac{1}{-1.5}=-0.66667$. The associated mode shapes are shown in Figure 1-10.

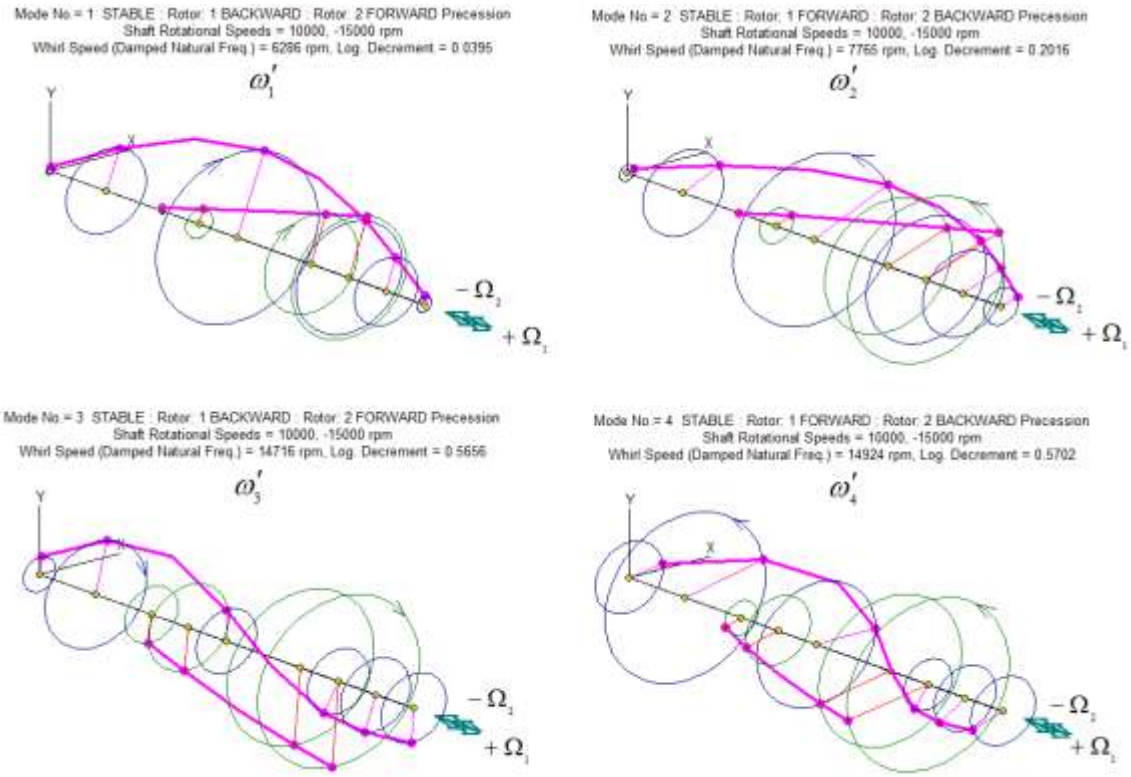

Figure 1-9 Precessional mode shapes at speed of Ω_1=10000, Ω_2= -15000 rpm

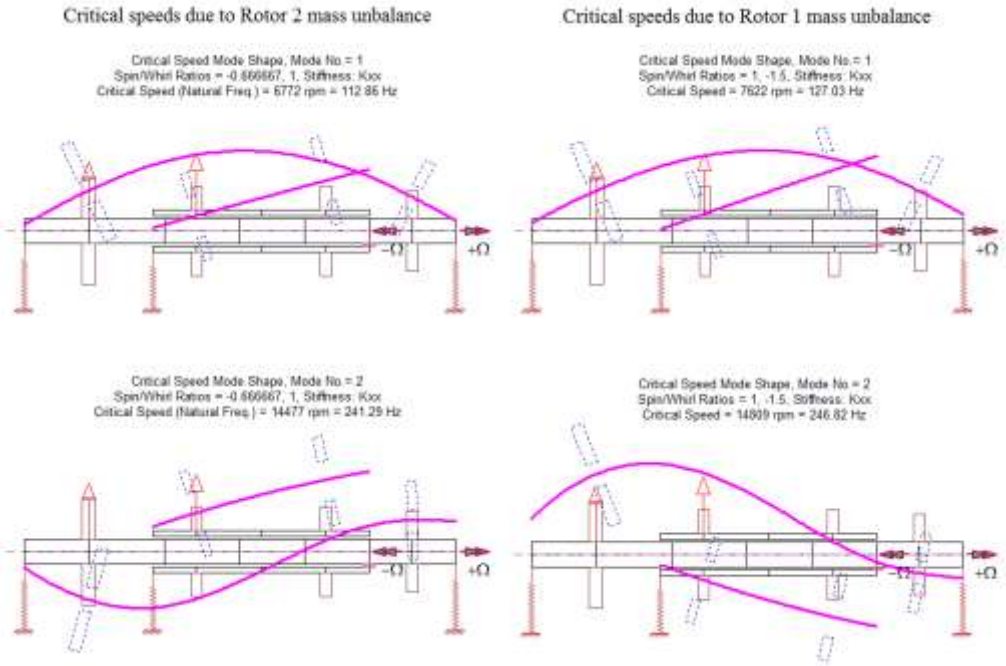

Figure 1-10 Critical speed mode shapes for $\Omega_2 = -1.5\,\Omega_1$

The rotor responses at station 2 (rotor 1) and station 9 (rotor 2) due to mass unbalance are shown in Figure 1-11. As expected, the peak responses occur at the critical speeds which are different from Case 1. Figure 1-12 shows the rotor steady state response with both mass unbalances at speed of (Ω_1=10000 rpm CCW and Ω_1=15000 rpm CW). It shows that the rotor 1 is whirling CCW and rotor 2 is whirling CW, both are corresponding to their own direction of rotation. Again, the whirling frequencies are the rotor speeds due to mass unbalances.

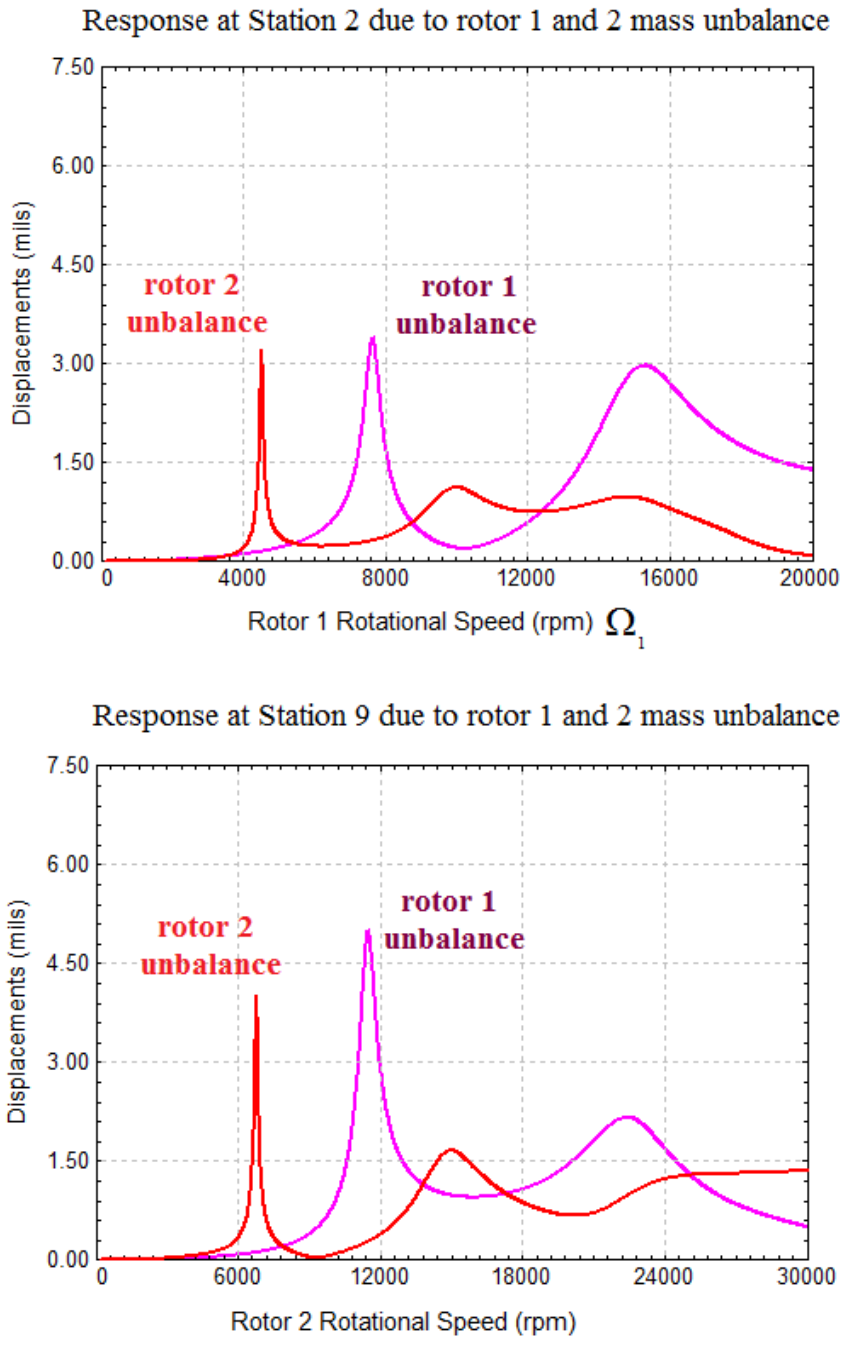

Figure 1-11 Rotor responses for $\Omega_2 = -1.5\,\Omega_1$

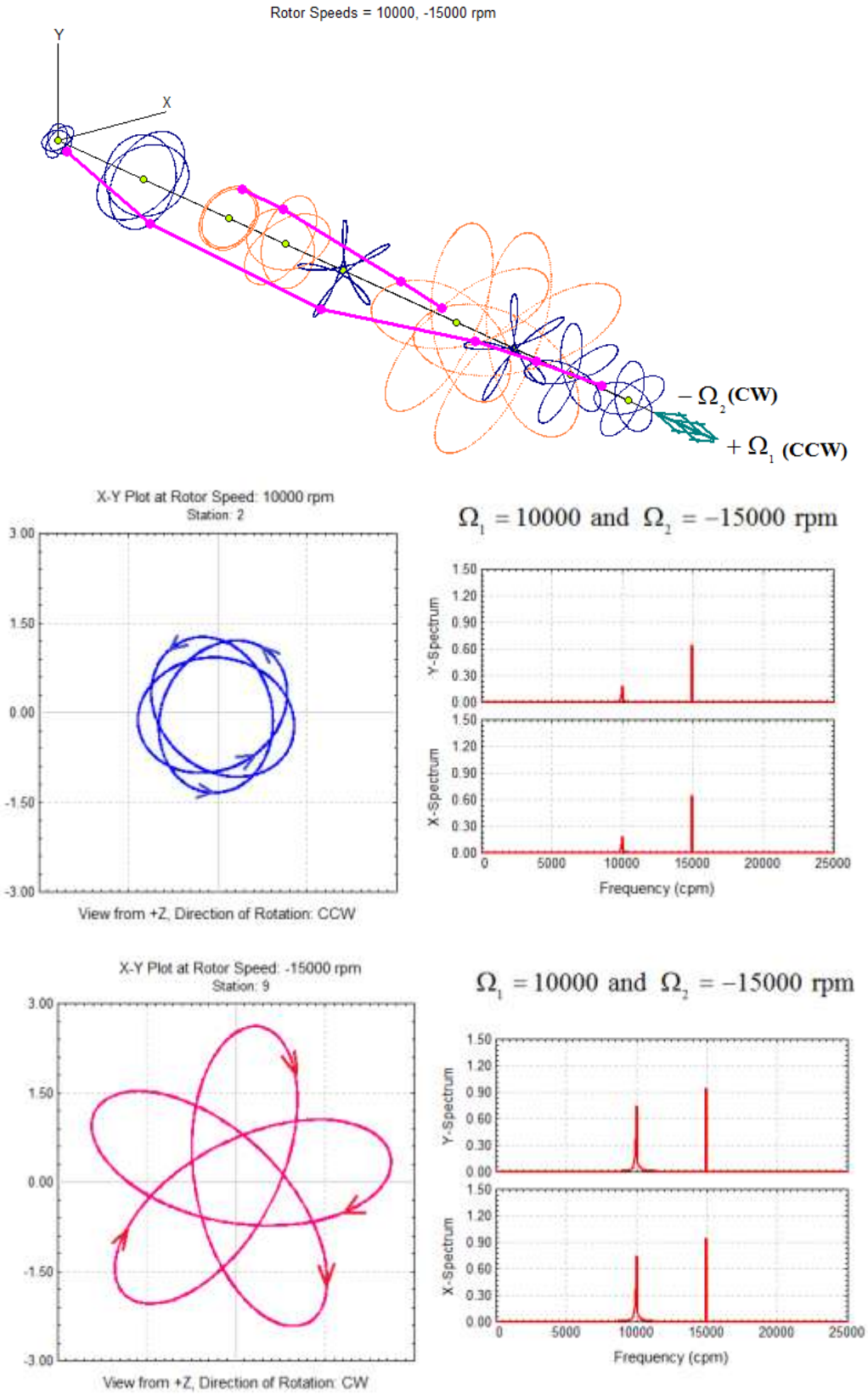

Figure 1-12 Rotor responses at speed Ω_1=10000 rpm CCW and Ω_2=15000 rpm CW

Case 3: $\Omega_2 = -1.5\,\Omega_1$**,** Ω_1 CW and Ω_2 CCW

For the completeness of the comparison, let us assume that the rotor 1 rotates CW and rotor 2 rotates CCW, as shown in Figure 1-13. The whirl speed map is shown in Figure 1-14. Note that the curves are generated from Case 3 and dots represent the results from Case 2. It shows that the frequency values are identical, however, the whirling direction are opposite, but consistent with the rotor direction of rotation. Therefore, the critical speeds due to rotor mass unbalances are identical to those in case 2, since the mass unbalance excites the forward modes, which whirl in the same direction as the rotor rotation. The critical speeds calculated using the critical speed analysis are also identical to those obtained in Case 2 and are not repeated here. The steady state unbalance responses are also the same as those in Case 2 Figure 1-11. Figure 1-15 shows the steady state responses at station 2 (rotor 1) and station 9 (rotor 2) at rotor speed of (Ω_1=10000 rpm CW and Ω_1=15000 rpm CCW) viewing from the +Z and –Z axis. Again, the response orbits whir in the same direction as the rotor rotation due to mass unbalance in this isotropic system.

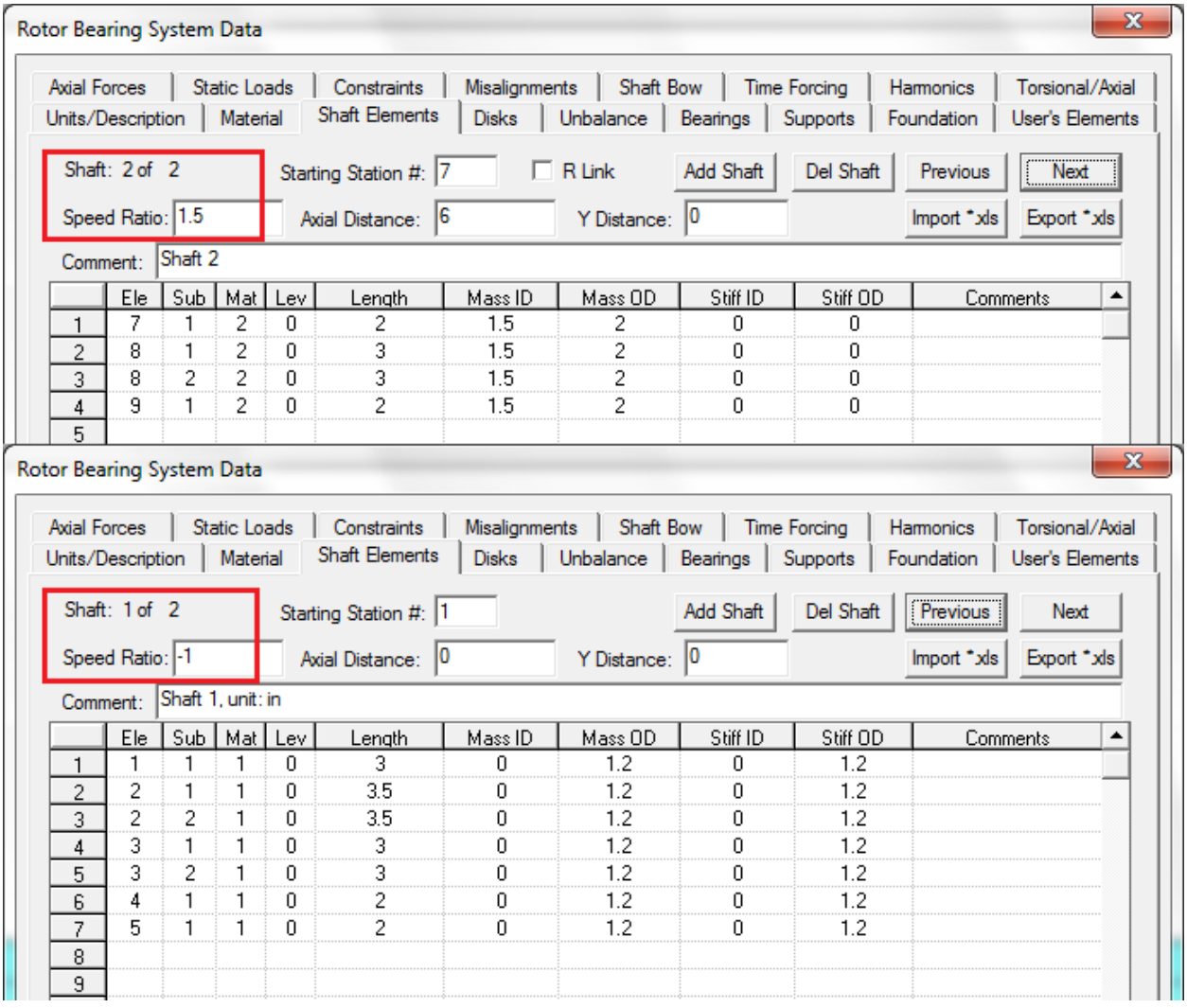

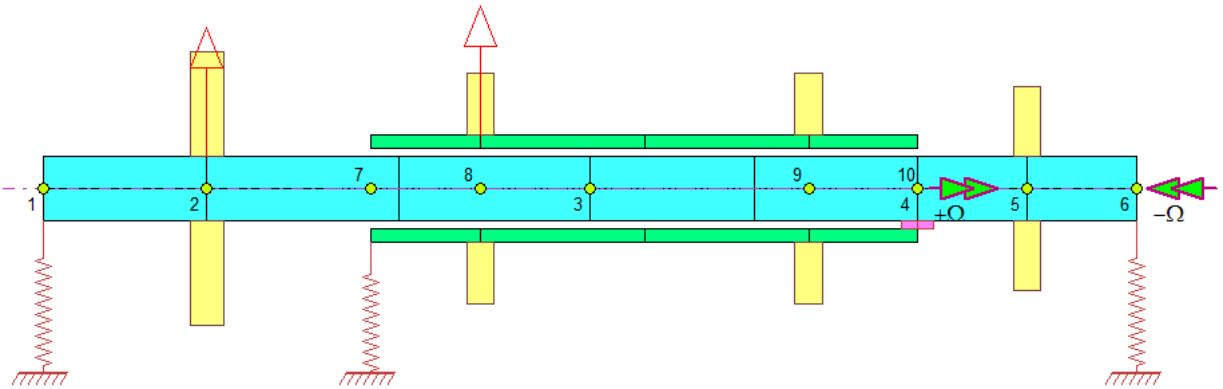

Figure 1-13 Dual rotor system, $\Omega_2 = -1.5\,\Omega_1$, Ω_1: CW and Ω_2: CCW

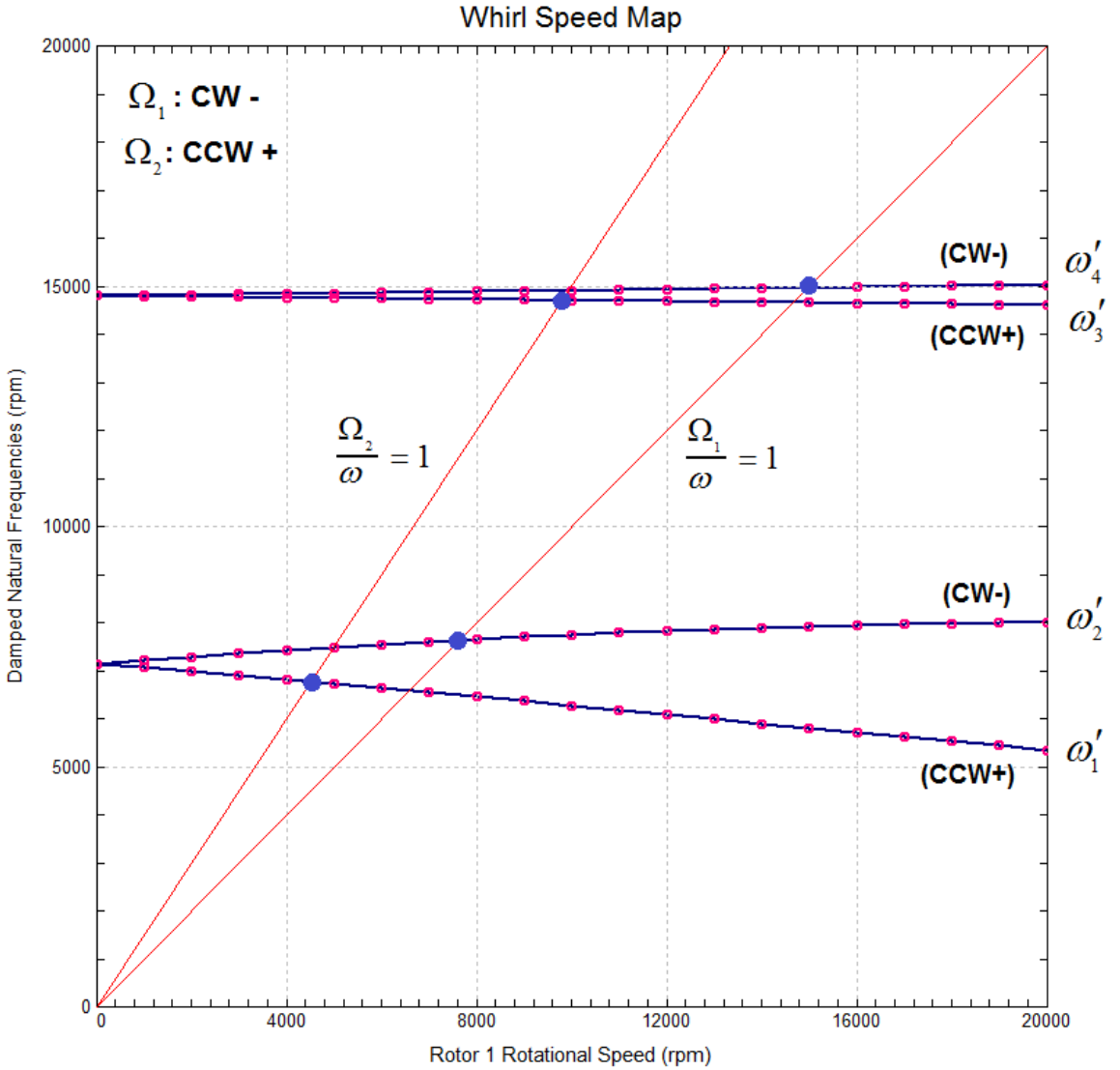

Figure 1-14 Whirl speed map for $\Omega_2 = -1.5\,\Omega_1$, Ω_1: CW and Ω_2: CCW

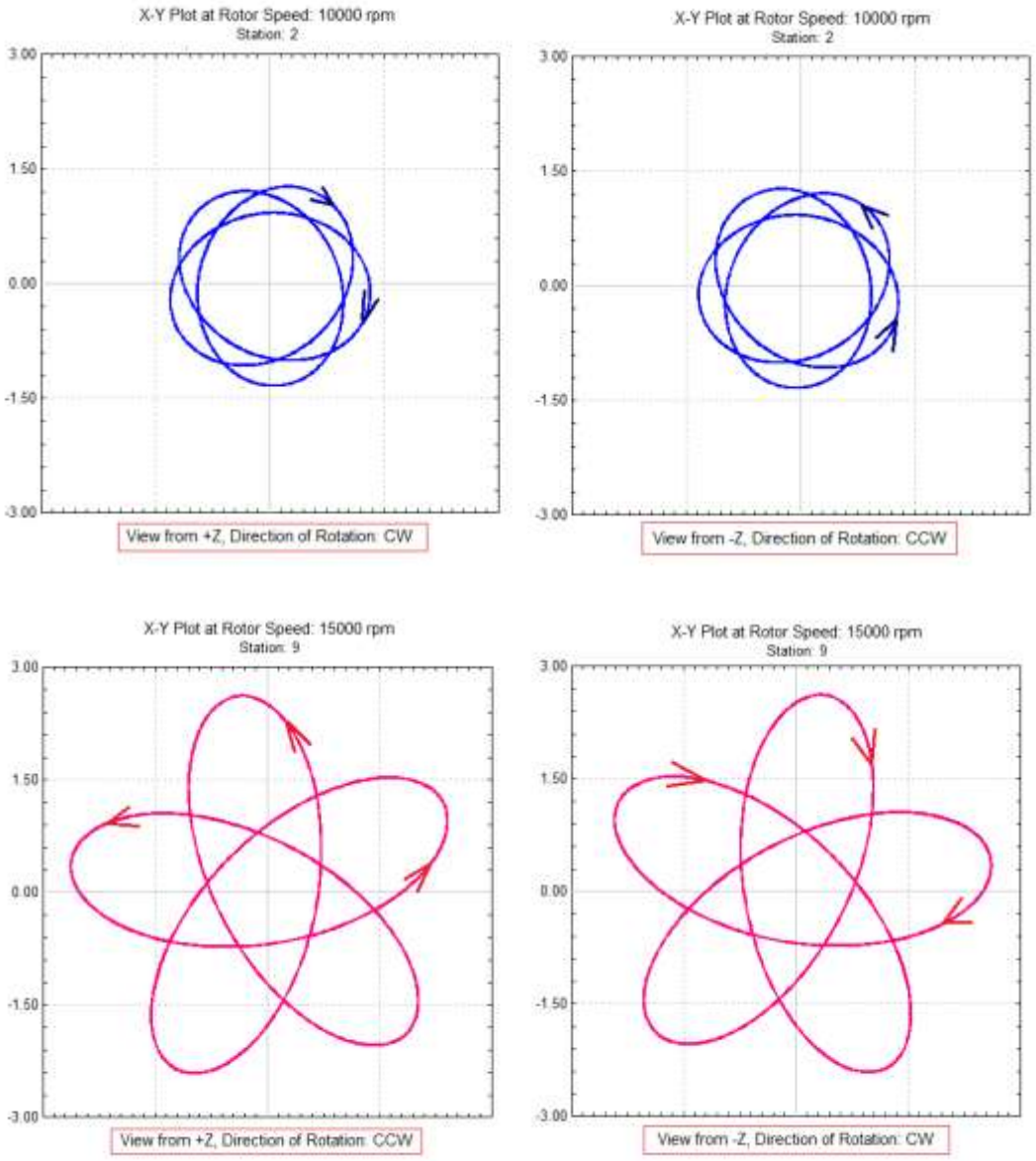

Figure 1-15 Rotor responses at speed Ω_1=10000 CW and Ω_2=15000 rpm CCW

Case 4: $\Omega_2 = 1.5\,\Omega_1$**,** Ω_1 CW and Ω_2 CW

Again, if both rotors rotate in the CW direction, the results will be identical to those presented in Case 1. The responses are also identical if viewed from the –Z axis. From Case 3 & Case 4, we learned that in all design practical purposes, for a single rotor system, the rotor direction of rotation can always be assumed in the CCW direction (+Z axis) without losing any accuracy and physical insights. For multiple rotor systems, the direction of rotation of rotor 1 can be assumed in the CCW direction (+Z axis) and others can be defined accordingly. The importance is the relationship in the direction of rotation for the multiple rotor system, not the exact direction of rotation of each rotor.

Example 2: A single rotor with cross-coupled bearing coefficients

Before we move on to the geared rotor system with multiple rotors running in different speeds and directions, let us examine another example to understand the coordinate relationship in more details. Consider a uniform shaft supported by two identical fluid film bearings, as shown in Figure 2-1. This system was first presented by Lund (1974) using the linearized bearing coefficients in the determination of damped critical speeds and instability threshold. It was then fully analyzed by Chen & Gunter (2005) in both linear and nonlinear analysis and results are well documented. This example used here is to address some necessary requirements and cautions in the coordinate transformation, in preparation for the analysis of complicated multiple shaft systems.

This uniform shaft has a length of 50 in., a diameter of 4 in., a Young's modulus of 3.0E07 psi, a shear modulus of 1.154E+07 psi, and a weight density of 0.283 Lb/in^3, is supported at the ends by two identical plain cylindrical fluid film bearings. For this uniform shaft, it has been demonstrated that the shaft shear deformation, rotatory inertia, and gyroscopic effects have a minimal influence on the dynamics of this rotor system, therefore, they are neglected here and focus is on the coordinate transformation. The two fluid film bearings are plain cylindrical journal bearings with a journal diameter of 4 in., a bearing radial clearance of 0.002 in., a bearing axial length of 1 in., and an oil viscosity of 6.9 centiPoise (1.0E-06 Reyns).

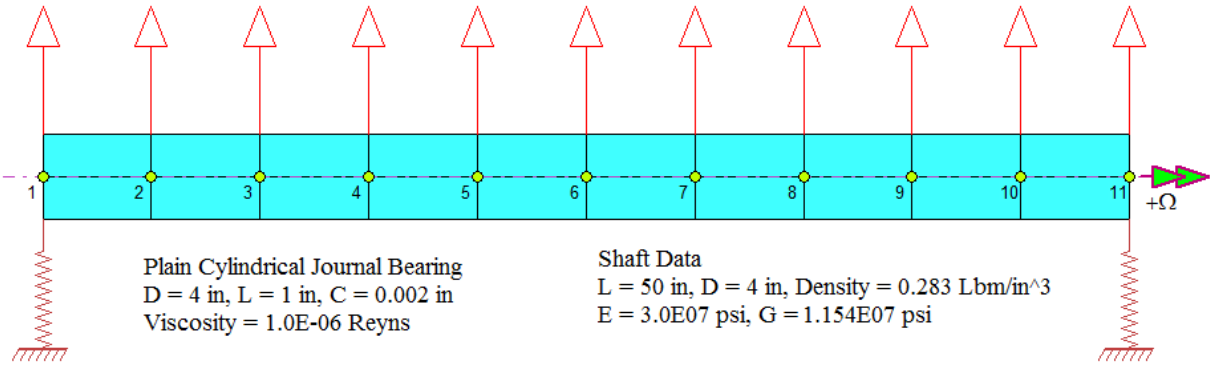

Figure 2-1 Uniform shaft supported by two plain cylindrical bearings

To perform the linear analysis on this rotor system, we need to analyze the bearings first to obtain the linearized bearing coefficients. Two bearing coordinate systems, as shown in Figure 1-2, are commonly used in the bearing analysis. The first one (X,Y), commonly used by the rotor dynamics analysts, is the same as the rotor coordinate system, that is X to the right and Y to the top and Z points to the viewer, regardless the bearing load vector. Then the bearing coefficients can be directly used in the rotor dynamic analysis. The second one (*x',y'*) is more frequently used by the bearing analysts where *x'*-axis is the same as the load vector and *y'* is perpendicular to the *x'*-axis. Once the linearized bearing coefficients are obtained from the (*x',y'*) coordinates system, it can be easily transformed into the standard (X,Y) coordinate system for the rotordynamic study. This coordinate transformation is described in details in Chen and Gunter and is given in Eq. 2-1.

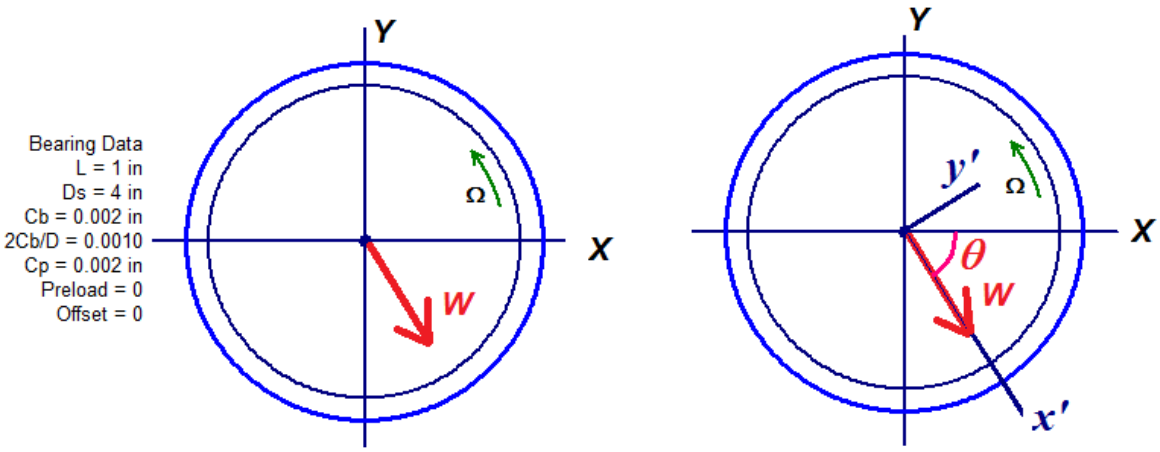

Figure 2-2 Bearing coordinates

$$\begin{bmatrix} k_{xx} & k_{xy} \\ k_{yx} & k_{yy} \end{bmatrix} = \begin{bmatrix} \cos\theta & \sin\theta \\ -\sin\theta & \cos\theta \end{bmatrix} \begin{bmatrix} k_{x'x'} & k_{x'y'} \\ k_{y'x'} & k_{y'y'} \end{bmatrix} \begin{bmatrix} \cos\theta & -\sin\theta \\ \sin\theta & \cos\theta \end{bmatrix}$$

where θ is the angle from x' to X axis. One critical assumption used in the above two coordinate systems for the bearing analysis is that the shaft direction of rotation is CCW in the Z direction. This assumption was not emphasized in many textbooks and papers, because for a single rotor system, we can always model the rotor system in the CCW direction of rotation without any problem as described in previous example. However, there will be different direction of rotations present for a geared system. Then caution needs to be taken to be sure that all the bearing coefficients have been converted into the coordinate system used for the rotor analysis.

Two scenarios are considered and shown in Figure 2-3, where (X,Y) are now the coordinates used to describe the rotor motion in the rotor dynamics analysis, and (X_b,Y_b) are the coordinates where the bearing linearized coefficients are obtained. When the rotor rotates CCW and the bearing coefficients are calculated based on the assumption of CCW shaft rotation, then (X,Y) and (X_b,Y_b) are the same, there is no need for any transformation and the bearing coefficients can be applied directly in the rotordynamic study. When the rotor rotates CW and the bearing coefficients are calculated based on the assumption of CCW shaft rotation, then the X and X_b are opposite to each other and Y and Y_b are the same. The linearized bearing forces acting on the rotor in both coordinate systems are:

In bearing coordinate system:

$$\begin{Bmatrix} F_x \\ F_y \end{Bmatrix}_b = -\begin{bmatrix} k_{xx} & k_{xy} \\ k_{yx} & k_{yy} \end{bmatrix}_b \begin{Bmatrix} x \\ y \end{Bmatrix}_b - \begin{bmatrix} c_{xx} & c_{xy} \\ c_{yx} & c_{yy} \end{bmatrix}_b \begin{Bmatrix} \dot{x} \\ \dot{y} \end{Bmatrix}_b$$

In rotor coordinate system:

$$\begin{Bmatrix} F_x \\ F_y \end{Bmatrix} = -\begin{bmatrix} k_{xx} & k_{xy} \\ k_{yx} & k_{yy} \end{bmatrix} \begin{Bmatrix} x \\ y \end{Bmatrix} - \begin{bmatrix} c_{xx} & c_{xy} \\ c_{yx} & c_{yy} \end{bmatrix} \begin{Bmatrix} \dot{x} \\ \dot{y} \end{Bmatrix}$$

Since we have the bearing forces and linearized coefficients in the bearing coordinate system and they need to be converted into the rotor coordinate system. The displacement, force, and coefficients transformations for scenario 2 are:

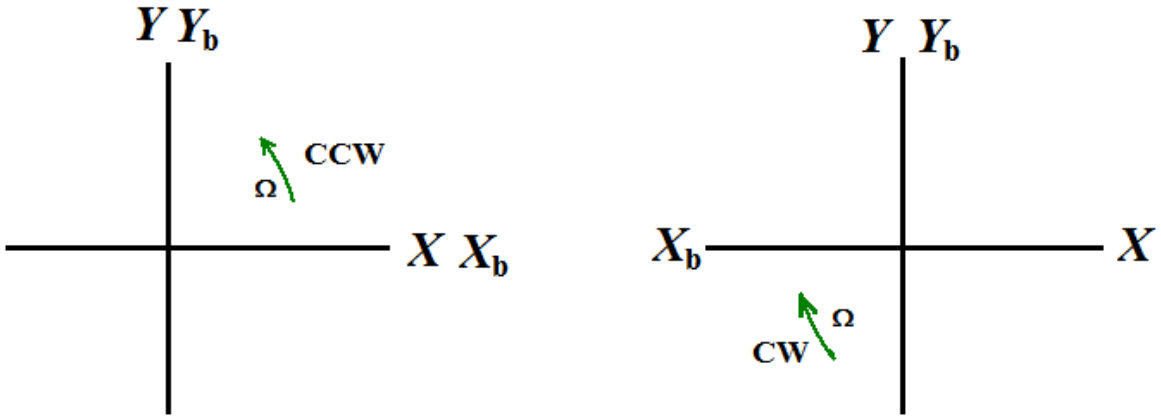

Figure 2-3 Rotor coordinates and bearing coordinates

$$\begin{Bmatrix} x \\ y \end{Bmatrix} = \begin{Bmatrix} -x \\ y \end{Bmatrix}_b = \begin{bmatrix} -1 & 0 \\ 0 & 1 \end{bmatrix} \begin{Bmatrix} x \\ y \end{Bmatrix}_b$$

$$\begin{Bmatrix} F_x \\ F_y \end{Bmatrix} = \begin{Bmatrix} -F_x \\ F_y \end{Bmatrix}_b = \begin{bmatrix} -1 & 0 \\ 0 & 1 \end{bmatrix} \begin{Bmatrix} F_x \\ F_y \end{Bmatrix}_b$$

and

$$\begin{bmatrix} k_{xx} & k_{xy} \\ k_{yx} & k_{yy} \end{bmatrix} = \begin{bmatrix} k_{xx} & -k_{xy} \\ -k_{yx} & k_{yy} \end{bmatrix}_b$$

$$\begin{bmatrix} c_{xx} & c_{xy} \\ c_{yx} & c_{yy} \end{bmatrix} = \begin{bmatrix} c_{xx} & -c_{xy} \\ -c_{yx} & c_{yy} \end{bmatrix}_b$$

For the stiffness and damping coefficients, only changes are the sign for the cross-coupled coefficients. The sign switch in the cross-coupled stiffness coefficients plays an important role in the rotor stability analysis. It is known that the cross-coupled stiffness coefficients generate the undesirable circulatory force and it contributes positive work done on the rotor system for a whirling orbit in the positive Z direction (CCW whirling orbit), and negative work done for a whirling orbit in the negative Z direction (CW whirling orbit). Positive work done indicates the

destabilizing effect and negative work done indicates the stabilizing effect. The work done by the cross-coupled stiffness coefficients over one cycle of a harmonic motion is given before and repeated here for easy reference:

$$W_{circulatory} = \left(k_{xy} - k_{yx}\right) \cdot \pi \left(a \cdot b\right)$$

where *a* and *b* are the semi-major and semi-minor axes of the elliptical orbit. Positive *b* indicates a CCW whirling orbit and negative *b* indicates a CW whirling orbit. $\pi\left(a \cdot b\right)$ is the area of the whirling elliptical orbit and positive area for a CCW whirling orbit and negative area for a CW whirling orbit. With the positive $(k_{xy} - k_{yx})$ term, this circulatory force destabilizes the CCW whirling modes, and stabilizes the CW whirling modes. Since for a single rotor system, we can always assume the rotor rotates CCW, therefore the CCW whirling modes are the so-called forward modes and CW whirling modes are backward modes. However, for a CW shaft rotation, the CW whirling modes are now the forward precessional modes and CCW whirling modes are the backward precessional modes. For the fixed-lobe fluid film bearings, with the positive Z shaft rotation, the $(k_{xy} - k_{yx})$ term is prone to be positive for the high speed and low load applications and it will tend to destabilize the forward modes with CCW precession. However, if the bearing coefficients are obtained based on the negative Z shaft rotation, then the $(k_{xy} - k_{yx})$ term is prone to be negative for the high speed and low load applications and it will tend to destabilize the forward modes with CW precession. Therefore, the sign switch in the cross-coupled stiffness coefficients is extremely important in the rotor stability analysis if the bearing is analyzed in the CW rotation. This is also valid for the so-called aerodynamic cross-coupling term *Q* used in the stability analysis by many Industry Standards, such as API. The purpose of introducing the aero-dynamic cross-coupling is to study the rotor stability and its sensitivity to the destabilizing force. The aerodynamic cross-coupling term is commonly treated (modeled) as a pseudo bearing with the following stiffness expression:

$$\begin{bmatrix} 0 & Q \\ -Q & 0 \end{bmatrix}$$ where *Q* is a positive value.

However, the Standard did not mention that it is customary to assume that the rotor is rotating CCW in the positive Z direction when the above expression is applied. If the rotor rotates in the CW direction, then the proper aerodynamic cross-coupling expression will be:

$$\begin{bmatrix} 0 & -Q \\ Q & 0 \end{bmatrix}$$ where *Q* is a positive value and Ω is CW rotation.

The aerodynamic cross-coupling term always destabilizes the forward modes, regardless the shaft rotation. The above discussion will be illustrated using this example. The bearing coefficients versus speeds and their coordinate definition are shown in Figure 1-4.

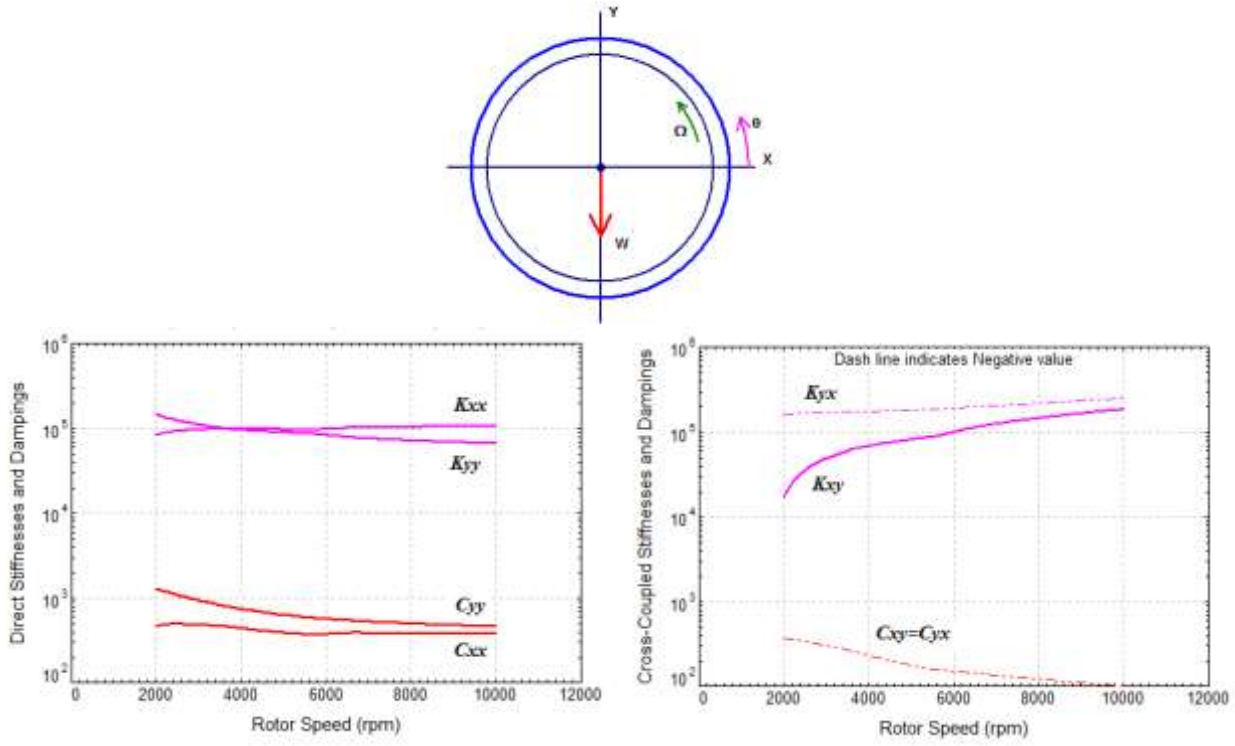

Figure 2-4 Bearing coordinates

Case 1: Ω is CCW rotation

Let us consider the conventional case, that is, the shaft is rotating CCW in the Z direction. Then, the bearing coefficients can be directly applied in the rotor dynamic study. Figures 2-5 and 2-6 show the whirl speed map and stability map. These two maps have been presented in this text many times. The only addition in the map is the direction of whirling for each mode. Since the rotor is rotating in the CCW direction, so the modes with CCW precessions are the forward modes, and with CW precessions are the backward modes. The first two backward modes are overdamped and not shown in the map. The first forward mode goes to unstable when the rotor speed exceeds 9120 rpm, which is commonly referenced as the instability threshold.

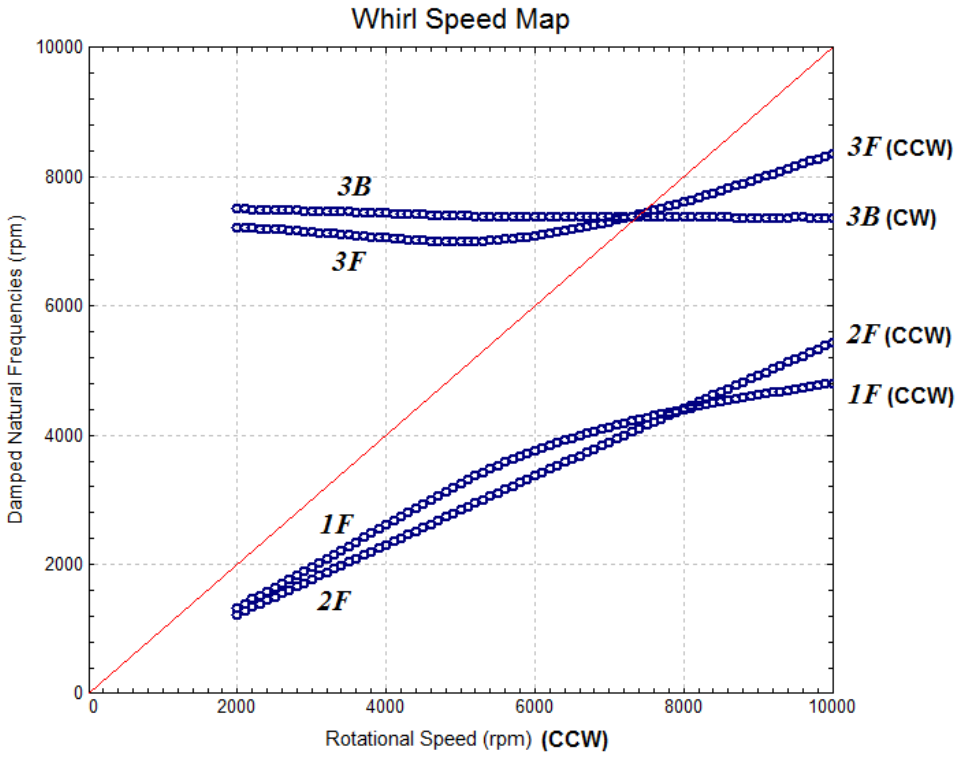

Figure 2-5 Bearing coordinates

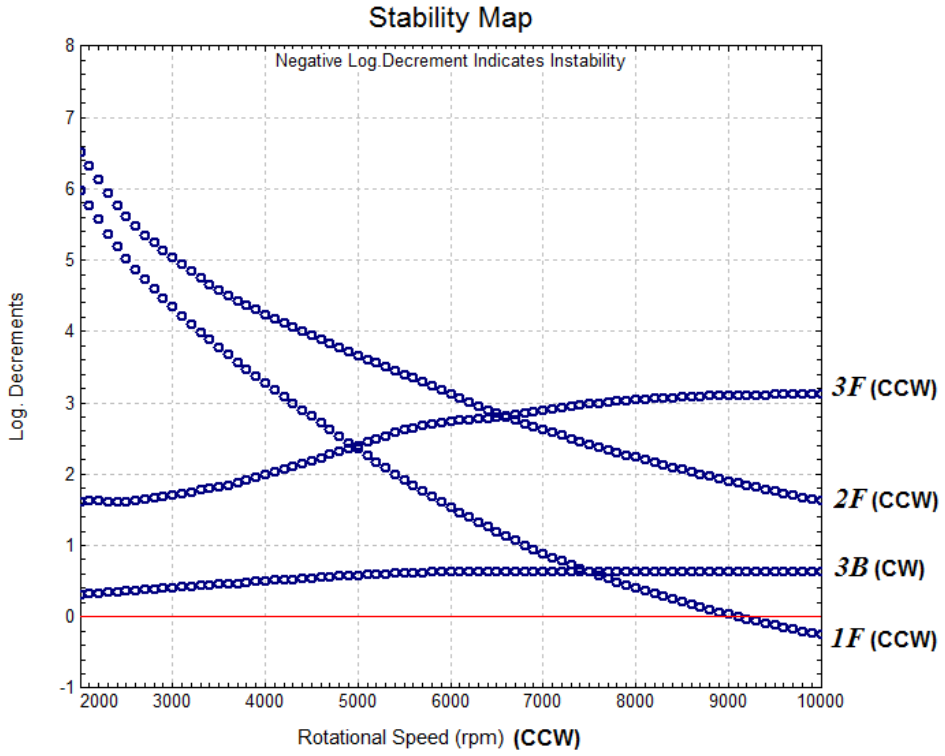

Figure 2-6 Bearing coordinates

With these linearized bearing coefficients, Figure 2-7 shows the steady state unbalance response at bearing station with 0.1 oz-in evenly distributed mass unbalance eccentricity. Figure 2-8 shows the bearing station displacement orbit at rotor speed of 5000 rpm. Note that the vibration is about the static equilibrium position for the linear analysis. The response orbit is whirling CCW in the direction of shaft rotation, which is a forward precession. Figure 2-9 shows response orbits for the linear analysis and nonlinear simulation about the bearing geometric center. Again, they are in the forward precessions and the orbit due to nonlinear simulation is a little smaller than that from the linear analysis due to nonlinearity.

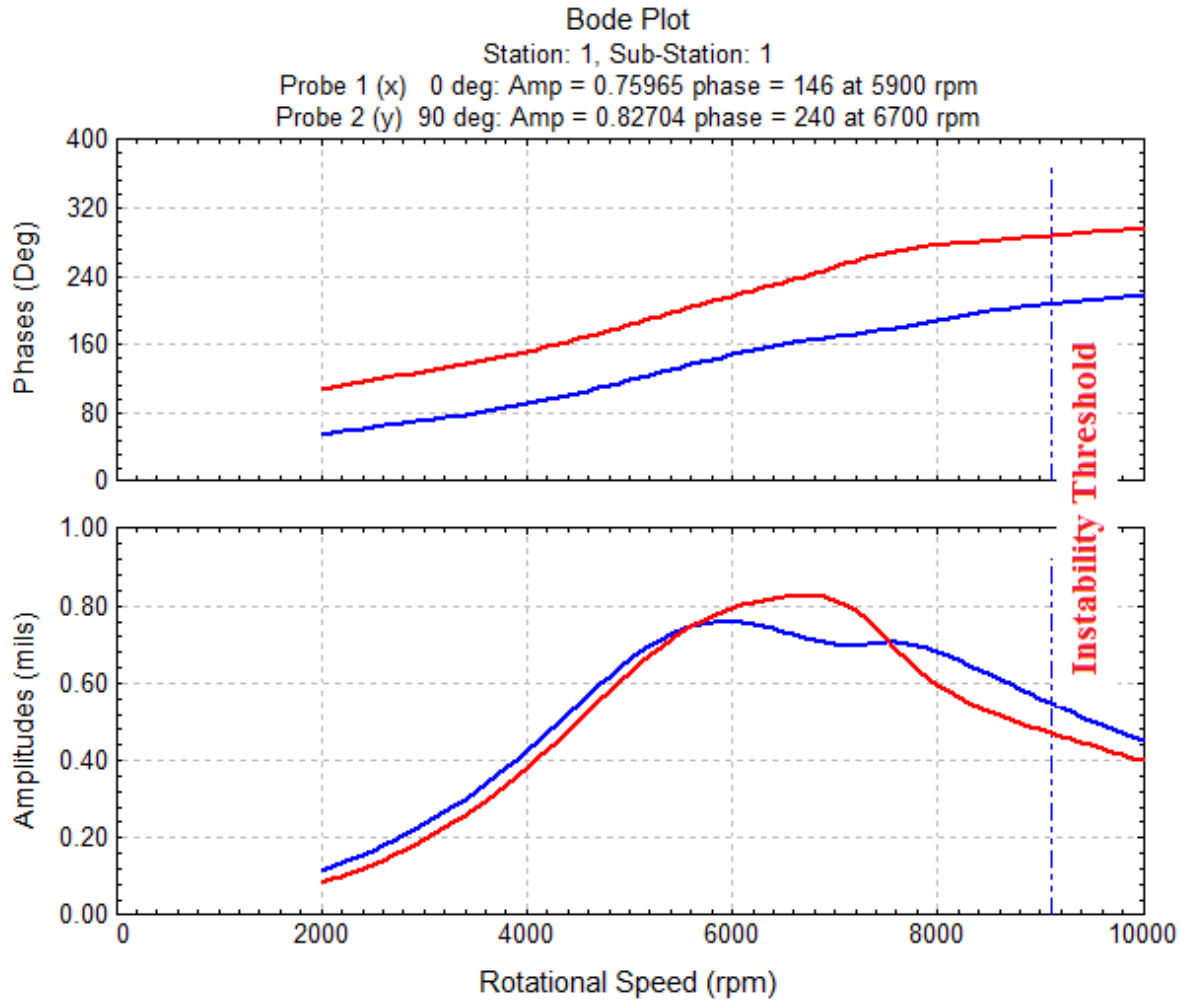

Figure 2-7 Steady state unbalance response at bearing station

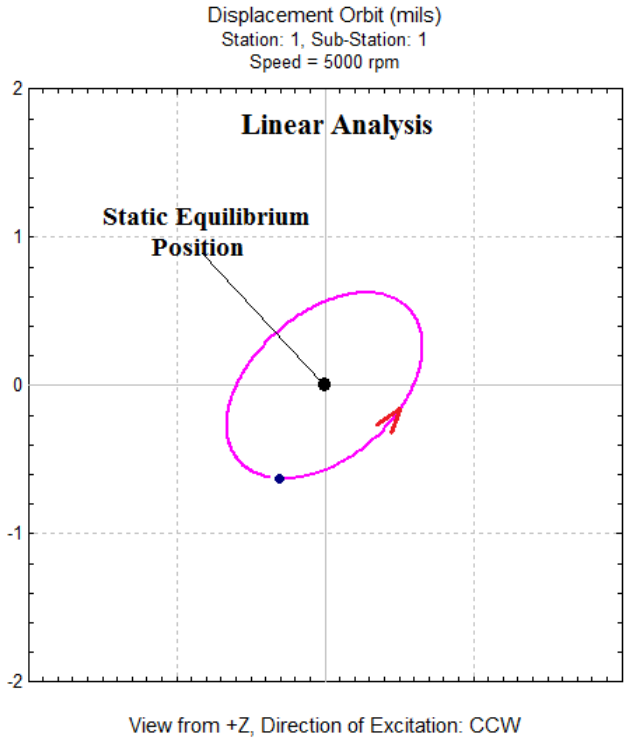

Figure 2-8 Bearing station linear displacement orbit at 5000 rpm

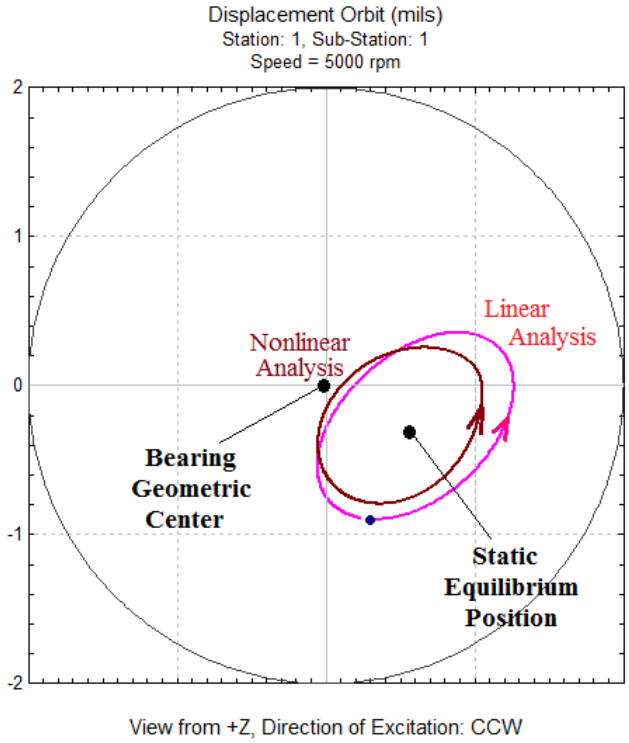

Figure 2-9 Bearing station linear and nonlinear displacement orbit at 5000 rpm

Since the instability threshold is around 9120 rpm from the stability map, therefore, the linear steady state unbalance response analysis is not valid after this speed and transient analysis is required. Figure 2-10 shows the transient response orbit at 10000 rpm with the linearized bearing coefficients. It shows that the response will grow out of the bearing clearance circle which is not physically feasible in practice and it demonstrates that the linear theory is not valid after the instability threshold and nonlinear theory should be applied. However, it shows that the response grows in the CCW direction, same as the direction of shaft rotation. It implies that the rotor is whirling with an unstable ***forward*** precessional mode, which is agreement with the stability map. Figure 2-11 shows that response orbit with nonlinear simulation. Again, it shows that the rotor is whirling CCW in the direction of shaft rotation, that is a forward precessional motion. And the orbit is constrained within the bearing clearance circle.

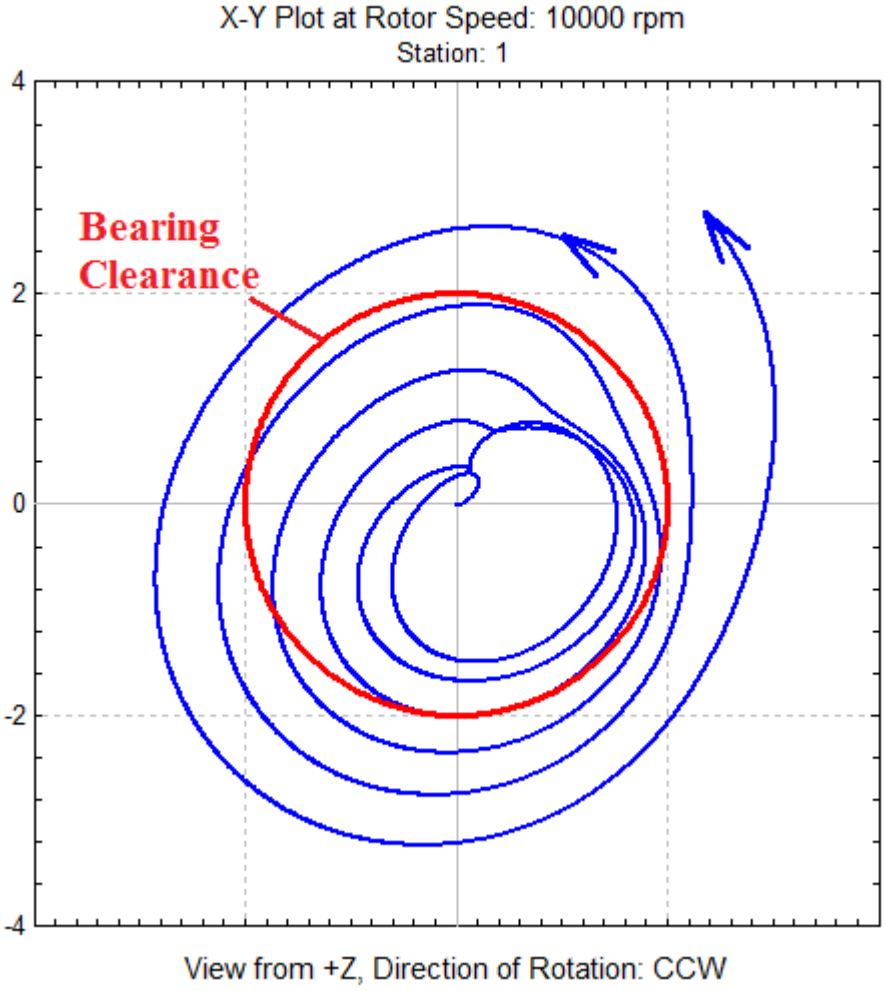

Figure 2-10 Transient response with linearized bearing coefficients at 10000 rpm

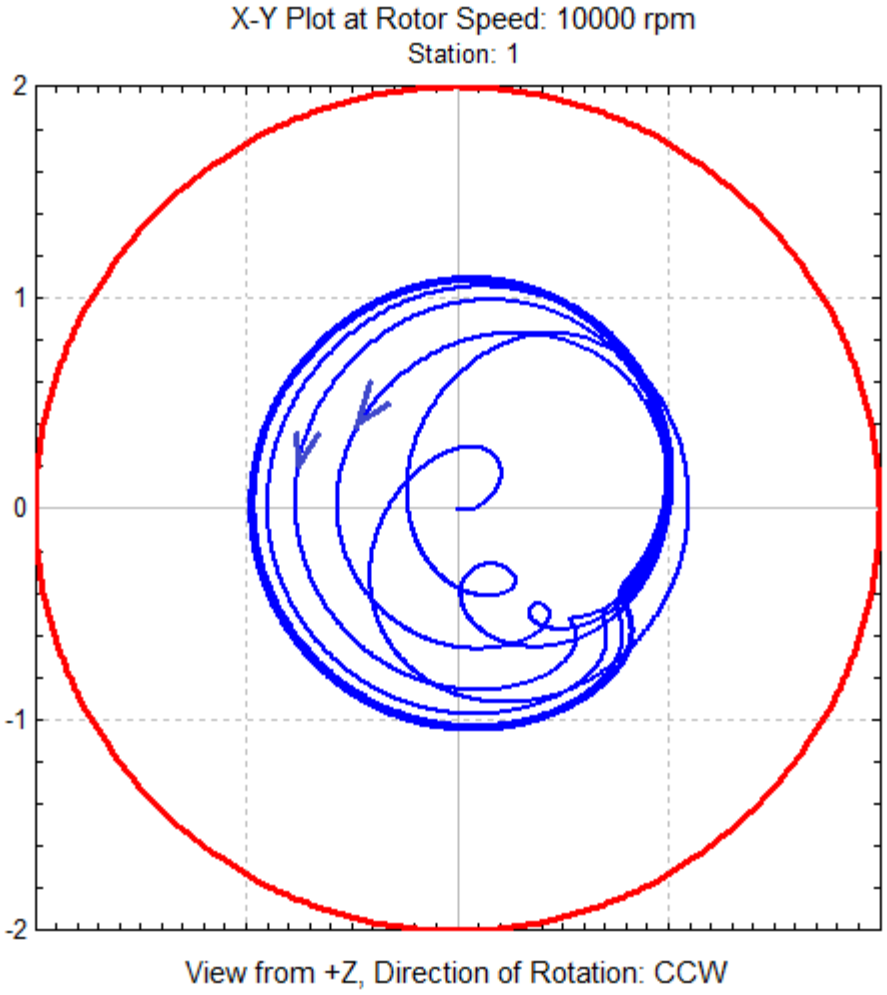

Figure 2-11 Transient response with nonlinear bearing forces at 10000 rpm

The above discussion provides a brief review on some important concepts that were presented before. The main objective here is to emphasize that the bearing coordinates and rotor coordinates must be in the same direction of rotation. Let us consider now the rotor rotates in the CW direction, as shown in Figure 2-12, and the bearing coefficients were obtained based on the CCW direction of rotation as before. Figures 2-13 and 2-14 show the whirl speed map and stability map with the original bearing coefficients. At the first glance, one may think that the results are identical to the previous discussion due to the same frequency values and the mode whirling directions, so it is unnecessary to switch the sign in the bearing cross-coupled coefficients. However, it is also noted that the rotor now rotates in the CW direction, so the CCW precessional modes becomes backward precessional modes and CW precessional modes become forward precessional modes. So, with these incorrect bearing coefficients, the backward mode becomes unstable, which is NOT the same as before. So, without the sing change in the bearing coefficients, the free vibration analysis provides incorrect results.

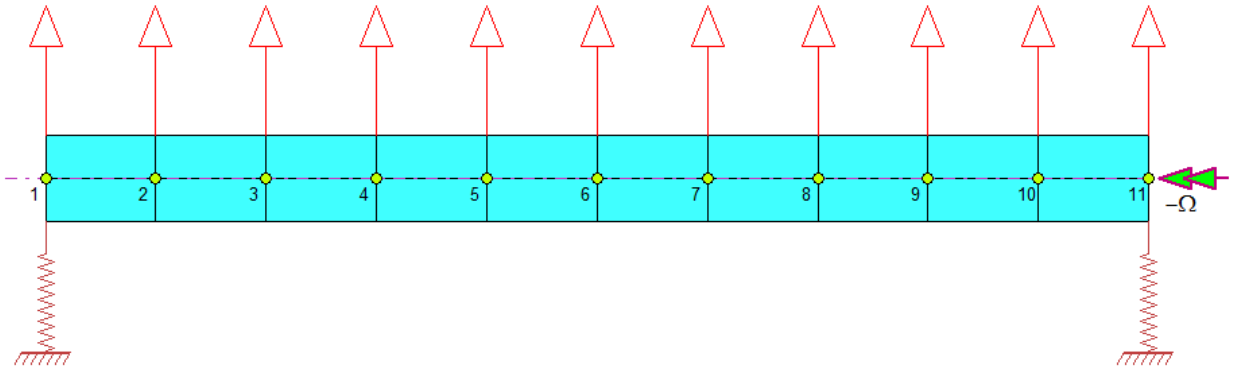

Figure 2-12 Shaft rotation CW

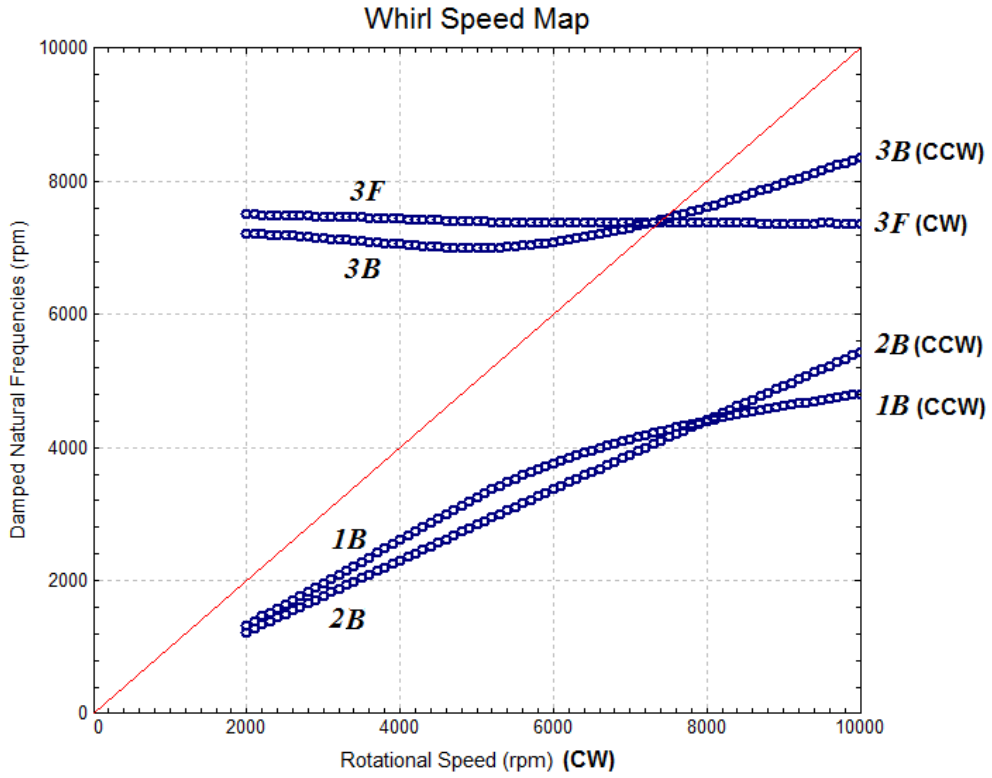

Figure 2-13 Whirl speed map with the INCORRECT bearing data

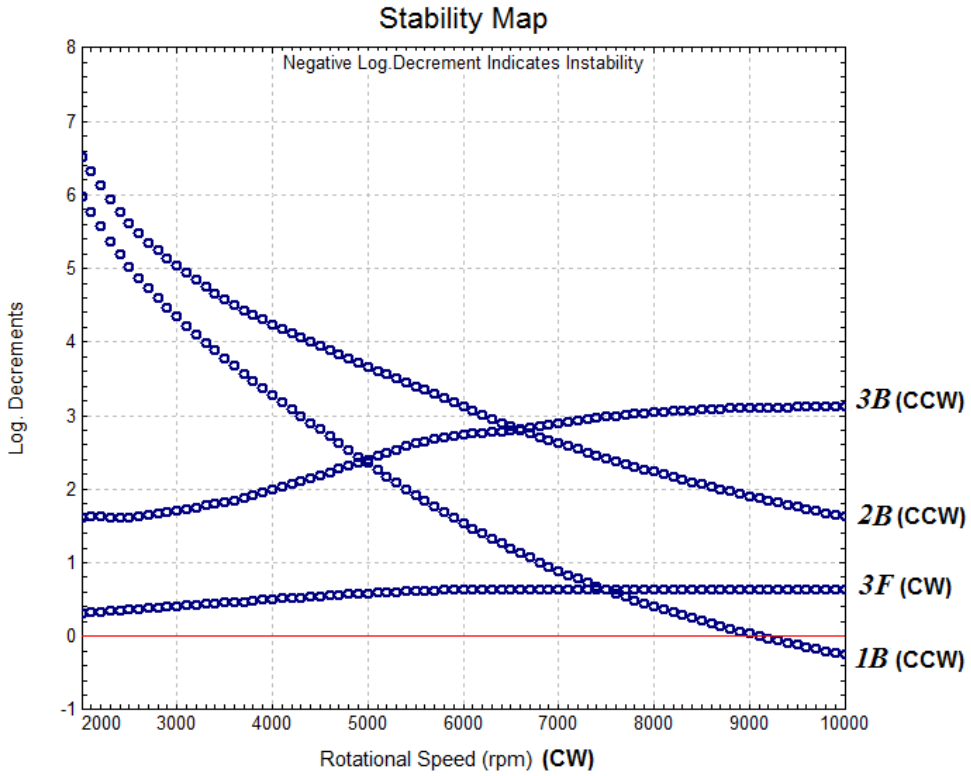

Figure 2-14 Stability speed map with the INCORRECT bearing data

Figure 2-15 shows the steady state unbalance response at the bearing station with the original bearing coefficients. Now, the significant difference is shown here with the previous result in Figure 2-7. Figure 2-16 shows the bearing station steady state response orbit at 5000 rpm viewed from both directions: +Z and –Z directions. It shows that the response orbit is whirling in the opposite direction from the direction of shaft rotation. This is also incorrect compared with previous results in Figure 2-8. Therefore, the sign switch in the bearing cross-coupled coefficients is important and needs special attention when the shaft direction of rotation is different from the bearing coefficients calculation.

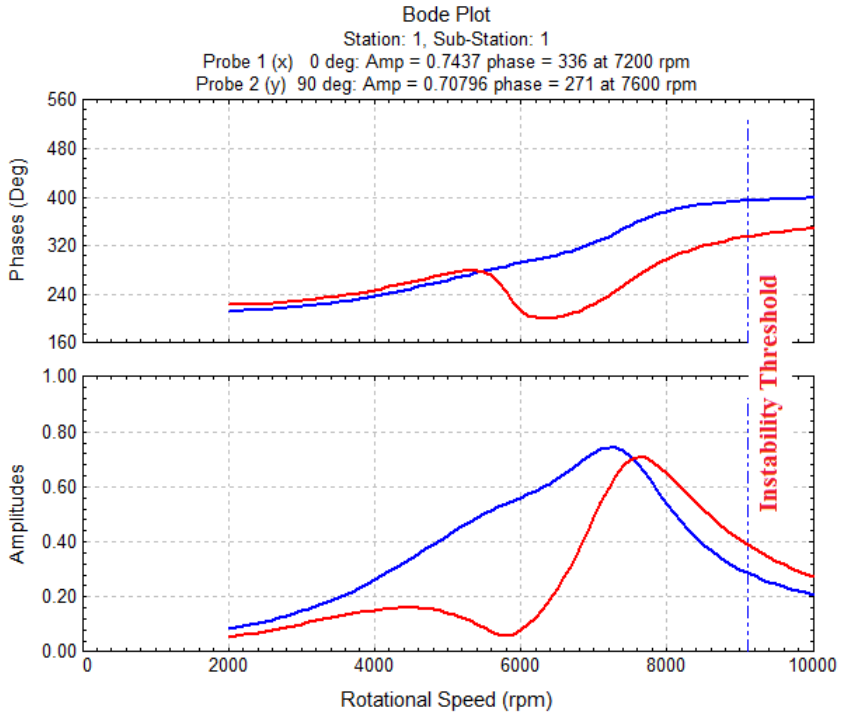

Figure 2-15 Steady state response with the INCORRECT bearing data

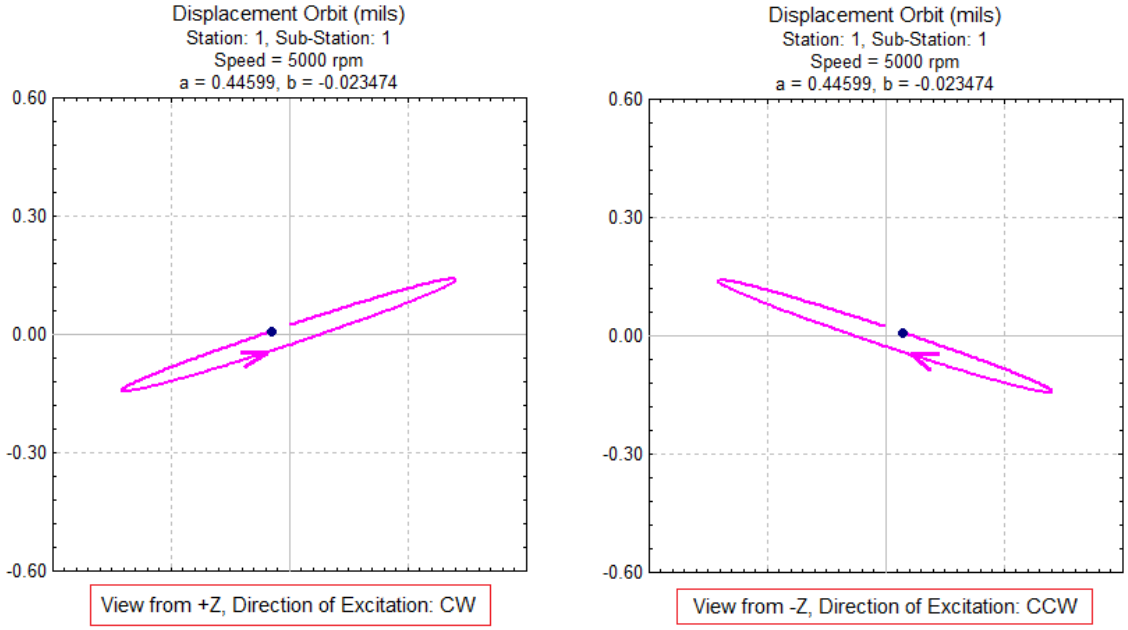

Figure 2-16 Steady state response at 5000 rpm with the INCORRECT bearing data

Figures 2-17 and 2-18 show the whirl speed map and stability map with the correct bearing coefficients, that is the sign change in the cross-coupled bearing coefficients. Now the results are identical to the original results. Although the forward precessional modes now are whirling in the CW direction, it is consistent with the shaft direction of rotation.

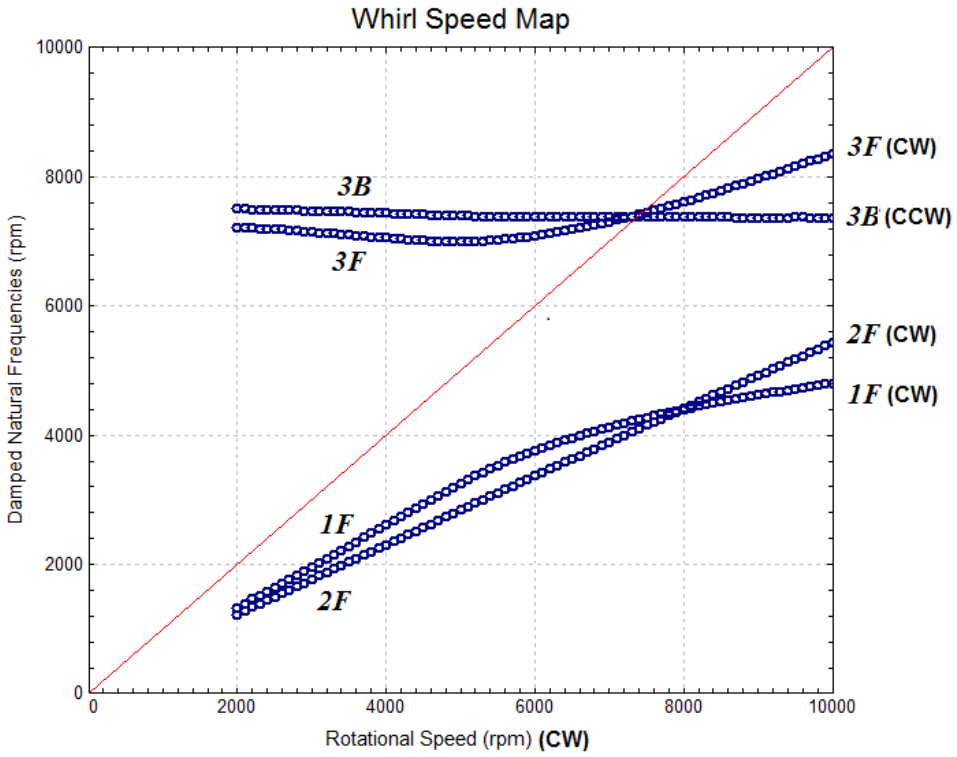

Figure 2-17 Whirl speed map with CORRECT bearing data

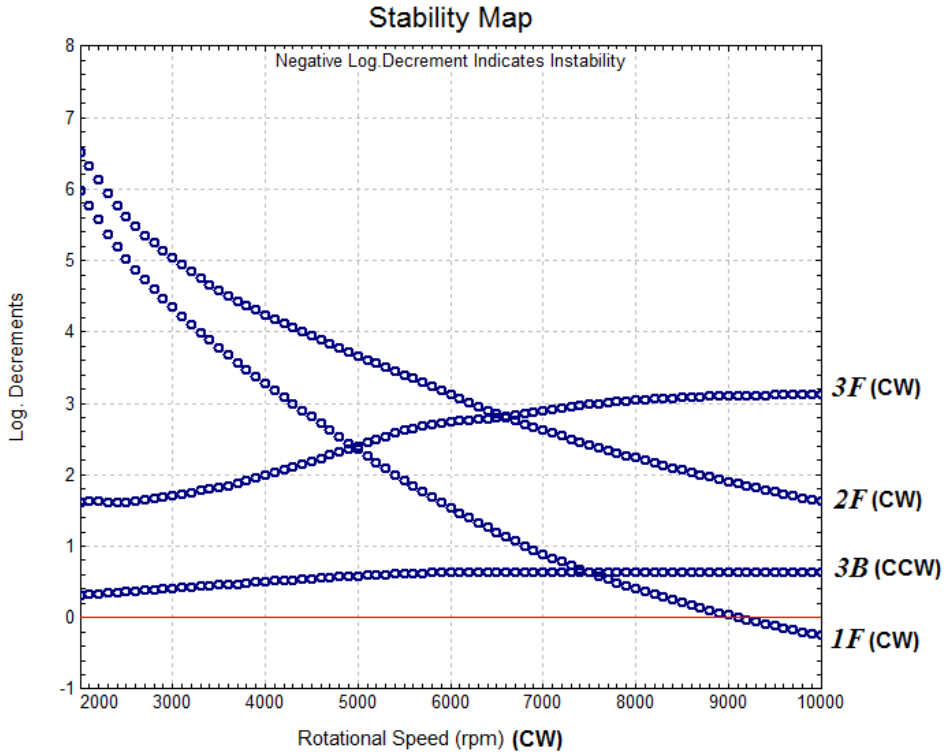

Figure 2-18 Stability map with CORRECT bearing data

The steady state unbalance response in Bode plot is identical to the correct result shown in Figure 2-7, and not shown here. The response orbit at bearing station at 5000 rpm and viewed from both +z and –Z directions, are shown in Figure 2-19. It shows that the results are identical to previous results if viewed from the correct direction. This example illustrates the importance of the shaft direction in the bearing coefficient calculation. In the rotordynamic study, the rotor rotation must be consistent with the bearing coefficients.

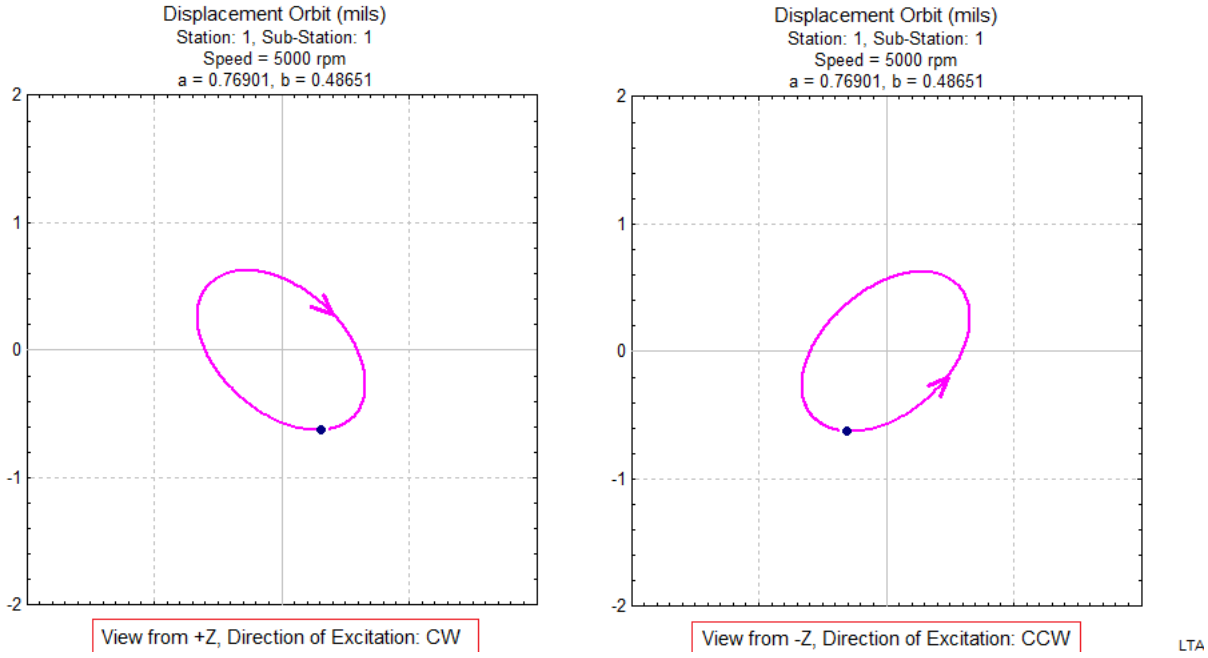

Figure 2-19 Bearing station response orbit with CORRECT bearing data

Example 3: 4 Stations Geared Model

A simple gear set with 4 finite element stations, as shown in Figure 3-1, is presented here as another example. The similar model was presented and analyzed in many publications, such as Iida et. al. (1980), Neriya et al (1985), and Kahraman et al (1992). A lumped model will be used here for illustration purposes. Station 1 is a motor which drives a gear set, and the gear set drives a load unit. In the previous publications, "pinion" and "gear" are used to describe station 2 and station 3, respectively. And station 4 is the load unit. However, in industry it will be more common to call the mating gear with larger pitch radius the "gear" and the smaller pitch radius the "pinion" (Shigley and Mischke, 1989). With this industrial nomenclature, station 2 will be called the gear and station 3 is the pinion.

The purpose here is to illustrate the combined lateral and torsional vibration due to the gear mesh effect, particularly the effect on the influence of the lateral vibration. For lateral vibration, consider only the translational motions at stations 2 and 3 without any gyroscopic moments. For torsional vibration, there is one torsional motion for every station and a total of 4 degrees of freedom. So, there are a combined of 8 degrees of freedom in this system, 4 lateral motions (x_2, y_2, x_3, y_3) and 4 torsional motions $(\theta_{z1}, \theta_{z2}, \theta_{z3}, \theta_{z4})$. In this example, the lateral governing equations of motion in X and Y directions are decoupled, also the lateral motion in Y direction is coupled with the torsional motion. The relevant parameters are listed below:

For pure lateral vibration:

m_2 = 16.96 kg with a mass unbalance of U_2 = 0.0003 kg-m
m_3 = 5.65 kg with a mass unbalance of U_3 = 0.00028 kg-m
Both are supported by an isotropic bearing with a stiffness of 2.75 E07 N/m

For pure torsional vibration:

J_1 = 0.459 kg-m^2 with a torsional synchronous excitation of T_1 = 1 N-m
J_2 = 0.0628 kg-m^2
J_3 = 0.03 kg-m^2
J_4 = 0.549 kg-m^2
The torsional stiffness connects stations 1 and 2, stations 3 and 4 is 115 N-m/rad.

The gear data:

Gear mesh connects stations 2 and 3
Spur gear and second rotor located at right hand side of the first rotor
First rotor (motor-gear) rotates CCW and the second rotor (pinion-load) rotates CW
Pitch radius for the gear at station 2 is 0.1015 m (P_d=0.203 m)
Pitch radius for the pinion at station 3 is 0.0564 m (P_d=0.1128 m)
The speed ratio, $\Omega_2 = -1.79965\,\Omega_1 = n\,\Omega_1$, where n = -1.79965
Only the tangential gear contact stiffness is considered, K_m=2E08 N/m

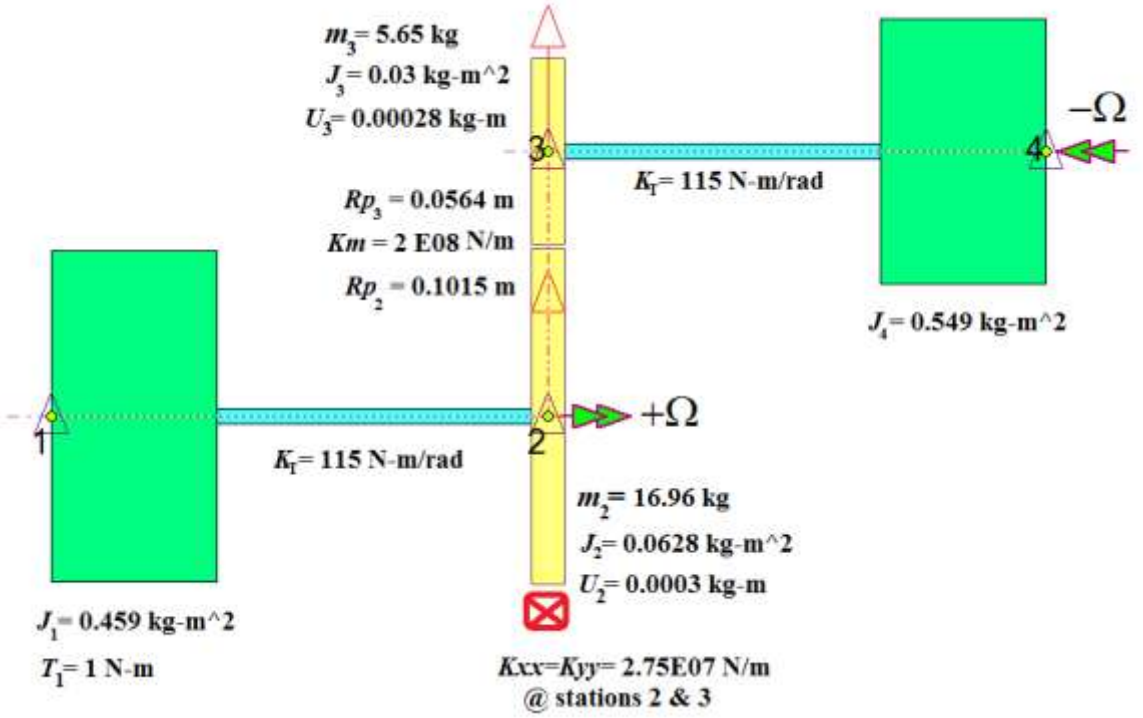

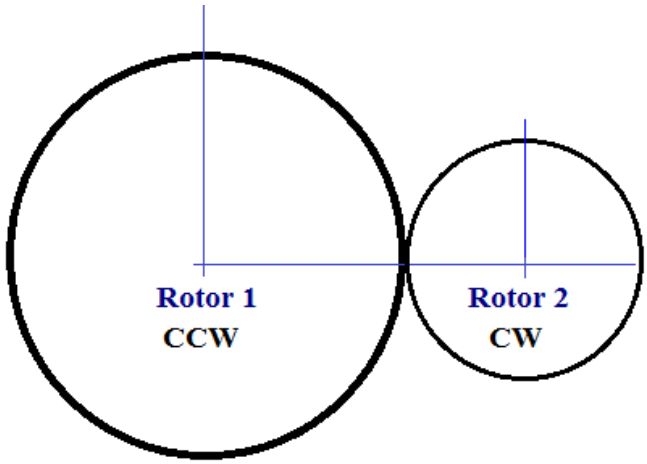

Figure 3-1 4-stations geared system

Gear mesh data is entered under the Torsional/Axial tab in the Data Editor option. In this example, the tangential stiffness is given and it is a spur gear, therefore there is no need to enter the pressure angle and helix angle. All other data can be entered just like doing the pure lateral and torsional analysis. When performing the Lateral-Torsional-Axial analysis option, one may select the types vibration be included in the analysis. In this example, Axial vibration is always be excluded, and torsional and lateral are included.

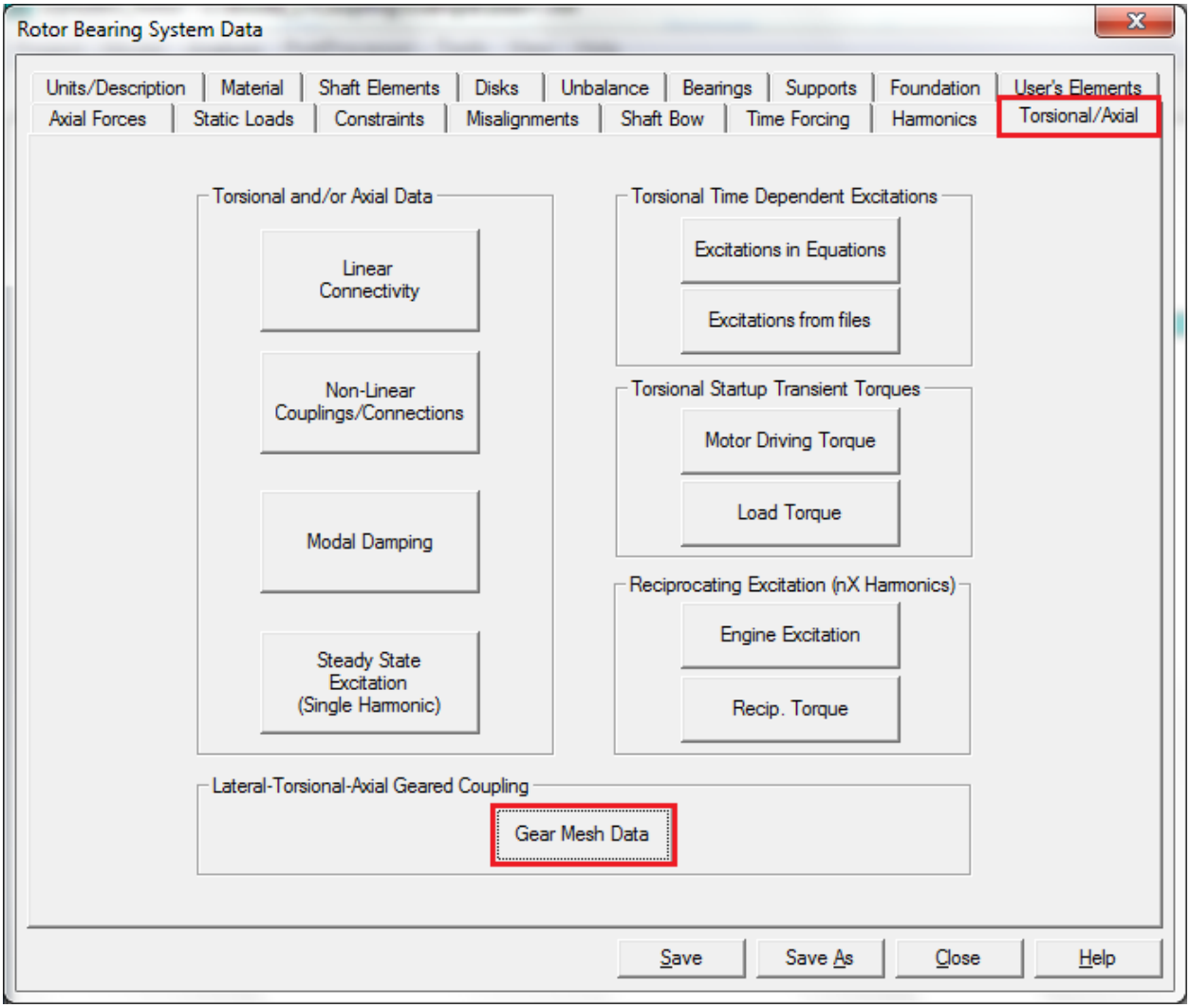
Rotor Bearing System Data
Units/Description
Material
Shaft Elements
Disks
Unbalance
Bearings
Supports
Foundation
User's Elements
Axial Forces
Static Loads
Constraints
Misalignments
Shaft Bow
Time Forcing
Harmonics
Torsional/Axial
Torsional and/or Axial Data
Linear Connectivity
Non-Linear Couplings/Connections
Modal Damping
Steady State Excitation (Single Harmonic)
Torsional Time Dependent Excitations
Excitations in Equations
Excitations from files
Torsional Startup Transient Torques
Motor Driving Torque
Load Torque
Reciprocating Excitation (nX Harmonics)
Engine Excitation
Recip. Torque
Lateral-Torsional-Axial Geared Coupling
Gear Mesh Data
Save
Save As
Close
Help

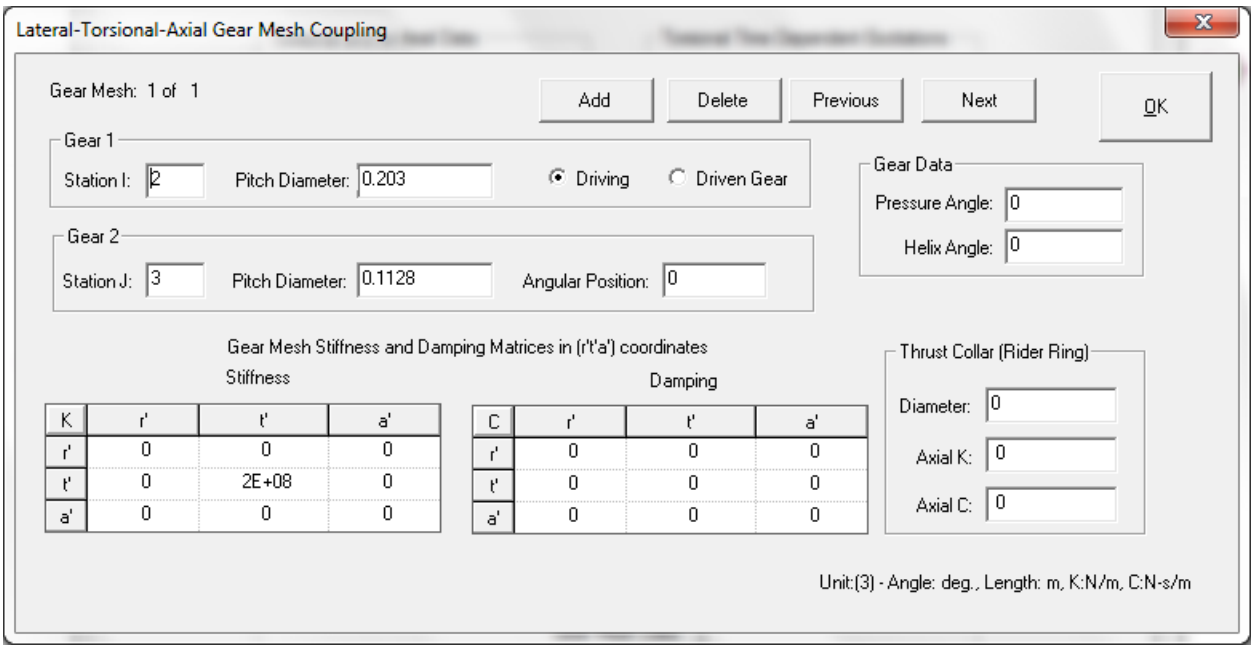
Lateral-Torsional-Axial Gear Mesh Coupling
Gear Mesh: 1 of 1
Add
Delete
Previous
Next
OK
Gear 1
Station I: 2
Pitch Diameter: 0.203
Driving
Driven Gear
Gear Data
Pressure Angle: 0
Helix Angle: 0
Gear 2
Station J: 3
Pitch Diameter: 0.1128
Angular Position: 0
Gear Mesh Stiffness and Damping Matrices in (r't'a') coordinates
Stiffness
K r' t' a'
r' 0 0 0
t' 0 2E+08 0
a' 0 0 0
Damping
C r' t' a'
r' 0 0 0
t' 0 0 0
a' 0 0 0
Thrust Collar (Rider Ring)
Diameter: 0
Axial K: 0
Axial C: 0
Unit:(3) - Angle: deg., Length: m, K:N/m, C:N-s/m

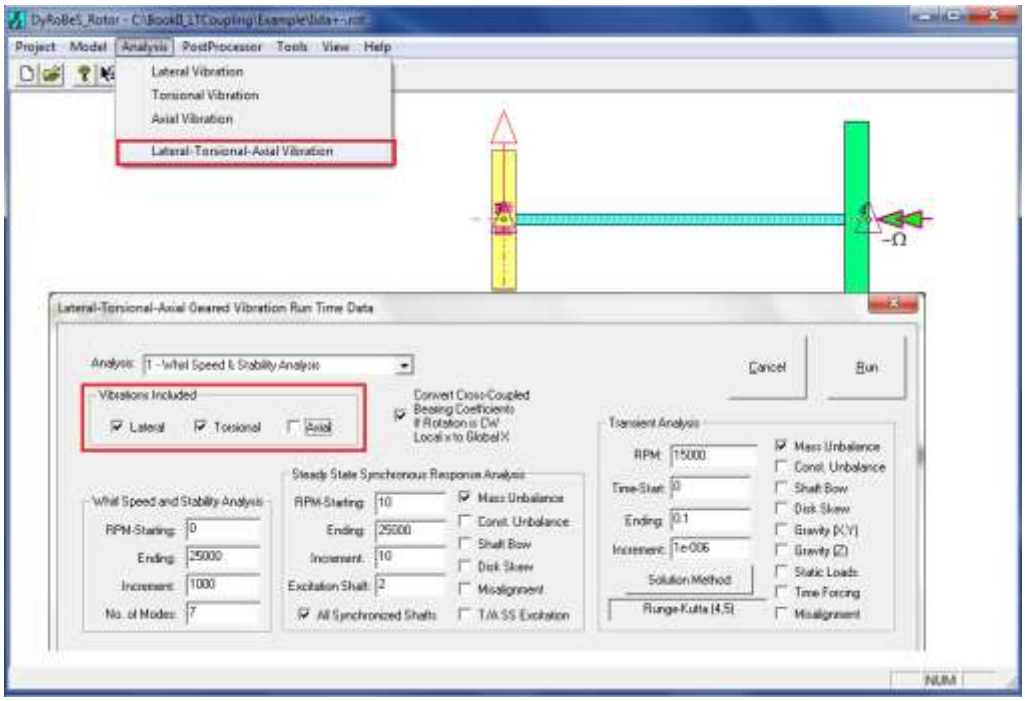

Both the free and forced vibrations are studied. For free vibration (natural frequency analysis), four cases are included.

1. The first case is the conventional purely torsional analysis with a rigid link in the gear mesh ($K_m = \infty$). With this rigid link between stations 2 and 3, the original 4 DOF torsional model has been reduced and become a 3 DOF torsional model. There are 3 natural frequencies are calculated: 0, 148, and 546 rpm. The zero natural frequency corresponds to the rigid body motion due to unconstrained torsional motion.

2. The second case is the torsional analysis with the flexible gear mesh (K_m=2E08 N/m). There are 4 natural frequencies: 0, 148, 546, and 70185 rpm. The 4th natural frequency is introduced by the flexibility of the gear mesh and this frequency value is extremely high. The 2nd and 3rd frequencies are essentially the same as the originally rigidly linked case. It is typically true that the torsional stiffness due to the gear mesh is much higher than the shaft torsional stiffness, and a rigid link can be reasonably assumed for the torsional analysis.

3. The third case is the purely lateral vibration. Since the bearings are isotropic and there are 2 natural frequencies for each rotor, one for each direction. The natural frequencies for rotors 1 and 2 can be easily determined by the following frequency equation: $\omega = \sqrt{\frac{k}{m}}$

   a. Rotor 1: $\omega_x = \omega_y = \sqrt{\frac{2.75E07}{16.96}} = 1273$ rad/sec = 12160 rpm

   b. Rotor 2: $\omega_x = \omega_y = \sqrt{\frac{2.75E07}{5.65}} = 2206$ rad/sec = 21068 rpm

4. The fourth case is the combination of the lateral and torsional vibration with the gear mesh effect. Once the gear mesh is included, the system is no longer an isotropic system. Asymmetry property is introduced by the gear mesh stiffness.

The results are summarized below:

	Purely Torsional ($K_m = \infty$)	Purely Torsional (K_m=2E08 N/m)	Purely Lateral	Combined Torsional & Lateral	Comments
Mode 0	0	0		0	Torsional Rigid Body
Mode 1	148	148		148	Torsional + weak *y*
Mode 2	546	546		546	Torsional + weak *y*
Mode 3			12160	10703	Lateral y_2 + Torsional
Mode 4			12160	12160	Lateral x_2
Mode 5			21068	17327	Lateral y_3 + Torsional
Mode 6			21068	21068	Lateral x_3
Mode 7		70185		96985	Torsional + Lateral *y*

The eigenvectors (modal displacements) for the vibratory modes are arranged in the following order, $\left(x_2, y_2, x_3, y_3, \theta_{z1}, \theta_{z2}, \theta_{z3}, \theta_{z4}\right)$, with translation motion first and then the torsional motion. However, for clarity and easy interpretation, the torsional displacements in rotor 2 are commonly converted into the equivalent displacements with the speed ratio. That is the torsional displacements $\left(\theta_{z3}, \theta_{z4}\right)$ will be expressed as $\left(\frac{\theta_{z3}}{n}, \frac{\theta_{z4}}{n}\right)$, where n = -1.79965. The modal displacements are summarized in the following table and shown in the Figure 3-2.

Displ.	Mode 1 148 rpm	Mode 2 546 rpm	Mode 3 10703 rpm	Mode 4 12160 rpm	Mode 5 17327 rpm	Mode 6 21068 rpm	Mode 7 96985 rpm
x_2	0	0	0	1	0	0	0
y_2	-4.0E-05	1.6E-05	-0.108	0	0.0617	0	0.0319
x_3	0	0	0	0	0	1	0
y_3	4.0E-05	-1.6E-05	0.033	0	0.197	0	0.0988
θ_{z1}	1	0.0462	-0.0002	0	-6.5E-05	0	-2.1E-06
θ_{z2}	0.0397	-0.5560	0.8580	0	0.8590	0	0.8600
θ_{z3}/n	0.0389	-0.5557	-0.5557	0	-0.5557	0	-0.5557
θ_{z4}/n	-0.2617	0.0381	0.0001	0	0.0000	0	1.1E-06
θ_{z3}	-0.0700	1	1	0	1	0	1
θ_{z4}	0.4710	-0.0685	-0.0002	0	-0.0001	0	-2.0E-06

Mode No.= 1 : Rotor: 1 STRAIGHT LINE Motion: Rotor: 2 STRAIGHT LINE Motion
Shaft Rotational Speeds = 0, -0 rpm
Whirl Speed (Damped Natural Freq.) = 148 rpm, Log. Decrement = -0.0000

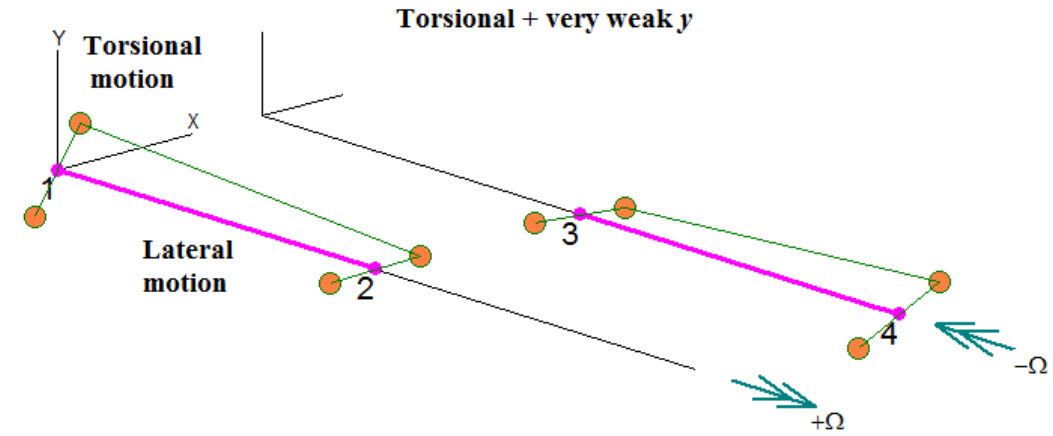

Mode No.= 2 : Rotor: 1 STRAIGHT LINE Motion: Rotor: 2 STRAIGHT LINE Motion
Shaft Rotational Speeds = 0, -0 rpm
Whirl Speed (Damped Natural Freq.) = 546 rpm, Log. Decrement = -0.0000

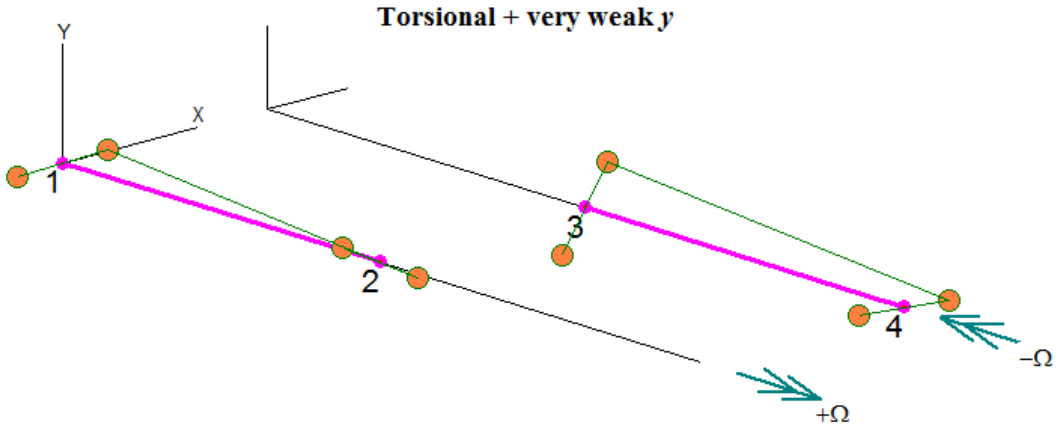

Mode No.= 3 : Rotor: 1 STRAIGHT LINE Motion: Rotor: 2 STRAIGHT LINE Motion
Shaft Rotational Speeds = 0, -0 rpm
Whirl Speed (Damped Natural Freq.) = 10703 rpm, Log. Decrement = -0.0000

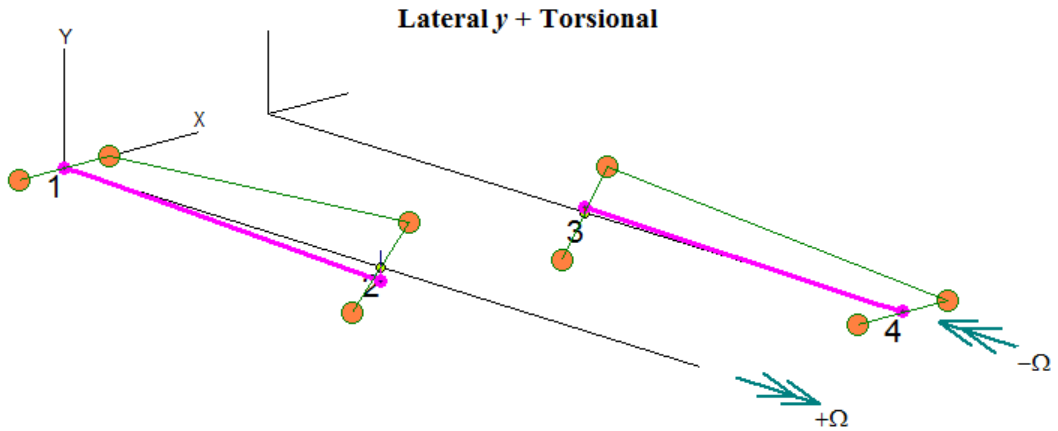

Mode No.= 4 : Rotor: 1 STRAIGHT LINE Motion: Rotor: 2 NO Precession
Shaft Rotational Speeds = 0, -0 rpm
Whirl Speed (Damped Natural Freq.) = 12160 rpm, Log. Decrement = -0.0000

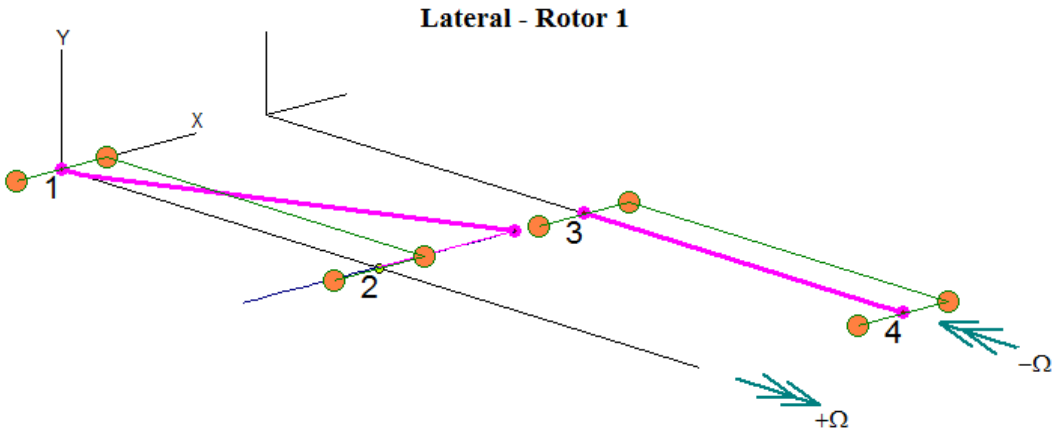

Mode No.= 5 : Rotor: 1 STRAIGHT LINE Motion: Rotor: 2 STRAIGHT LINE Motion
Shaft Rotational Speeds = 0, -0 rpm
Whirl Speed (Damped Natural Freq.) = 17327 rpm, Log. Decrement = -0.0000

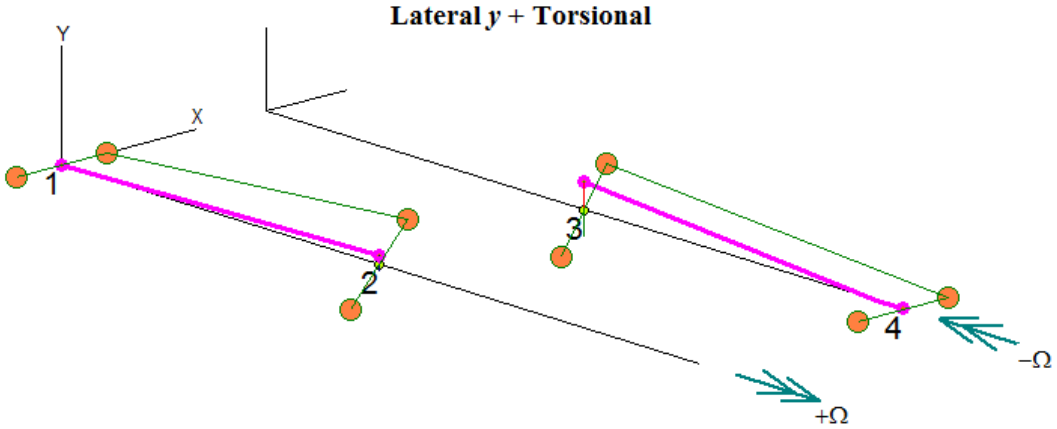

Mode No.= 6 : Rotor: 1 NO Precession: Rotor: 2 STRAIGHT LINE Motion
Shaft Rotational Speeds = 0, -0 rpm
Whirl Speed (Damped Natural Freq.) = 21068 rpm, Log. Decrement = -0.0000

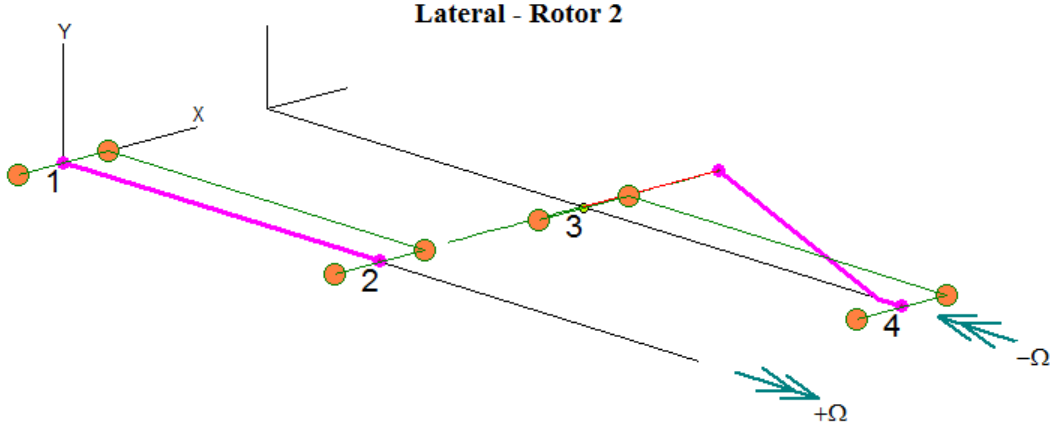

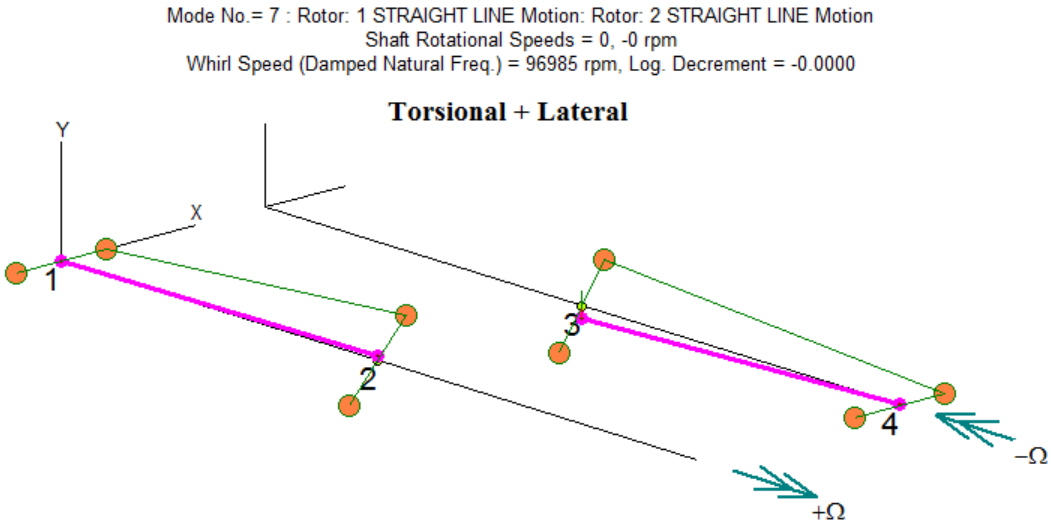

Figure 3-2 Mode shapes

It shows that mode 1 and mode 2 are primary torsional motions, there is extremely small relative torsional motion occurs at station 2 and 3 $\left(\theta_{z2}, \theta_{z3}/n\right)$ which causes insignificant movements at *y* direction for stations 2 and 3. The frequencies are basically the same as the purely torsional analysis without the lateral vibration. Again, in this example, only the lateral motion in Y direction is coupled with the torsional motion and lateral motion in X direction is decoupled from other motions.

The mode 3 shows the strong coupling between the torsional motion and the lateral motion of rotor 1 and again only in the y direction. Mode 5 shows the strong coupling between the torsional motion and the lateral motion of rotor 2 and also only in the y direction. Due to the large relative movement at the gear contact point, it acts like a flexible support underneath the bearings, so the frequencies are lower than those obtained from the pure lateral motion.

Modes 4 and 6 are the purely lateral motion at the X direction for the rotor 1 and rotor 2 and the frequencies are the same as the pure lateral vibration. Mode 7 is the torsional motion coupled with the weak lateral motion and it raises the frequency from the purely torsional motion.

Since there is no gyroscopic effect present and the bearings are isotropic, the system natural frequencies do not vary with the rotor speed. Figure 3 shows the whirl speed map with both rotor speeds are labeled in the X-axis. Each mode can be excited by the synchronous excitations. The critical speeds for the first 6 modes below 25000 rpm of rotor 1 speed are summarized in table 2.

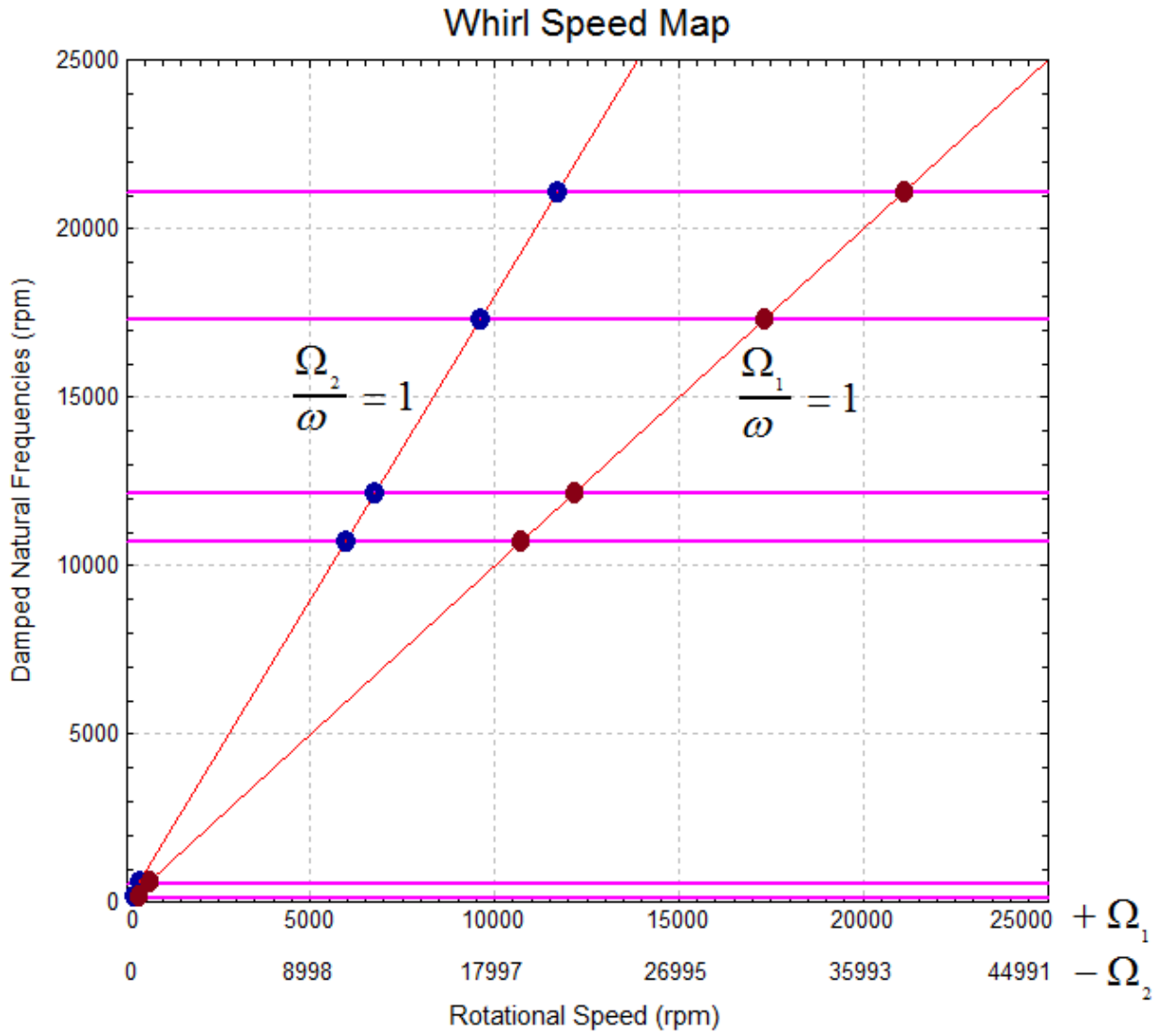

Figure 3-3 Whirl speed map

Mode	Critical speeds due to rotor 1 synchronous excitation		Critical speeds due to rotor 2 synchronous excitation	
(rpm)	Rotor 1 speed, Ω_1	Rotor 2 speed, Ω_2	Rotor 1 speed, Ω_1	Rotor 2 speed, Ω_2
148	148	$\Omega_2 = 1.79965\ \Omega_1$	$\Omega_1 = \Omega_2 / 1.79965$	148
546	546	$\Omega_2 = 1.79965\ \Omega_1$	$\Omega_1 = \Omega_2 / 1.79965$	546
10,703	10,703	$\Omega_2 = 1.79965\ \Omega_1$	$\Omega_1 = \Omega_2 / 1.79965$	10,703
10	12,160	$\Omega_2 = 1.79965\ \Omega_1$	$\Omega_1 = \Omega_2 / 1.79965$	12,160
17,327	17,327	$\Omega_2 = 1.79965\ \Omega_1$	$\Omega_1 = \Omega_2 / 1.79965$	17,327
21,068	21,068	$\Omega_2 = 1.79965\ \Omega_1$	$\Omega_1 = \Omega_2 / 1.79965$	21,068

Now, let us investigate the steady state synchronous response due to rotor 1 unbalance, rotor 2 unbalance, and motor torsional excitation. The objective here is to study the dynamic characteristics of the system due to various excitations, and not focus on the exact response amplitude since no damping is introduced in this system. The steady state response was analyzed from 10 rpm to 25,000 rpm with an increment of 10 rpm.

Case 1: Motor synchronous excitation, T_1=1 N-m

With the torsional synchronous excitation at the motor (station 1), Figures 3-4 and 3-5 show the lateral response at stations 2 (rotor 1) and 3 (rotor 2). As expected, the peaks were observed for modes 1, 2, 3, and 5 with *Y* displacements only. There is no response for the *X* displacement since the lateral-torsional coupling occurs in the *Y* displacement only in this rotor arrangement. The responses are straight line motions. Modes 4 and 6 are the pure lateral vibration modes in the X direction which are not excited by the torsional excitation. Figures 3-6 and 3-7 show the torsional displacements at stations 2 and 3 and again only the modes 1, 2, 3, and 5 are excited. Figure 3-8 shows the gear dynamic force due to this torsional excitation.

It is noted that although the bearings are isotropic, however the lateral orbits at stations 2 and 3 are straight line motion due to torsional effect and not circular as observed in lateral vibration analysis only, which implies that with this torsional vibration coupling, the system is no longer isotropic.

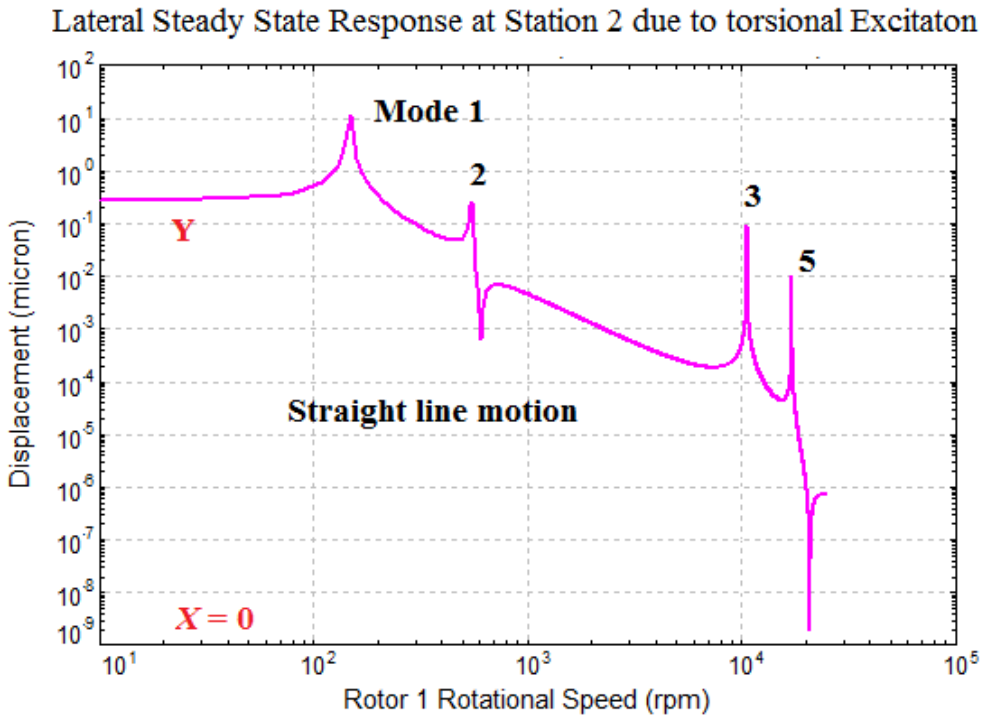

Figure 3-4 Lateral steady state response at station 2 due to torsional excitation at station 1

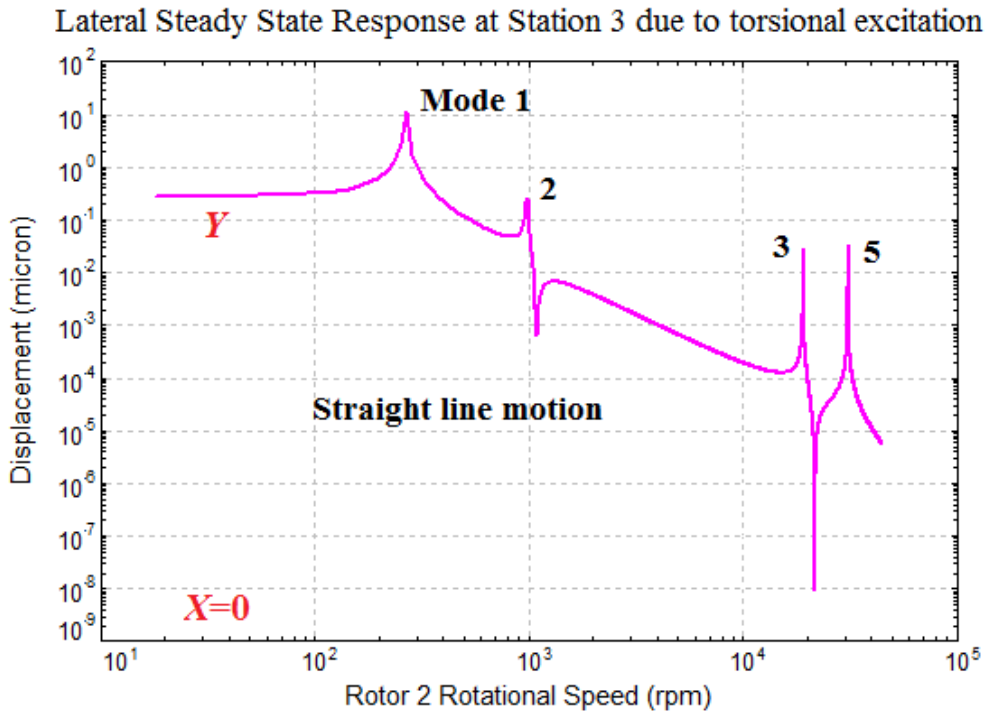

Figure 3-5 Lateral steady state response at station 3 due to torsional excitation at station 1

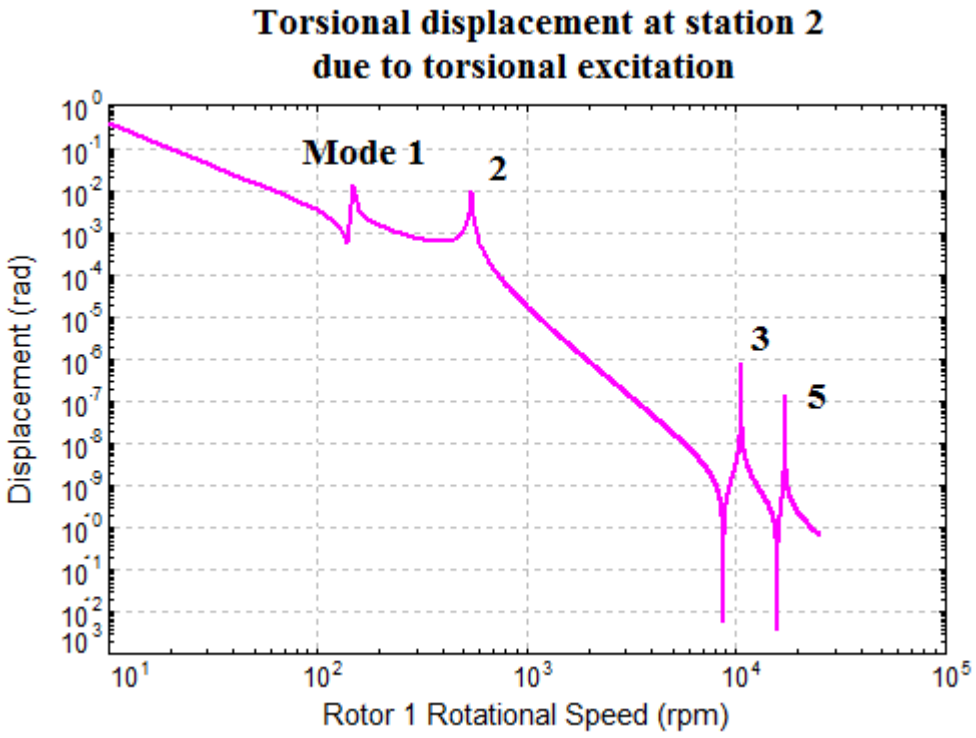

Figure 3-6 Torsional response at station 2 due to torsional excitation at station 1

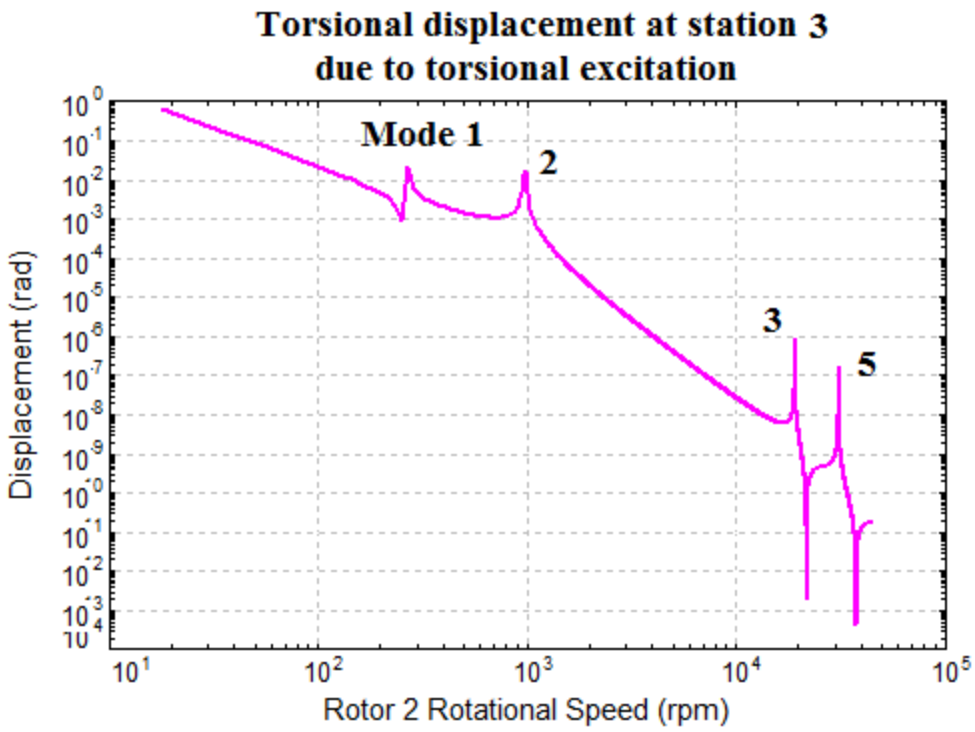

Figure 3-7 Torsional response at station 3 due to torsional excitation at station 1

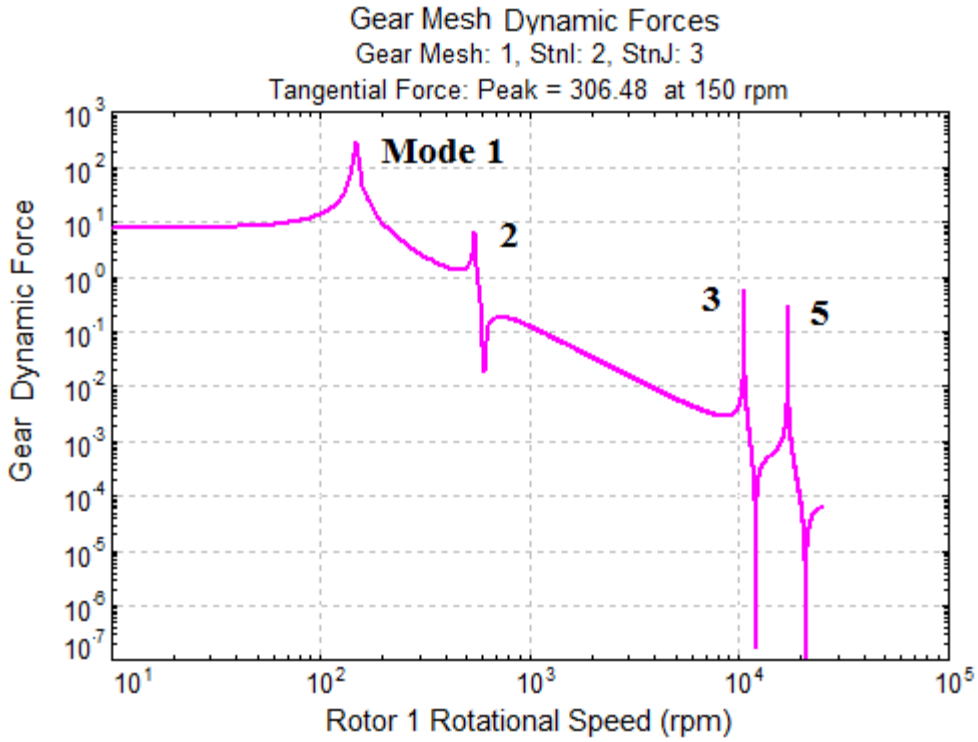

Figure 3-8 Gear dynamic force due to torsional excitation at station 1

Case 2: Rotor 1 mass unbalance excitation, U_2 = 0.0003 kg-m

Figure 3-9 shows the lateral steady state response at station 2 due to rotor 1 unbalance. It shows that there is only one peak in the X direction at mode 4 critical speed and two peaks in the Y direction occurring at modes 3 and 5 critical speeds. These results are consistent with the observation from the modal displacements (mode shapes). Again, the system is no longer isotropic due to the coupled lateral and torsional motions and the orbits are highly elliptical near critical speeds for station 2. Figure 3-10 shows the lateral steady state response at station 3 due to rotor 1 unbalance. It shows that there are 2 peaks in the Y direction due to resonances at modes 3 and 5. However there is no motion in the X direction. As explained before, the motion in the X direction is not coupled with the torsional motion. The motion at station 3 due to rotor 1 unbalance is a straight line motions along the Y axis.

Figure 3-11 is the torsional response at station 2 due to rotor 1 unbalance. Figure 3-12 is the gear dynamic force due to rotor 1 unbalance. Both figures show that the lateral and torsional motions are strongly coupled for modes 3 and 5.

Further examine the station 2 lateral response orbits at various rotor speeds, as shown in Figure 3-13. At low speed, the orbit is near circular and forward precession which indicates that the torsional influence is insignificant. As speed increases, the orbit becomes more elliptical and the major axis is aligned with the Y axis. At mode 3 resonance, the motion becomes a straight line. After resonance, the orbit becomes backward precession and the major axis gradually turns to be in-line with the X-axis. After the mode 4 resonance, the orbit becomes forward precession again.

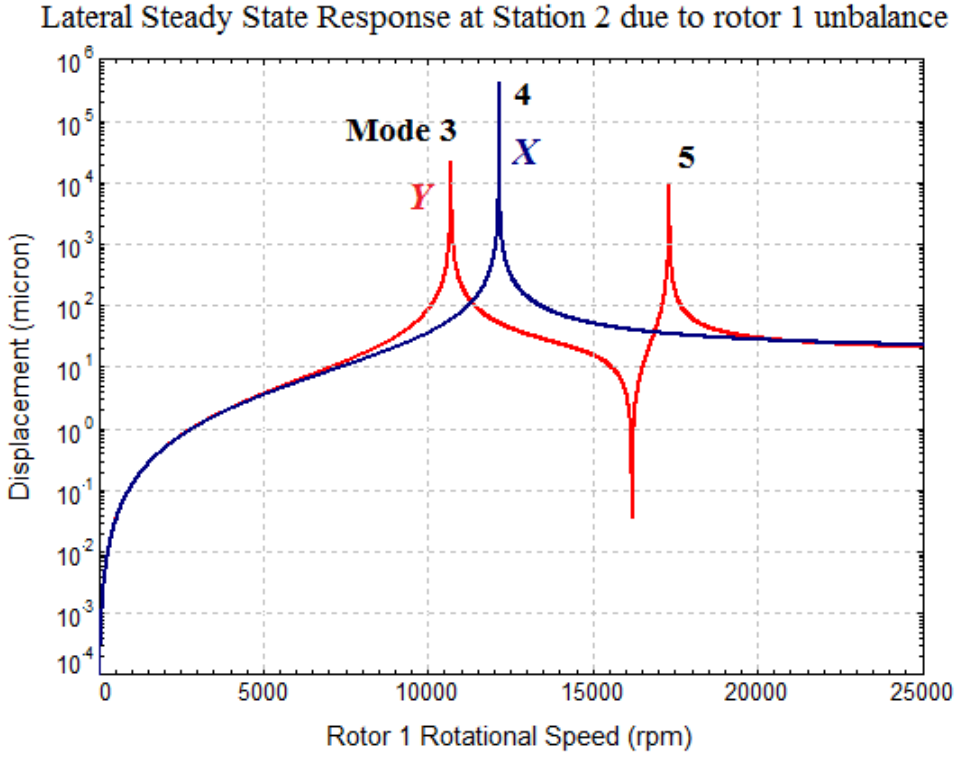

Figure 3-9 Lateral steady state response at station 2 due to rotor 1 unbalance

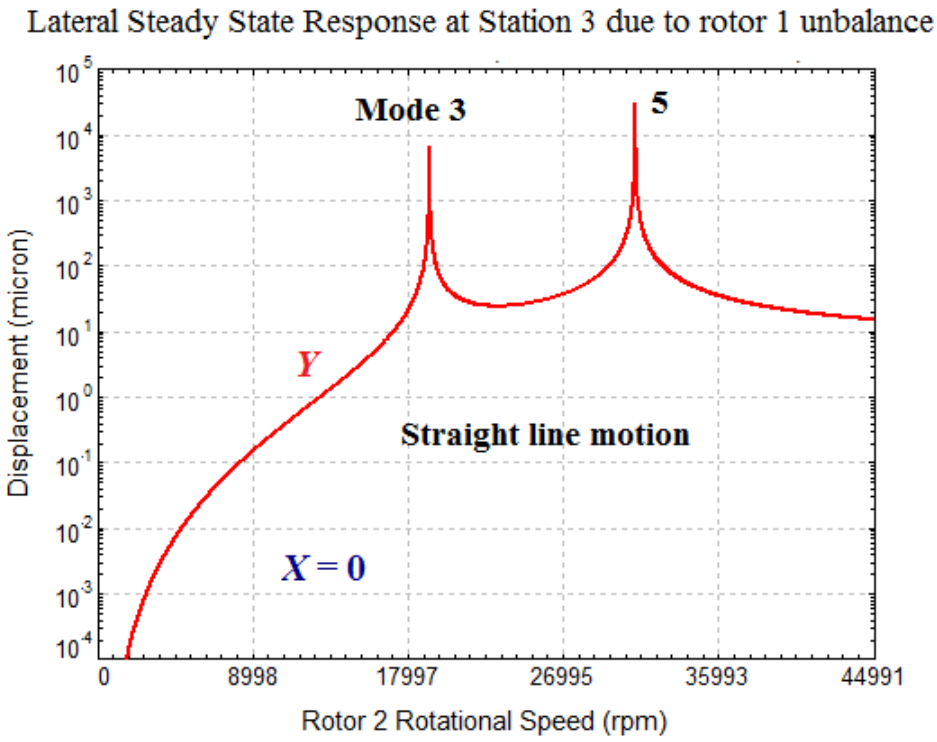

Figure 3-10 Lateral steady state response at station 3 due to rotor 1 unbalance

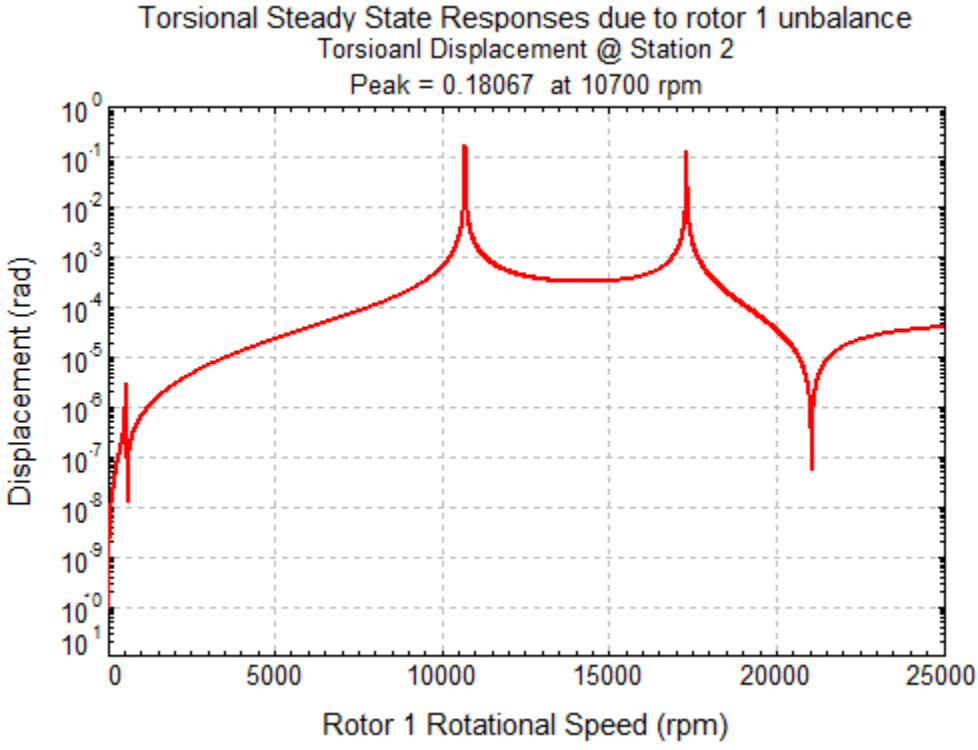

Figure 3-11 Torsional response at station 2 due to rotor 1 unbalance

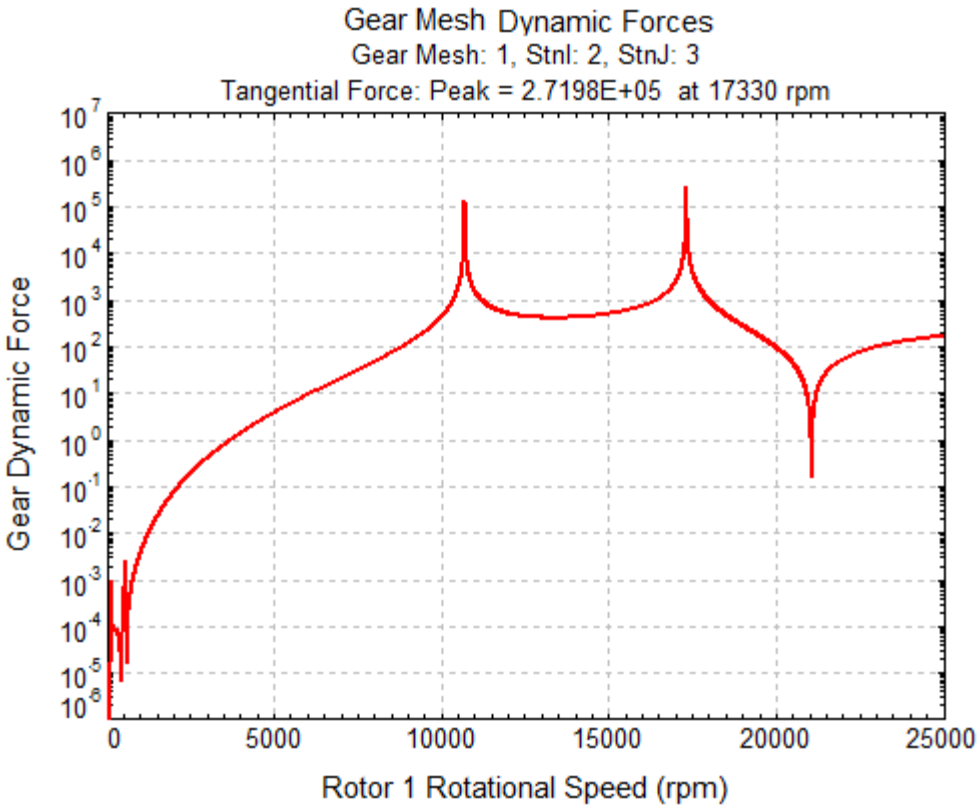

Figure 3-12 Gear dynamic force due to due to rotor 1 unbalance

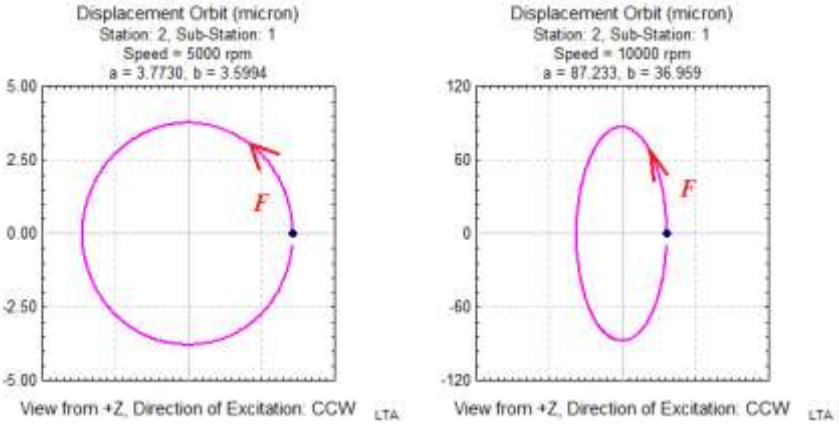

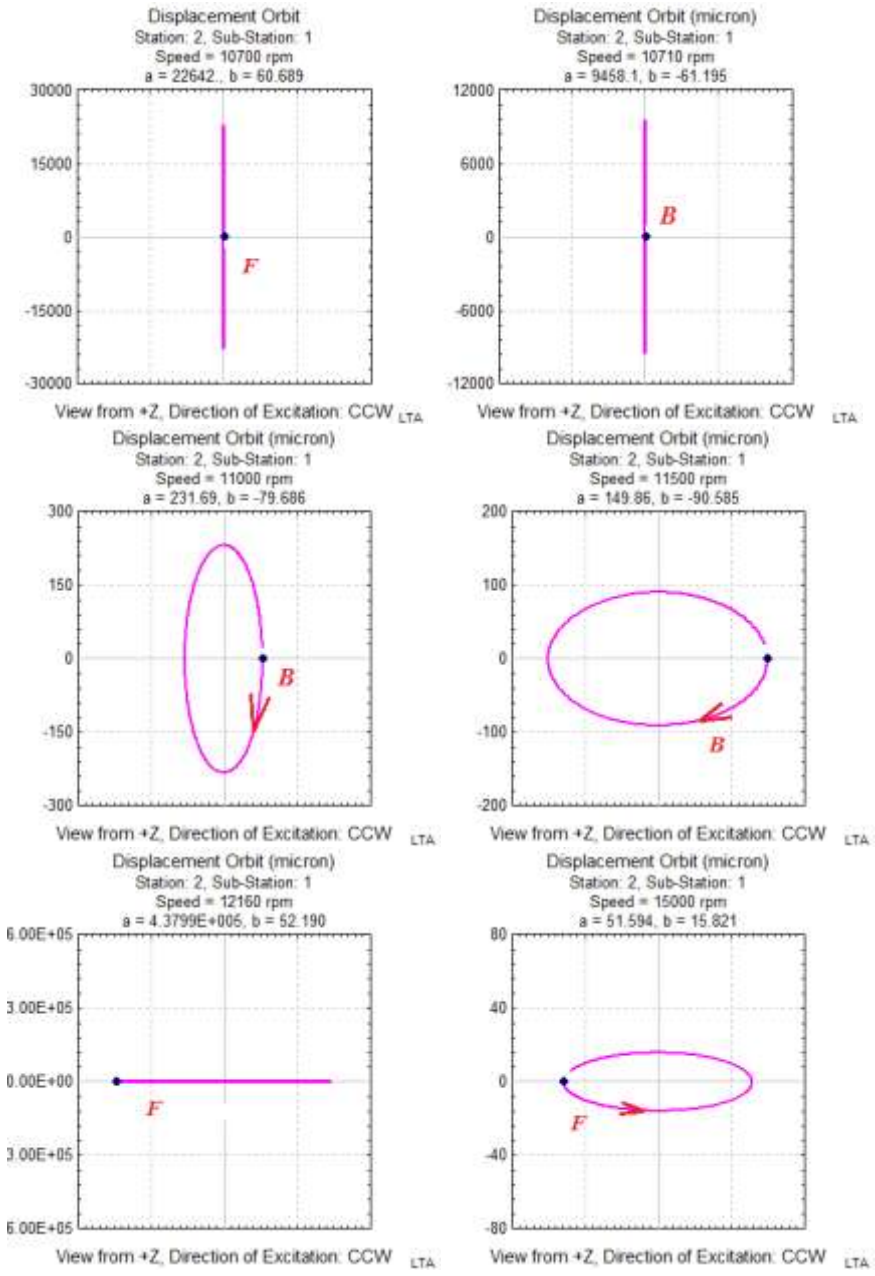

Figure 3-13 Lateral response orbits at station 2 for various rotor speeds due to rotor 1 unbalance

Case 3: Rotor 2 mass unbalance excitation, U_3 = 0.00028 kg-m

Now let us consider the steady state response due to rotor 2 mass unbalance at station 3 only. Figure 3-14 shows the lateral steady state response at station 2 (rotor 1) due to rotor 2 unbalance. It shows that the response at Y direction has two peaks due to modes 3 and 5 resonances, and the response at X direction is null. So, the response at station 2 is a straight line motion along the Y axis due to rotor 2 unbalance.

Figure 3-15 shows the lateral steady state response at station 3 (rotor 2) due to rotor 2 unbalance. It shows that the response at Y direction has two peaks due to modes 3 and 5 resonances, and the response at X direction has one peak due to mode 6 resonance. The discussions on this case are similar to the previous case. Again, there are backward whirl between mode 5 and 6 at station 3.

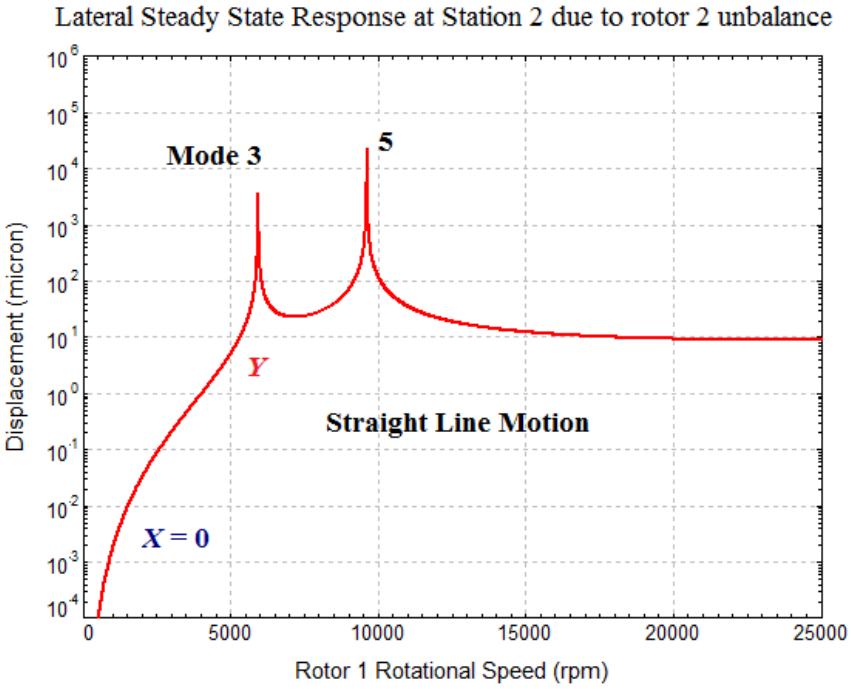

Figure 3-14 Lateral steady state response at station 2 due to rotor 2 unbalance

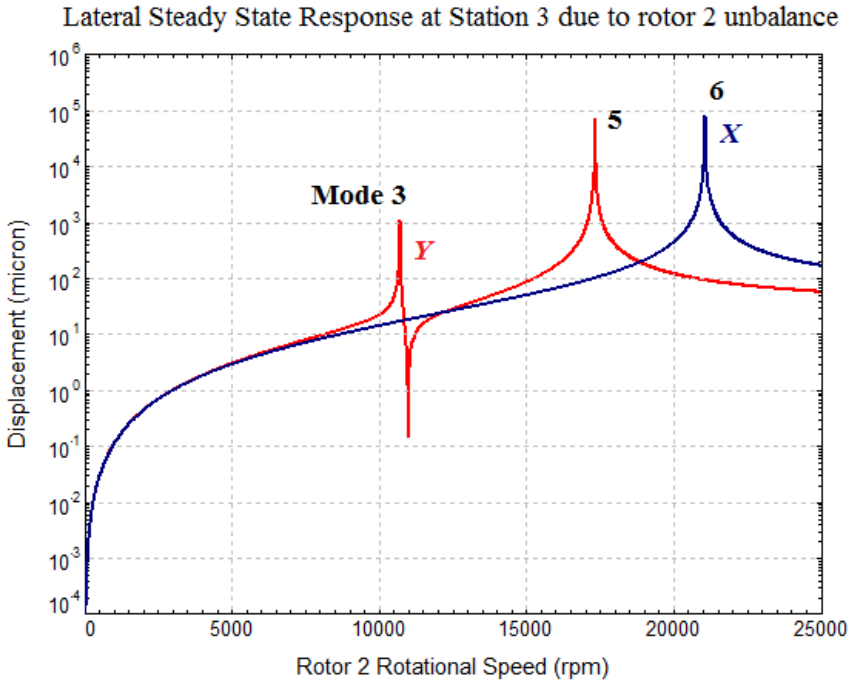

Figure 3-15 Lateral steady state response at station 3 due to rotor 2 unbalance

Case 4: Angular position of rotor 2 is not zero

Note that the above discussion is based on the rotor 2 is at zero angular position in the horizontal line from rotor 1, therefore the torsional motion couples the Y displacements only. Let us consider another scenario that is the rotor 2 is located at 45 degree with respect to rotor 1, as shown in Figure 3-16. Then, the torsional motion couples both X and Y directions. The values of the system natural frequencies are identical to the previous case, except the X and Y lateral motions are now both coupled with the torsional motion in modes 1, 2, 3, 5, and 7. Modes 4 and 6 are still purely lateral motions along the gear center line without torsional effect. Mode shapes for modes 4, 5 and 6 are shown in Figure 3-17.

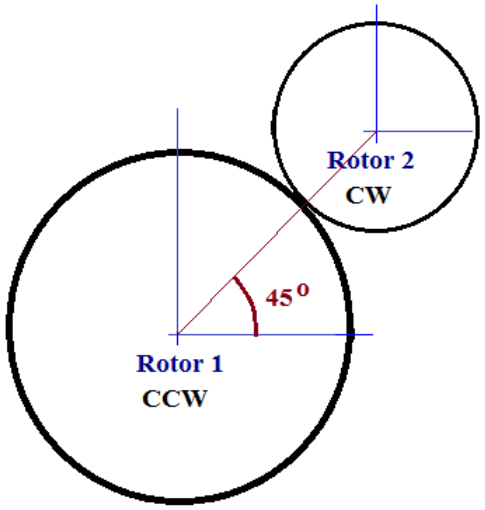

Figure 3-16 Rotor center line is not in the X-axis

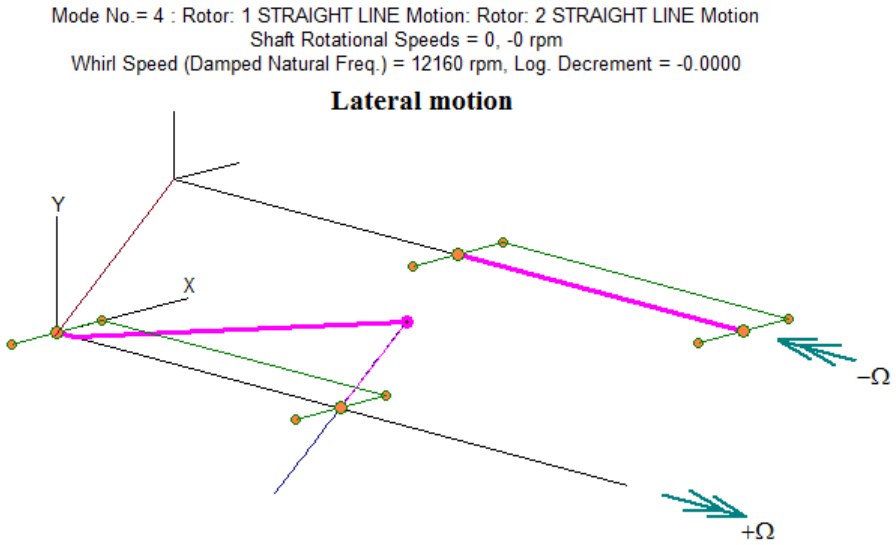

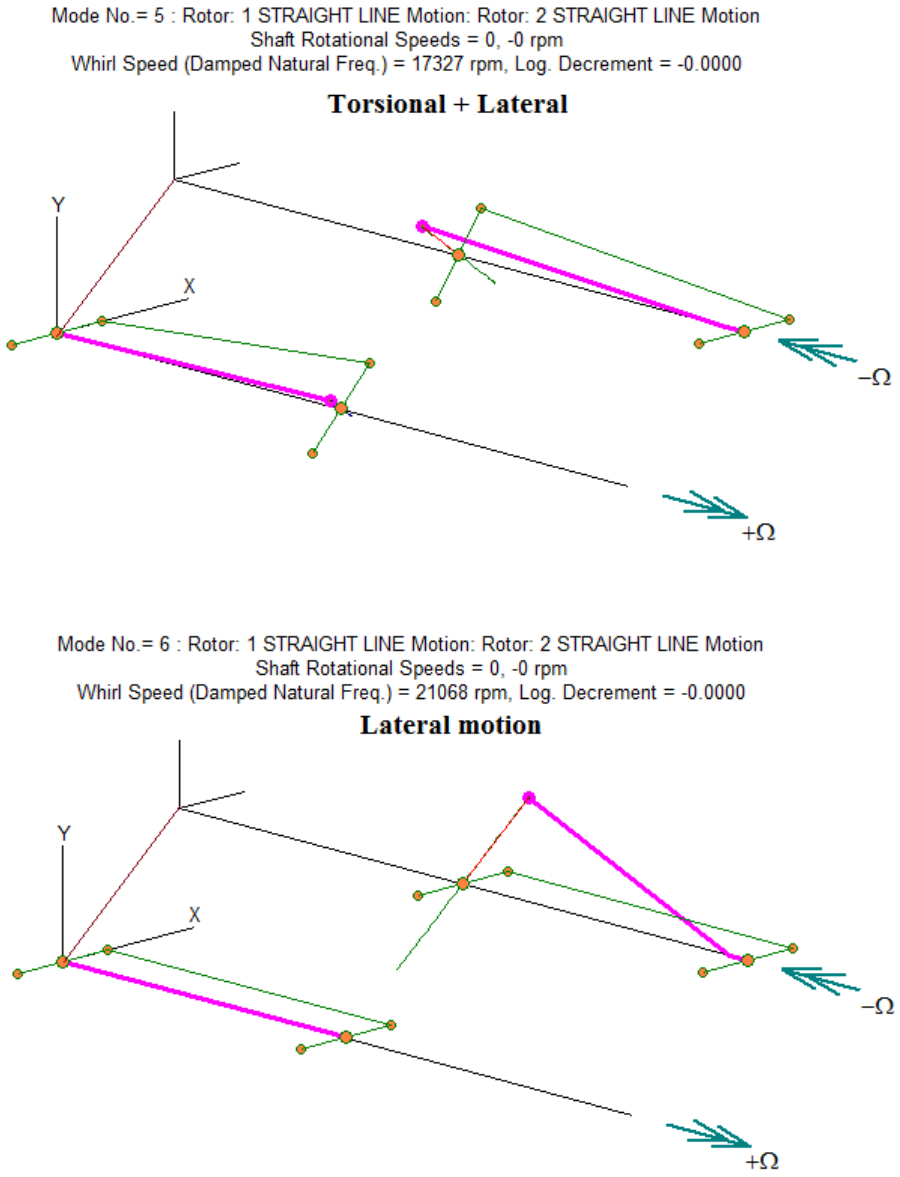

Figure 3-17 Mode shapes for modes 4, 5, and 6

Next let us consider the forced response. Figure 3-18 is the steady state response at station 2 due to the torsional excitation, same as case 1 discussed before. It shows that modes 1, 2, 3, 5 are excited by the torsional excitation and purely lateral modes 4 and 6 are decoupled from the torsional motion and not excited by the torsional excitation. The displacements in X and Y directions have the same amplitude but different phase. The lateral response orbit now is a straight line in 45 degree along the pressure line, as shown in Figure 3-19, not in Y direction as discussed in case 1.

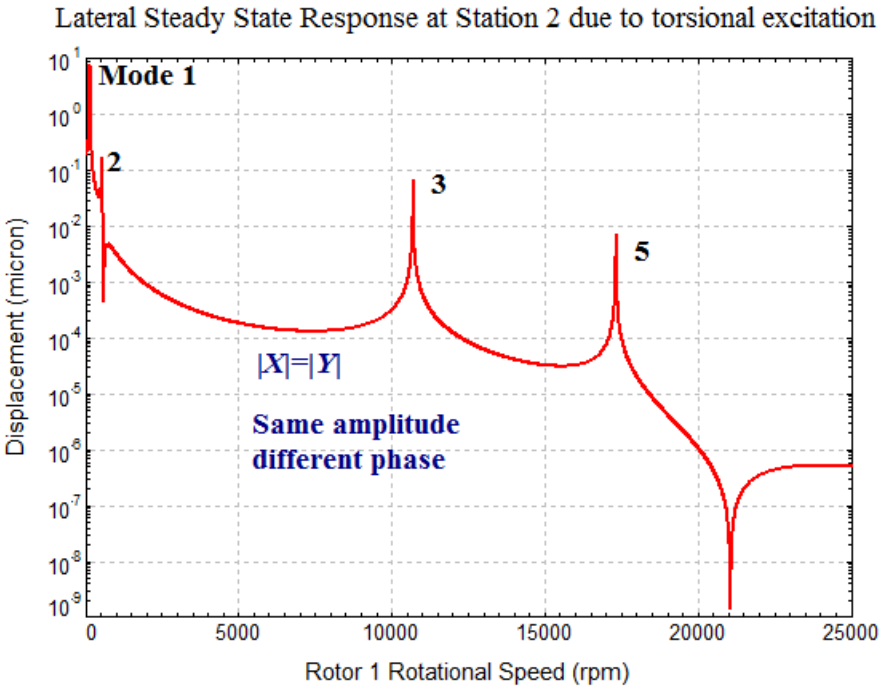

Figure 3-18 Lateral steady state response at station 2 due to torsional excitation at station 1

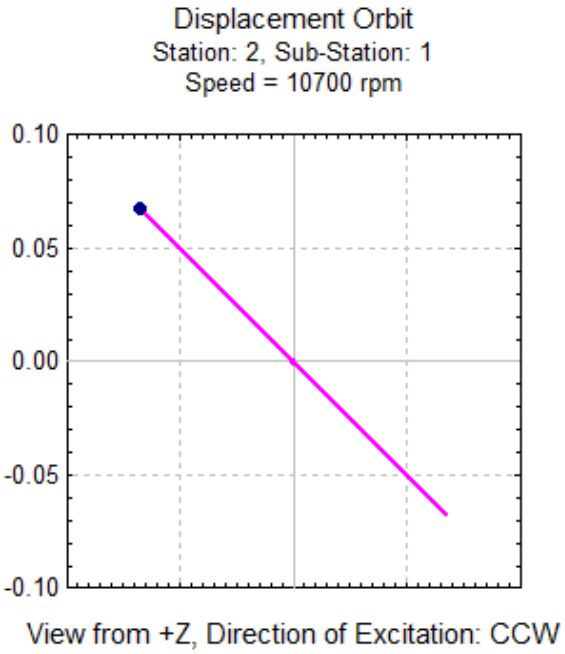

Figure 3-19 Lateral response orbit at station 2 due to torsional excitation at station 1

Figure 3-20 shows the lateral steady state response at station 2 due to rotor 1 unbalance. Again, modes 3, 4, and 5 were excited by rotor 1 unbalance and the amplitudes in X and Y directions are the same, but phases are different.

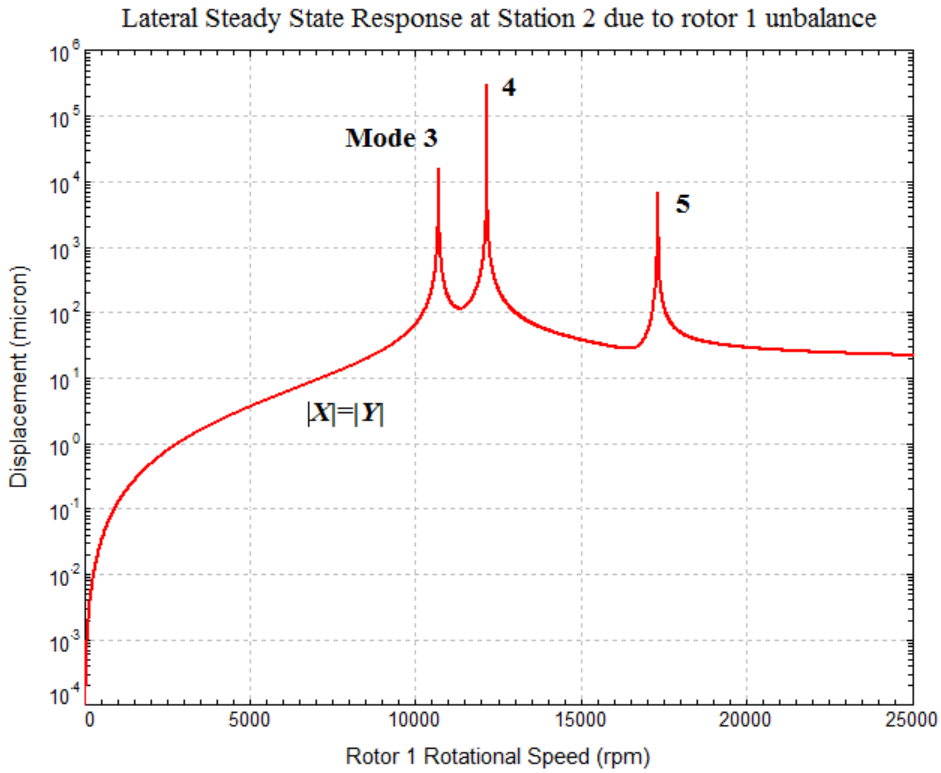

Figure 3-20 Lateral steady state response at station 2 due to rotor 1 unbalance

Figure 3-21 shows the lateral steady state response at station 3 due to rotor 1 unbalance. Modes 3 and 5 were excited by rotor 1 unbalance and the amplitudes in X and Y directions are the same, but phases are different. Mode 4 is a purely lateral motion at station 2, therefore, not shown at station 3 in Figure 3-21.

Again, although the bearings are isotropic, however, the orbits in general are not circular and backward whirl exists between critical speeds. Figure 3-22 shows the response orbits at station 2 due to rotor 1 unbalance in various speeds. Again, backward whirl occurs between 2 critical speeds.

It shows that the anisotropy of the support property is due to the effect of gear mating.

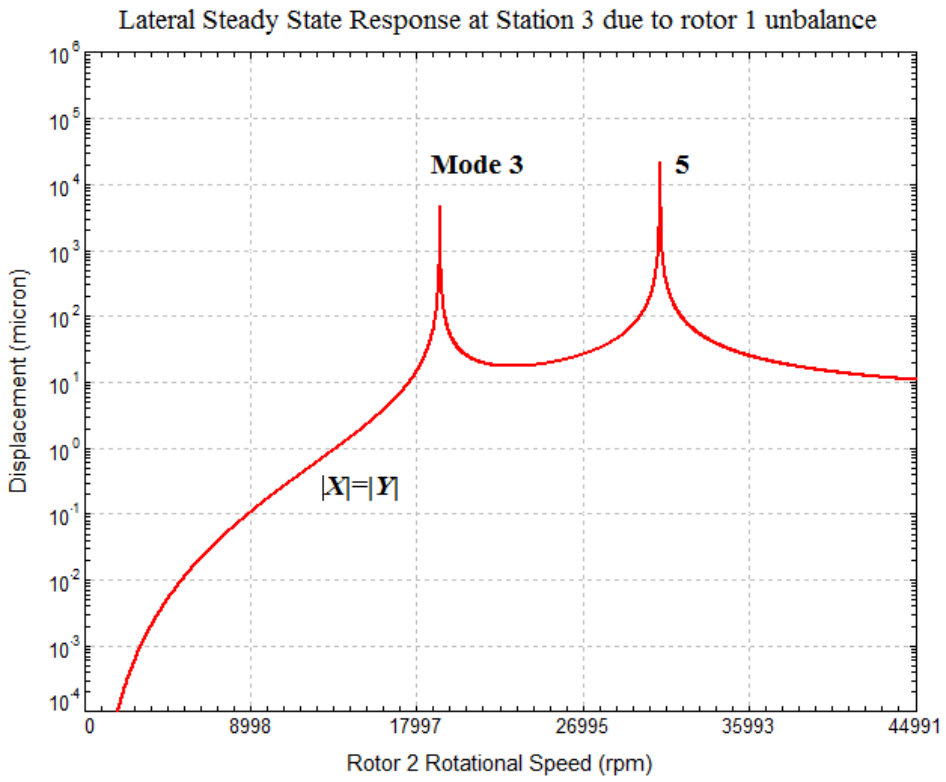

Figure 3-21 Lateral steady state response at station 3 due to rotor 1 unbalance

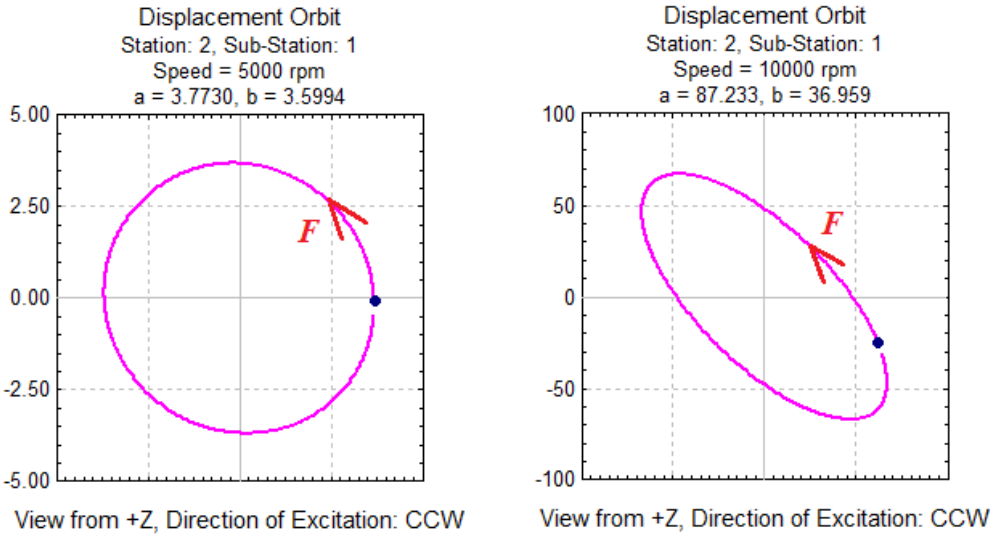

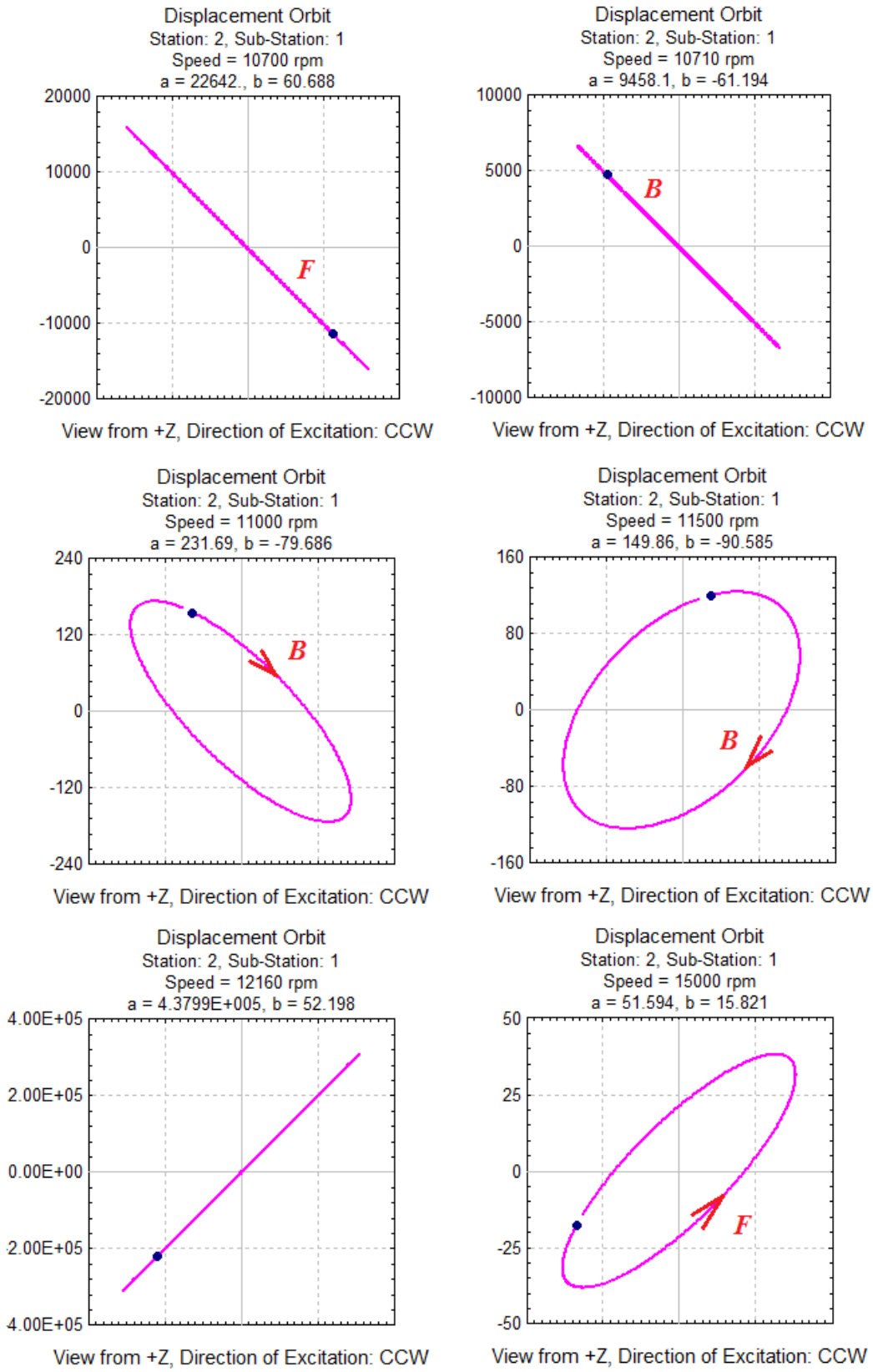

Figure 3-22 Lateral response orbits at station 2 for various speeds due to rotor 1 unbalance

Example 4: NASA test rig

A NASA test rig, shown in Figure 4-1, is used as a fourth example before we move on to an industrial application. This spur geared system has been presented in numerous publications (Kahraman, etal, 1990, 1992, Singh, et al, 1990). The natural frequencies at zero speed were presented in all the publications and compared here. For comparison purpose, the shaft shear deformation is neglected in the analysis. The 2 shafts have the same pitch radii (same speed). The relevant parameters are shown in the Figure 4-1. To draw the a bearing using a block, go to Project – Preferences Settings – Model Display Settings – Set Bearing Length = -1 or 0, then, adjust the Bearing Width.

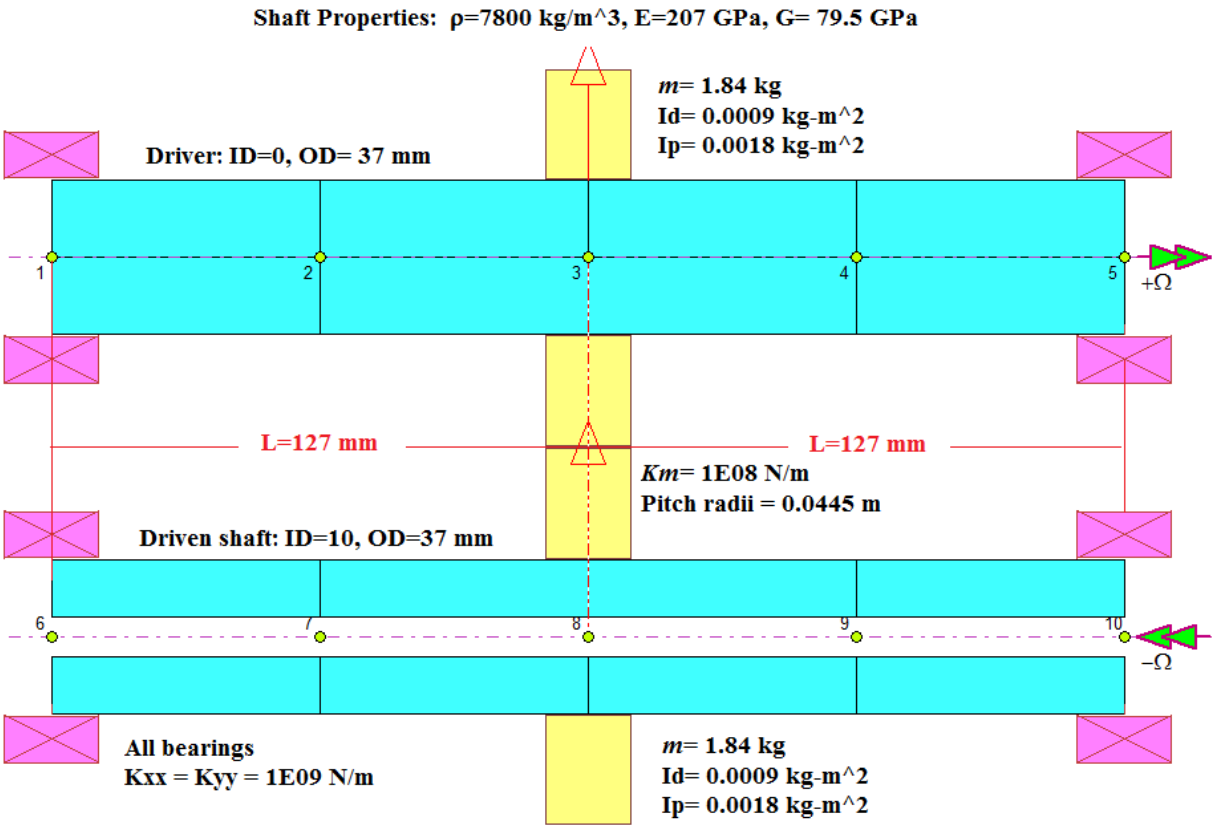

Figure 4-1 Two shafts system

To compare the results is an easy task and is not the only purpose here. The objective is to fully understand the dynamics of a multiple rotor system using the available knowledge. It is strongly recommended that each rotor should be analyzed before analyzing the entire system. At zero speed, the first 4 natural frequencies of rotor 1 (driving shaft) are: 687, 687, 3387, and 3387 Hz. The first 4 natural frequencies of rotor 2 (driven shaft) are: 695, 695, 3454, and 3454 Hz. These 8 natural frequencies can be obtained from analyzing each individual rotor or analyzing the entire rotor model with lateral vibration analysis without gear mesh effect.

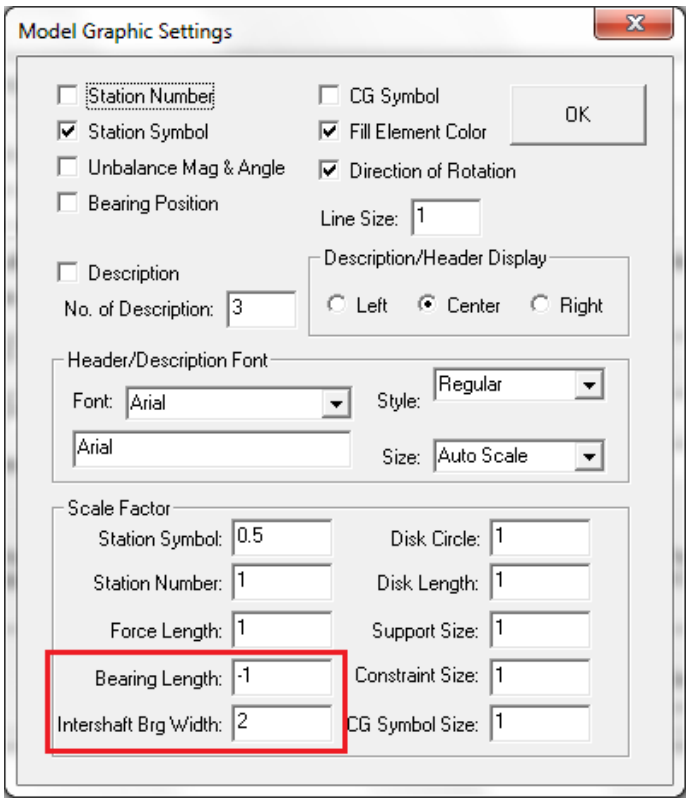

The mode shapes from analyzing the entire system without gear mesh are shown in Figure 4-2. As expected that the first pair natural frequencies are corresponding to the first bending mode in the X and Y directions, respectively. And the second pair natural frequencies are corresponding to the second bending mode in the X and Y directions, respectively. Noted that the gears (disks) are at the center of the shaft, therefore, the first two modes (the first bending mode) of each rotor are not affected by the disk gyroscopic effect due to zero slope at disk. The third and fourth modes (the second bending mode) of each rotor are strongly affected by the disk gyroscopic effect due to large slope at disk. Further, the gears (disks) are at the nodal point for the second bending modes, they are not influenced by the torsional vibration. This will be illustrated by the whir speed map later.

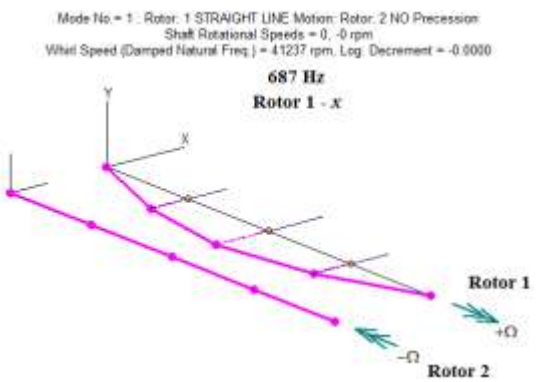

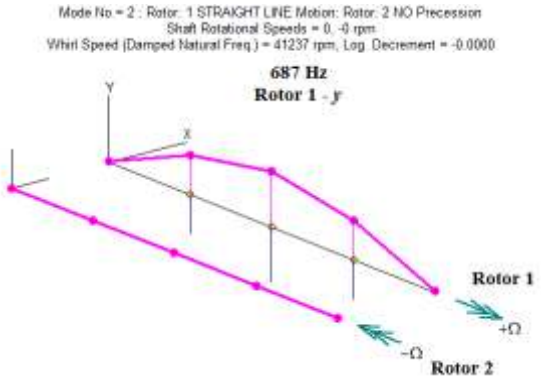

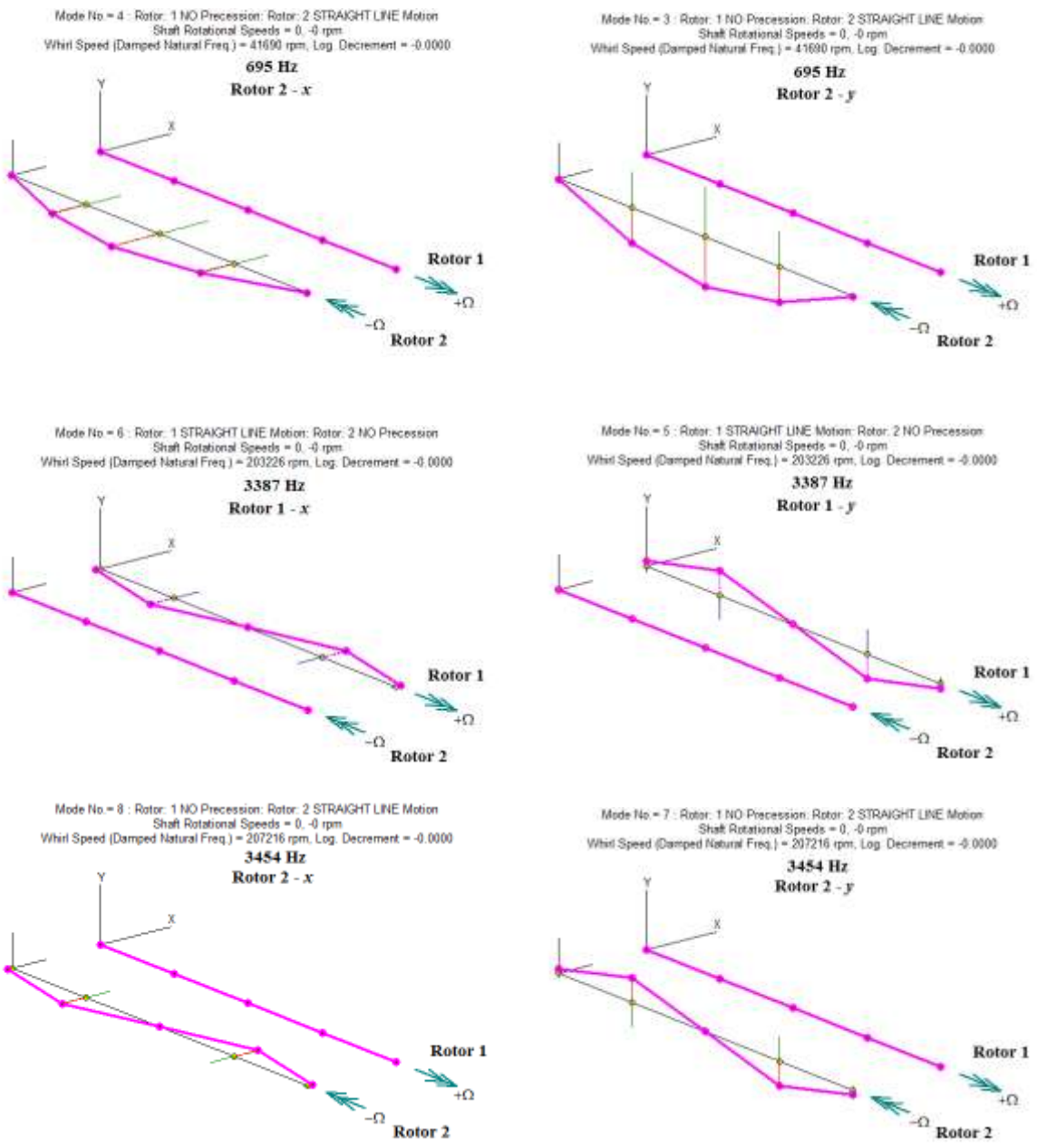

Figure 4-2 Mode shapes for lateral vibration

The first purely torsional natural frequency of the entire system is 2136 Hz. Note that in this mode each rotor acts as a rigid rotor and the only torsional flexibility is in the gear mesh. For gear dynamics, this mode needs a great attention since the gears move out of phase. Also, this mode will be influenced by the lateral-torsional coupling effect. The mode shape for this torsional mode is shown in Figure 4.3.

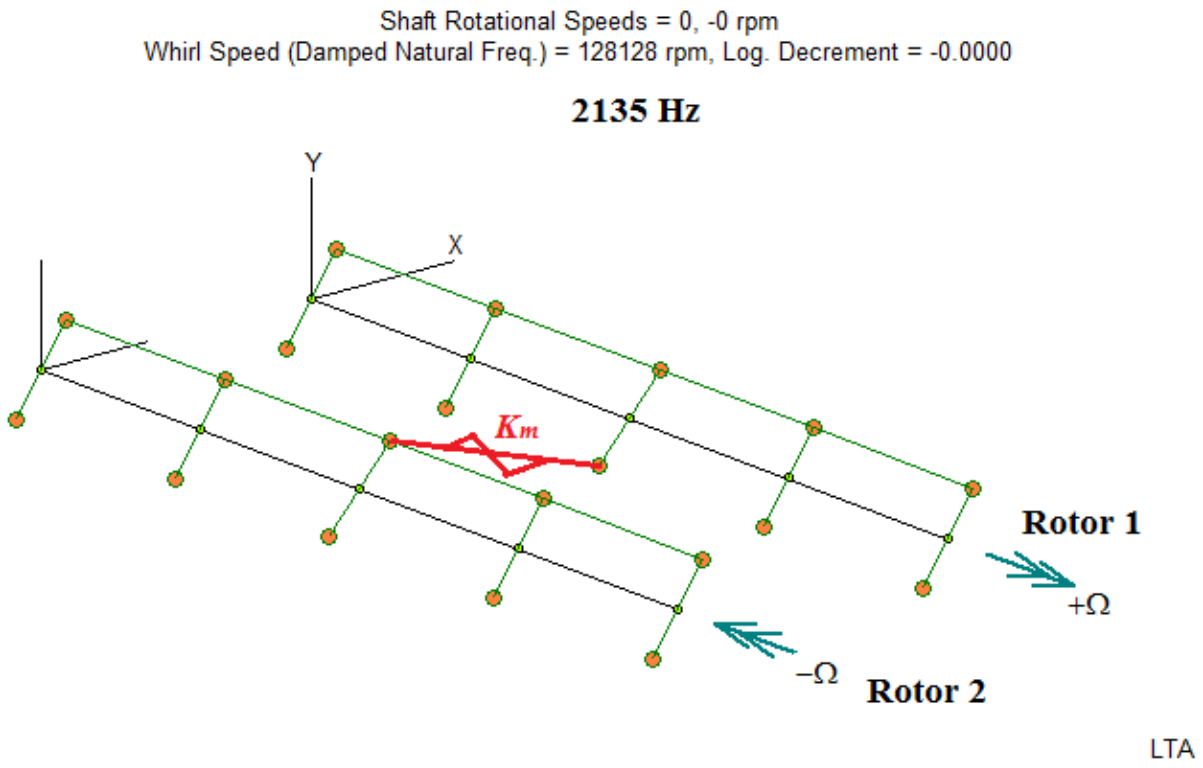

Figure 4-3 Mode shape for torsional vibration

Table 1 summarizes the first several natural frequencies of the entire system (2 rotors) at zero speed for comparison.

Mode	Purely Torsional	Rotor 1 Lateral	Rotor 2 Lateral	Combined Lateral-Torsional	NASA GRD	Mode Description
1		687		582	582	Lateral + Torsional
2		687		687	687	Lateral – Rotor 1 *x*
3			695	691	691	Lateral + Torsional
4			695	695	695	Lateral – Rotor 2 *x*
5	2136			2525	2531	Torsional + Lateral
6		3387		3387	3387	Lateral – Rotor 1
7		3387		3387	3387	Lateral – Rotor 1
8			3454	3454	3456	Lateral – Rotor 2
9			3454	3454	3456	Lateral – Rotor 2

The mode shapes for the first 5 modes with the combined lateral and torsional motions at zero speed are shown in Figure 4-4. It shows that the first mode (582 Hz) is the combined lateral motions of two rotors in Y direction with the torsional motion. Note that in this mode, rotor 1 and rotor 2 vibrates out of phase in the Y direction with large relative torsional displacements at the gear contact. The second mode (687 Hz) is an uncoupled lateral motion (X direction) for

rotor 1. The third mode (691 Hz) is again a combined lateral and torsional mode. However, unlike mode 1, both rotors now vibrate in phase in the Y direction with small relative torsional displacements at gear contact in this mode. The fourth mode (695 Hz) is an uncoupled lateral motion (X direction) for rotor 2. The fifth mode (2525 Hz) is a combined torsional and lateral mode with very large relative torsional displacements at gear contact and small lateral motion in Y direction for both rotors. Among these 5 modes, for the gear dynamic study, modes 1, 3, and 5 are of the critical modes, which coupled torsional and lateral motions. Modes 6, 7, 8, and 9 are purely lateral vibration with nodal point at the gear location, therefore, no influence from the torsional motion on these modes.

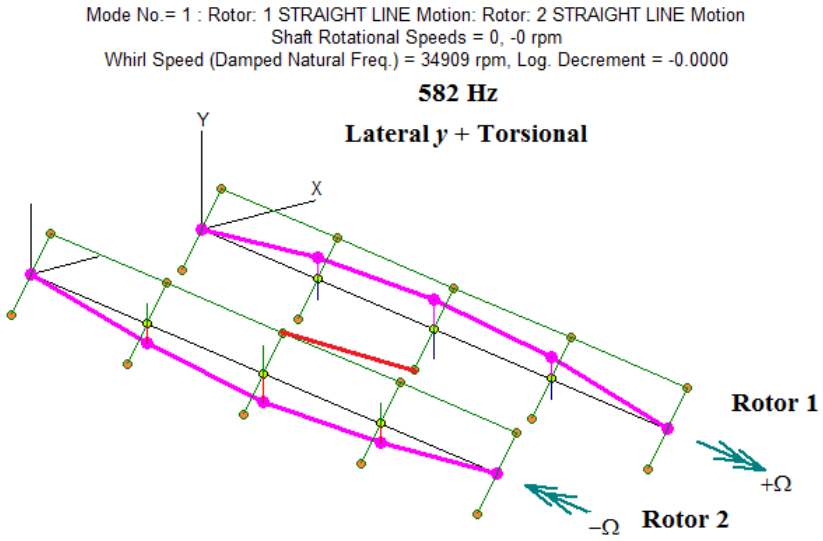

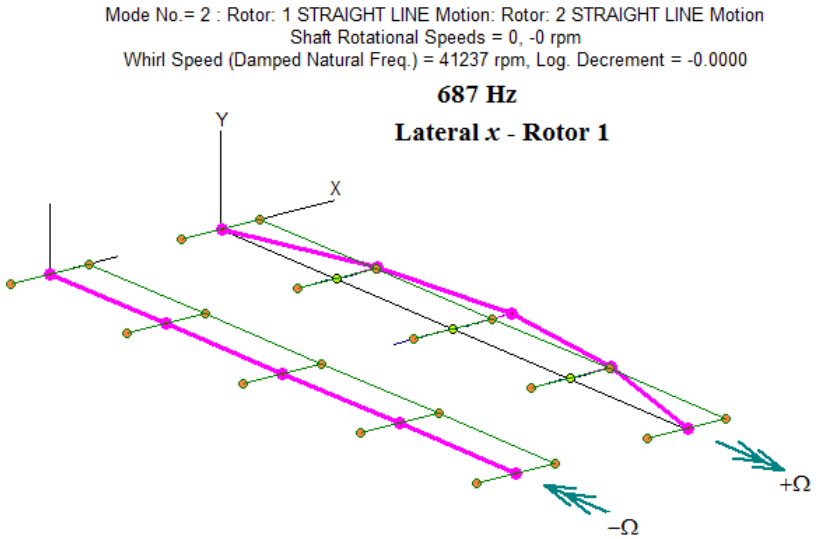

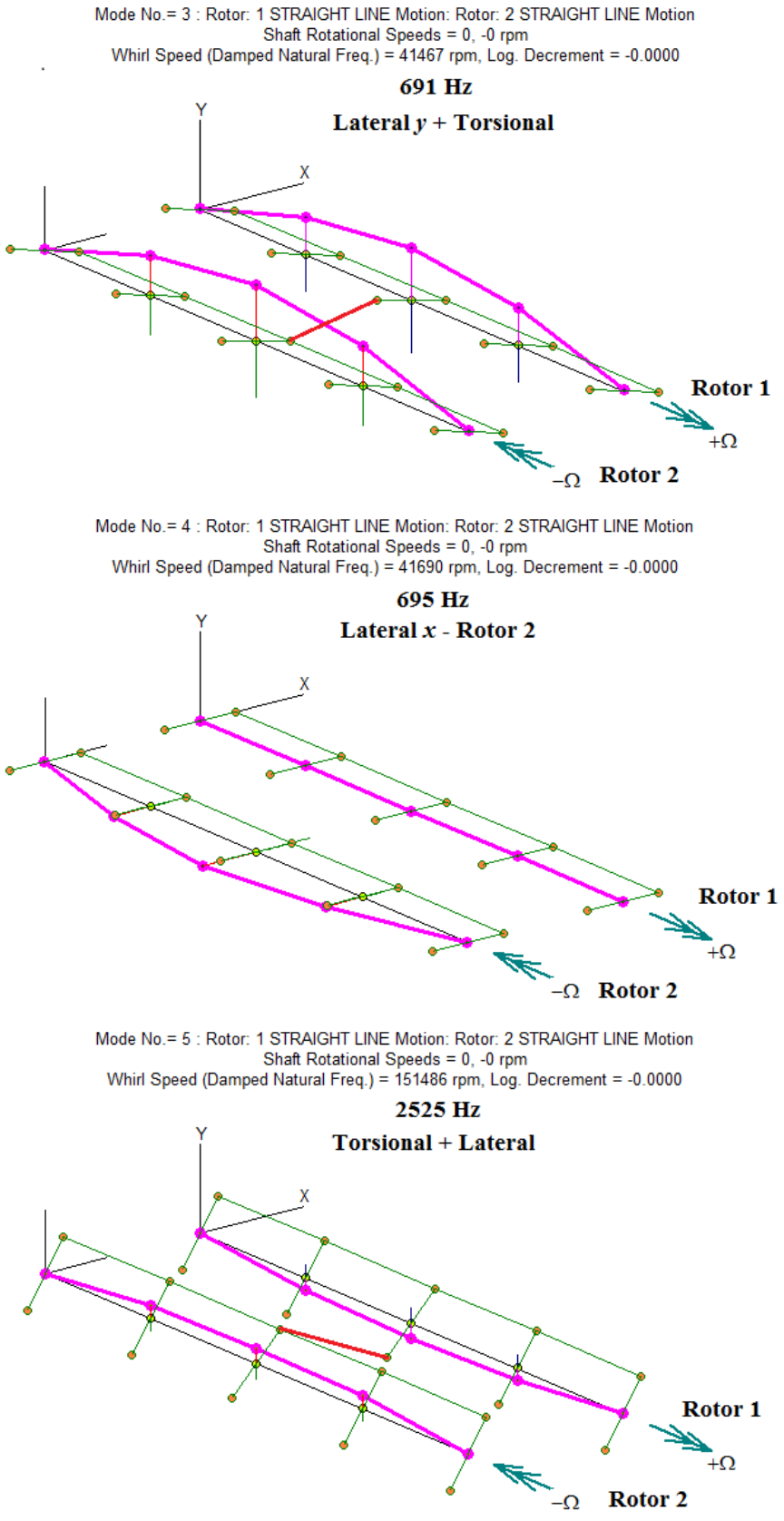

Figure 4-4 Mode shape for the combined system

The whirl speed map for the first 9 natural frequencies is shown in Figure 4-5. It shows that the gyroscopic effect has little influences on the lowest 5 modes, since the disks (gears) are at the center of shafts with zero gyroscopic moments in these modes. However, the gyroscopic effect is significant as speed increases in modes 6, 7, 8, and 9 due to large slope at the gears.

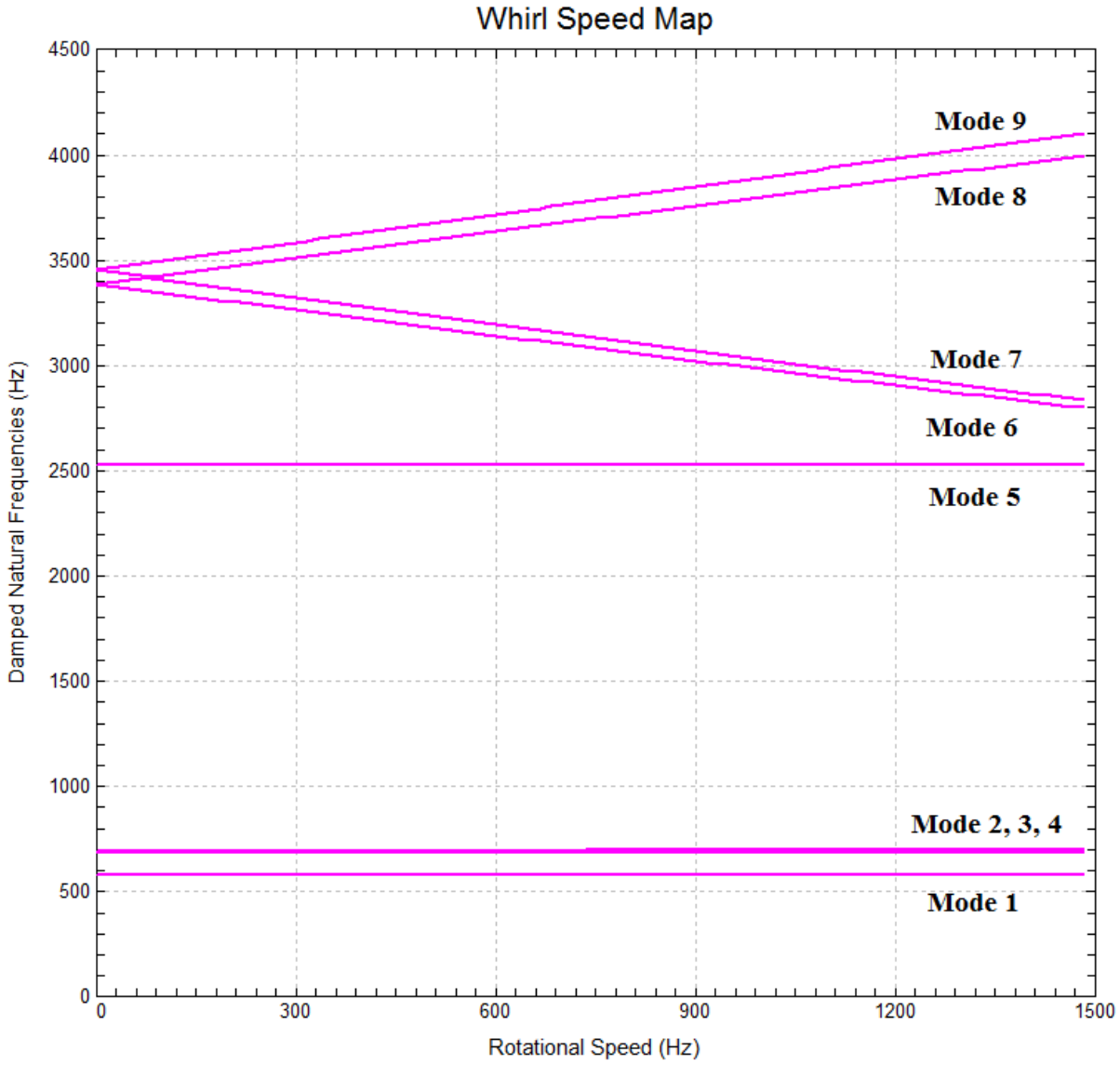

Figure 4-5 Whirl speed map for 2 shafts system

Example 5: A geared industrial compressor

An industrial 3 stages compressor driven by an electrical motor, as shown in Figures 5-1 and 5-2, is used in this example. Again, it is strongly recommended that each rotor to be analyzed before performing the lateral-torsional-axial coupled vibration. So, the combined effect can be studied and also it will minimize unnecessary mistakes which may be caused in the complete system.

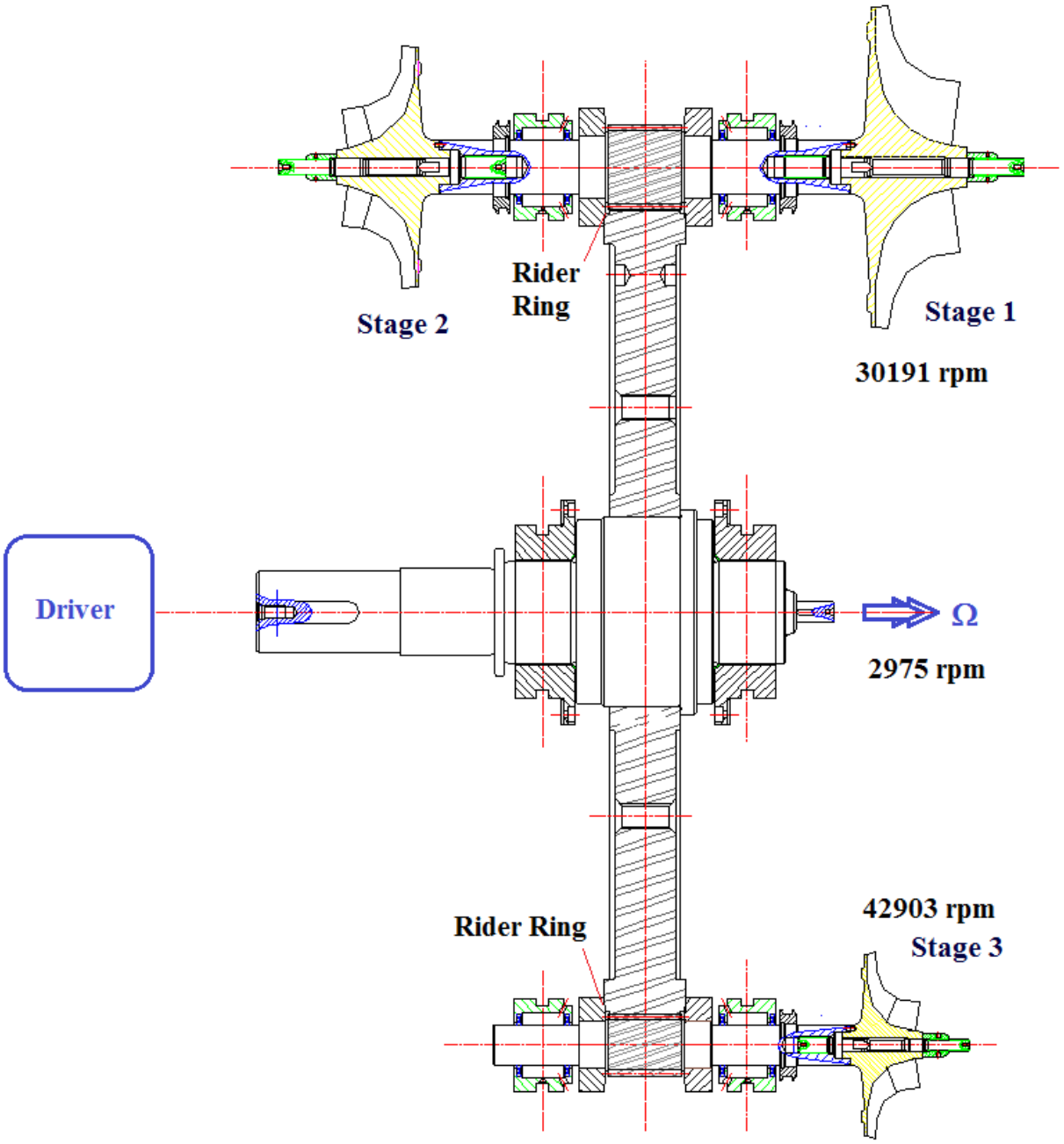

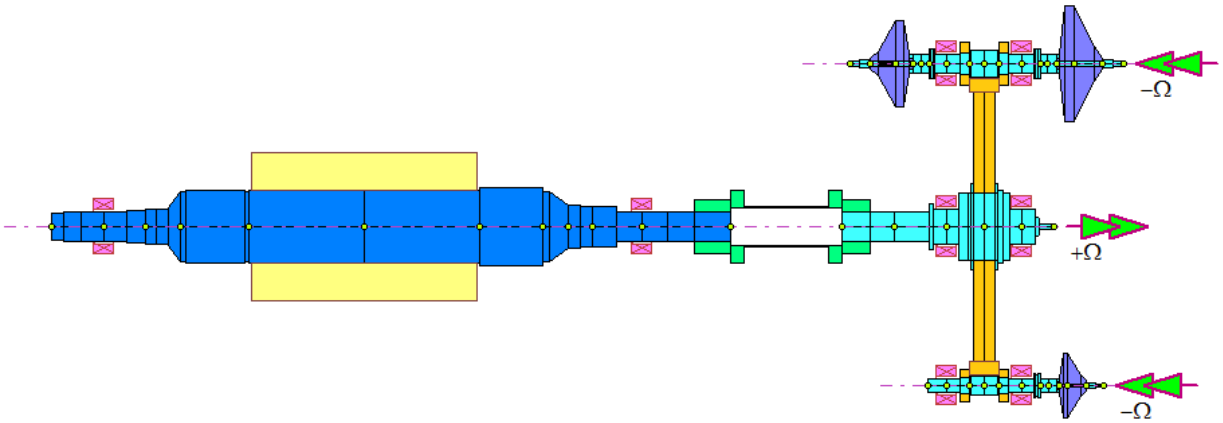

Figure 5-1 A geared compressor model

The bull gear rotates CCW when viewing from the air discharge side into the motor. Typically, the bull gear rotor is designed such that the operating speed is far below the first critical speed and can be reasonably considered as a rigid rotor. Since stability is not an issue for the bull gear rotor, 2-axial grooved bearings or elliptical bearings are commonly used in bull gear rotor bearings. For the compressor pinions, typically their operating speeds are above the critical speeds. The first pinion has 2 stages compressor with a design speed of 30191 rpm. The stage 3 compressor is in the second pinion with a design speed of 42903 rpm. Both pinions are supported by two 4-pads tilting pad bearings. Note that the rider ring (thrust collar) is used to transfer the pinion thrust loads into the low speed bull gear thrust bearing. Due to the aero thrusts, the thrust loads from the pinions are transmitted to bull gear from the collars at the motor side. The entire rotor assembly is axially constrained by the bull gear thrust bearing, however not constrained in torsional motion. Therefore there is one rigid body torsional mode with zero frequency present.

To obtain the linearized bearing coefficients, we need to calculate the bearing loads first. The bearing loads due to gear forces and aero thrusts, viewed from both sides, are shown in Figure 5-2. It should be noted that almost every bearing analysis program is based on the CCW shaft rotation for the bearing coefficients. Proper bearing orientation is extremely important to ensure the bearing performance reflect the design intention. For the current tilting pad bearings, the bearings are oriented such that the loads are between pads. The relevant bearing parameters are given in Figure 5-3.

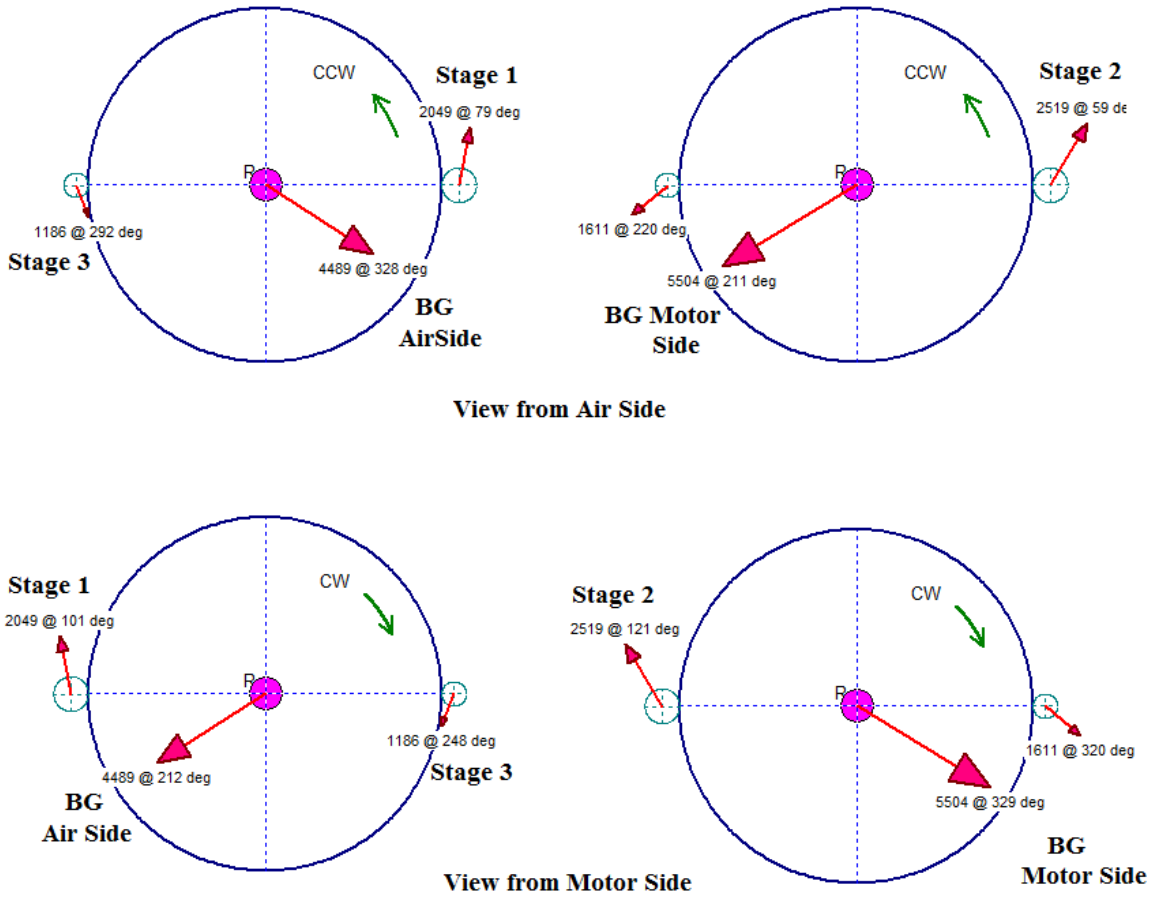

Figure 5-2 Bearing loads

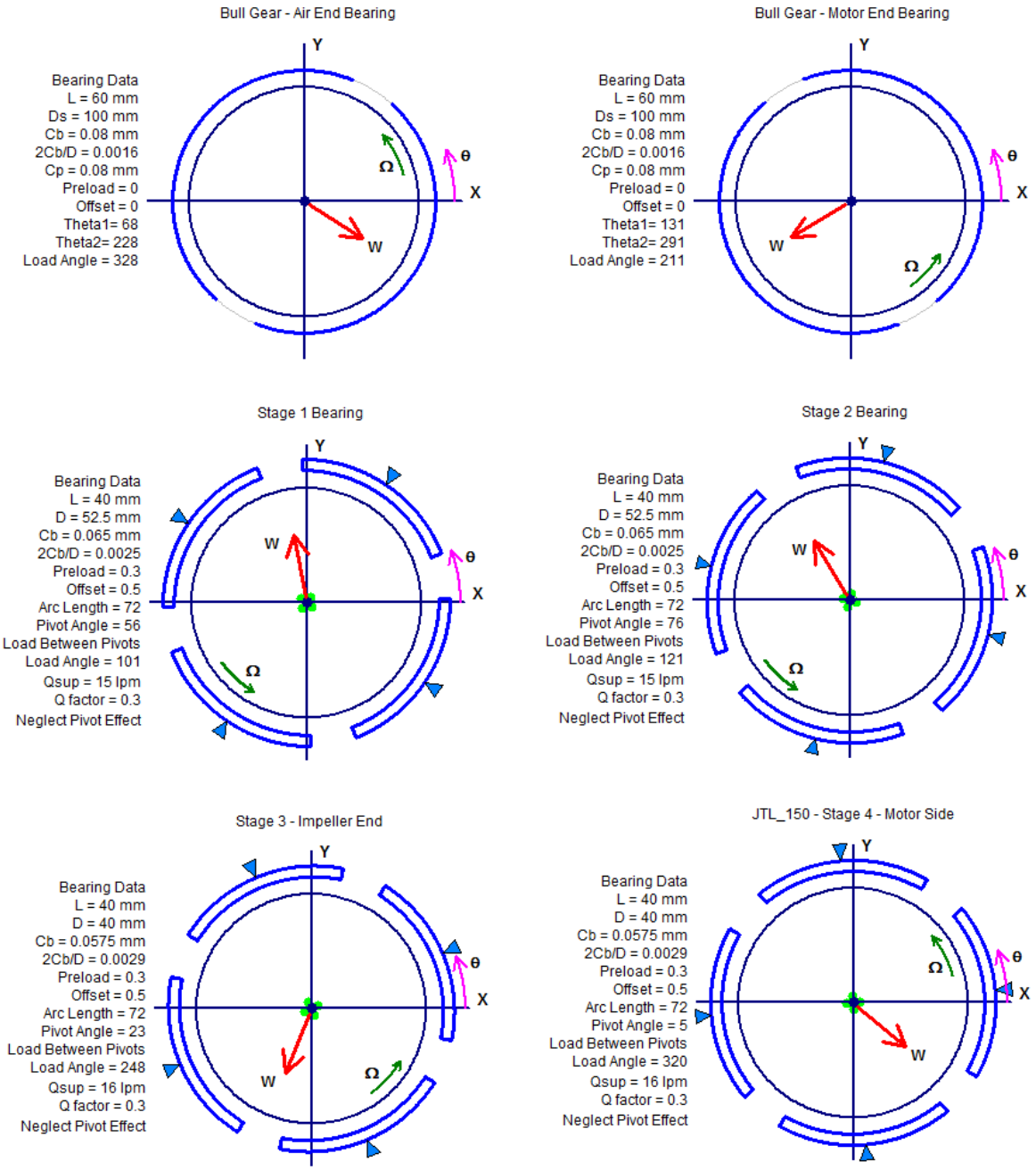

Figure 5-3 Bearing data

Again, in order to fully understand the dynamics of the entire rotor system, it is strongly recommended that each rotor be analyzed separately first for the lateral vibration, as shown in Figure 5-4. For the torsional analysis, the entire train must be considered and it has little significance for the individual rotor to be analyzed for the torsional vibration since the torsional motion for the first torsional mode is typically occurred around the coupling connected the driver and driven unit.

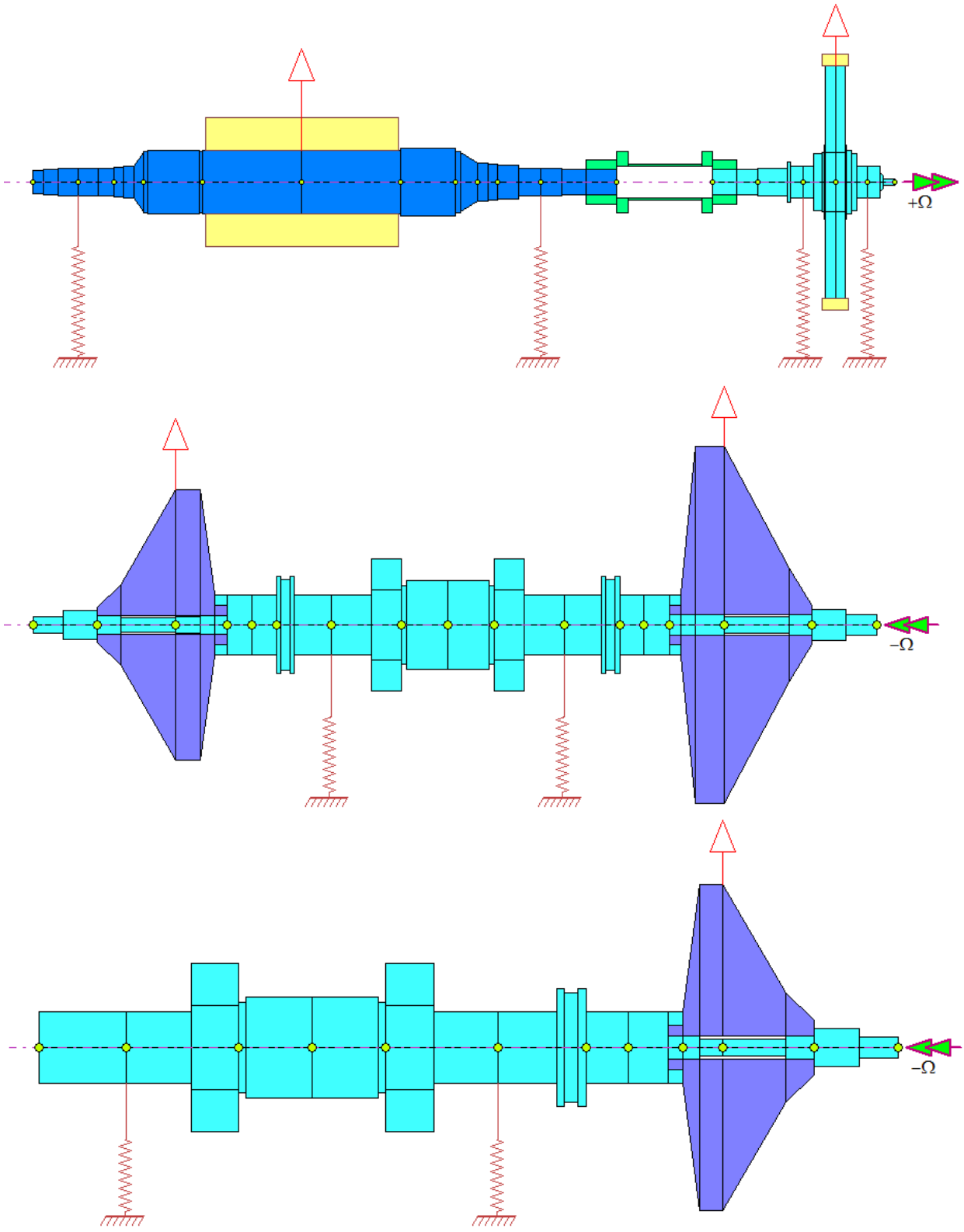

Figure 5-4 Individual rotor model

Although the program is capable of including or neglecting the lateral, torsional, or axial vibrations as shown below for the combined entire rotor system, it can also be used to verify the results from the individual rotor analysis.

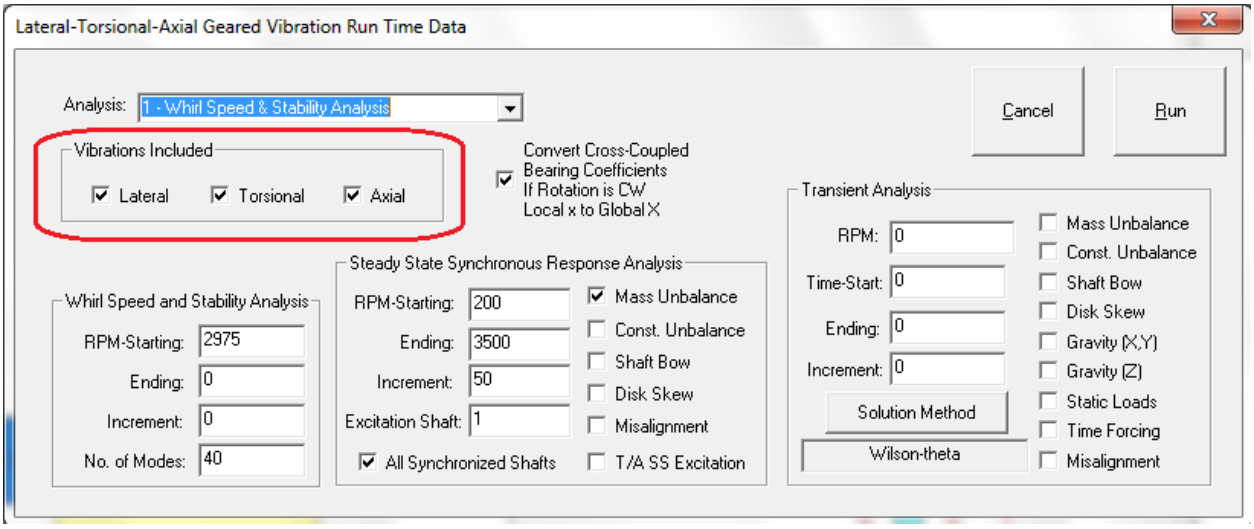

The natural frequencies at the motor design speed of 2975 rpm for the torsional, axial, individual lateral, and combined effect are summarized in Table.

Mode	Torsion	Axial	Motor + BG	Pinion 1	Pinion 2	Combined	Description
0	0						Torsional Mode
1	1225					1225	Torsional + very weak lateral on BG
2			1262			1245	Lateral BG + Axial
3			1657			1659	Lateral Motor + BG + weak Axial
4			1803			1803	Lateral Motor + weal Axial
5			3260			3220	Lateral BG + weak Axial
6			4892			4890	Lateral Motor + weak Axial
7			5287			5287	Lateral Motor + weak Axial
8				7262		7058	Lateral BG + Pinion 1 (high damping)
9			7631			7252	Lateral Pinion 1 (high damping)
10					7794		Overdamped in combined system
10		8576				8576	Axial motion only
11				11245		11292	Lateral Pinion 1
12				16650		16599	Lateral Pinion 1
13					17963	17981	Lateral Pinion 2
14				21064		20358	Lateral Pinion 1 & Pinion 2
15				21186		21629	Lateral Pinion 2
16			21648		21543	21631	Lateral Driver + Axial
17			23304			23276	Lateral Driver + Pinion 1 + Axial
18						23909	Lateral Pinion 1
19	25080					26837	Lateral Driver

20			26943			26856	Lateral Driver + weak Axial
21			27042			30809	Lateral Pinion 1 + Driver
22					32398	38579	Lateral Pinion 2
23				33185		39979	Lateral + Torsional + Axial
24					40873	41828	Lateral Driver
25			42974			41972	Lateral Driver
26			42102			42285	Torsional + Lateral + Axial
27	42282					47446	Lateral Pinion 1 + Pinion 2
28			43393			50045	Lateral Pinion 1 + Pinion 2
29	46001					51605	Lateral Driver

The mode shapes for some interesting modes of the combined effects are shown in Figure 5-5 and brief discussion is also provided.

Note that there is a rigid body mode with zero frequency for the torsional vibration and not shown here. The first flexible mode of 1225 rpm is a primary torsional mode with very weak coupling in Y direction of the bull gear where the gear is located and lateral motion of the first pinion. The major torsional deflection occurs around the coupling as expected. Here, torsional vibration is indicated by the bar symbol and lateral vibration is by the purple line and blue whirling orbits. The axial vibration is indicated by the dot symbol along the rotor center lines. This mode has no axial vibration shown. The low log decrement is because this mode is mainly torsional mode and there is no external torsional damping is applied in this example.

Modes 2 to 7 are mainly lateral motion in the driver (motor + BG) coupled with axial vibration. The log decrements of modes 2 to 6 are all far above 1 which indicates they are critically damped modes and not a concern. Mode 7 has a log. Decrement of 0.35, but it is far above the synchronous excitation from the driver, so not a concern too.

The second mode of 1245 rpm is a lateral mode coupled with the axial vibration. The lateral motion occurs at the bull gear and the motor side is whirling backward and air end is whirling forward. The axial vibrations for two high speed pinions are moving out of phase, one to the right and the other to the left. There is no torsional motion involved in this mode. The third mode of 1659 rpm is a lateral mode with motion in most entire rotor 1 coupled with very weak axial vibration. Most of the rotor is whirling forward, except very small session in the right (air) side of the bull gear is whirl backward. The log decrement of this mode is very high (4.23) and it is a critically damped mode.

Modes 8 and 9 are also primary lateral motion. Mode 8 is the lateral motion in bull gear and pinion 1, mode 9 is the lateral motion in pinion 1 only. Mode 10 is a purely axial motion in the driver. Modes 11 to 22 are primary lateral motions.

Mode No.= 1 : Rotor: 1 MIXED (86% F, 9% B) Whirl: Rotor: 2 MIXED (48% F, 48% B) Whirl: Rotor: 3 FORWARD Precession
Shaft Rotational Speeds = 2975, -30191, -42903 rpm
Whirl Speed (Damped Natural Freq.) = 1225 rpm, Log. Decrement = 0.0001

Torsional + very weak Lateral on BG and Pinion 1

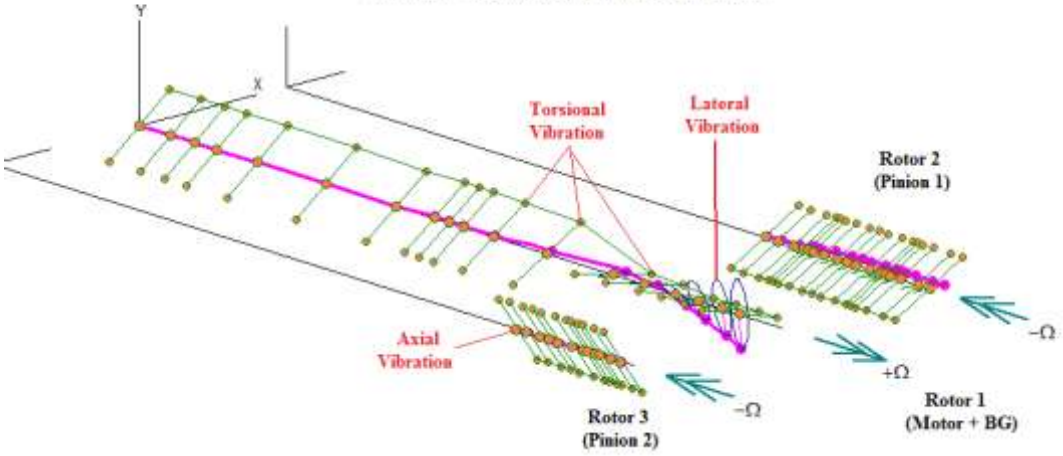

Mode No.= 2 STABLE : Rotor: 1 MIXED (51% F, 48% B) Whirl: Rotor: 2 BACKWARD : Rotor: 3 MIXED (47% F, 52% B) Whirl
Shaft Rotational Speeds = 2975, -30191, -42903 rpm
Whirl Speed (Damped Natural Freq.) = 1245 rpm, Log. Decrement = 12.5130

Lateral + Axial

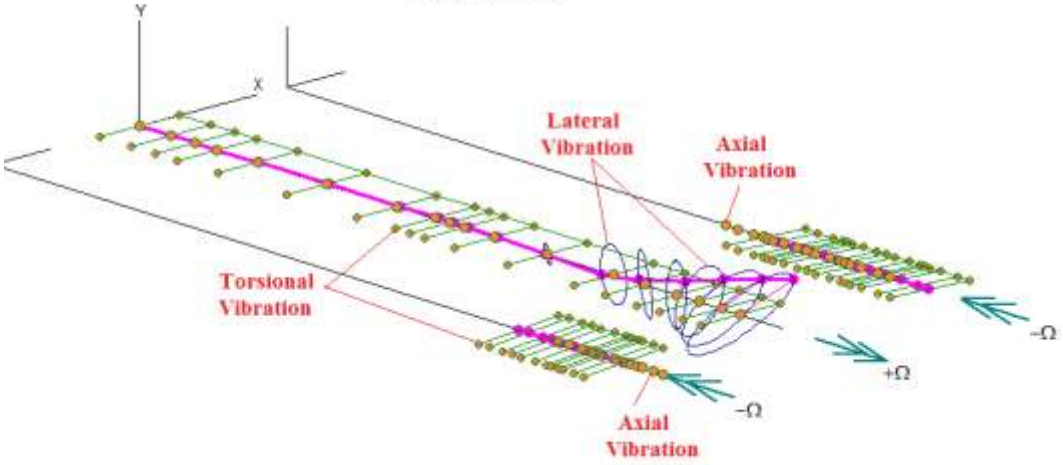

Mode No.= 3 STABLE : Rotor: 1 MIXED (95% F, 4% B) Whirl: Rotor: 2 MIXED (35% F, 61% B) Whirl: Rotor: 3 MIXED (79% F, 20% B) Whirl
Shaft Rotational Speeds = 2975, -30191, -42903 rpm
Whirl Speed (Damped Natural Freq.) = 1659 rpm, Log. Decrement = 4.2308

Lateral + very weak Axial

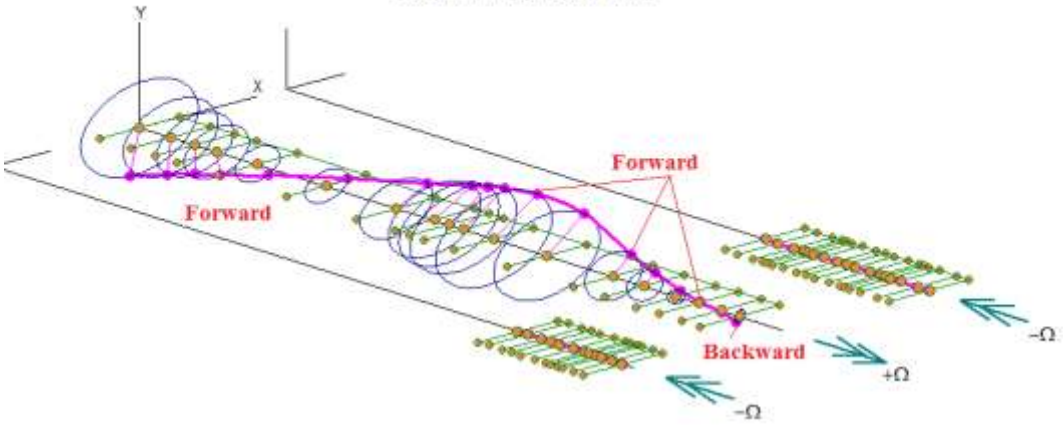

Mode No.= 8 STABLE : Rotor: 1 MIXED (84% F, 15% B) Whirl: Rotor: 2 MIXED (8% F, 91% B) Whirl: Rotor: 3 MIXED (18% F, 81% B) Whirl
Shaft Rotational Speeds = 2975, -30191, -42903 rpm
Whirl Speed (Damped Natural Freq.) = 7058 rpm, Log. Decrement = 2.4199

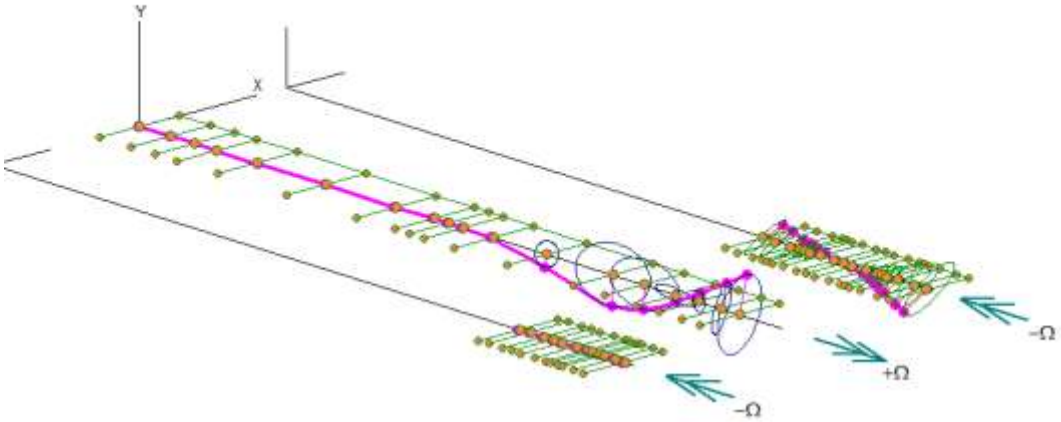

Mode No.= 9 STABLE : Rotor: 1 MIXED (88% F, 11% B) Whirl: Rotor: 2 MIXED (2% F, 97% B) Whirl: Rotor: 3 MIXED (13% F, 69% B) Whirl
Shaft Rotational Speeds = 2975, -30191, -42903 rpm
Whirl Speed (Damped Natural Freq.) = 7252 rpm, Log. Decrement = 0.9770

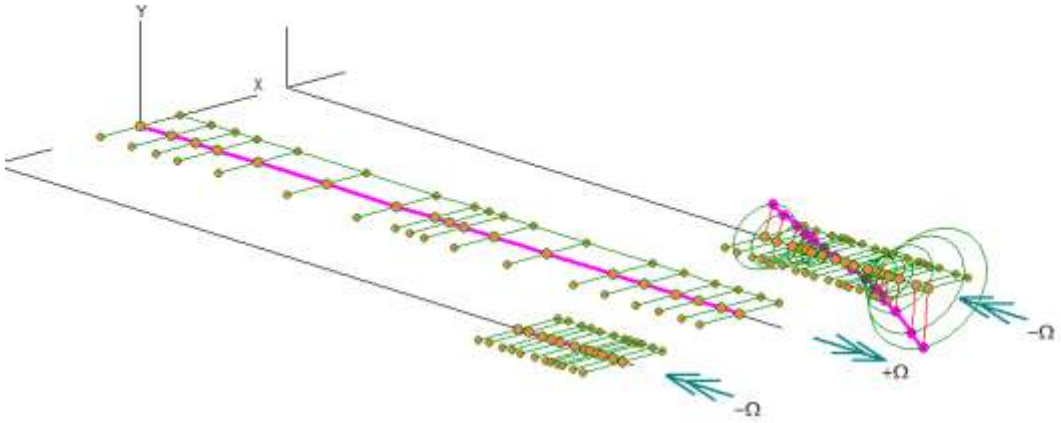

Mode No.= 10 : Rotor: 1 MIXED (73% F, 11% B) Whirl: Rotor: 2 MIXED (60% F, 36% B) Whirl: Rotor: 3 BACKWARD Precession
Shaft Rotational Speeds = 2975, -30191, -42903 rpm
Whirl Speed (Damped Natural Freq.) = 8576 rpm, Log. Decrement = 0.0000

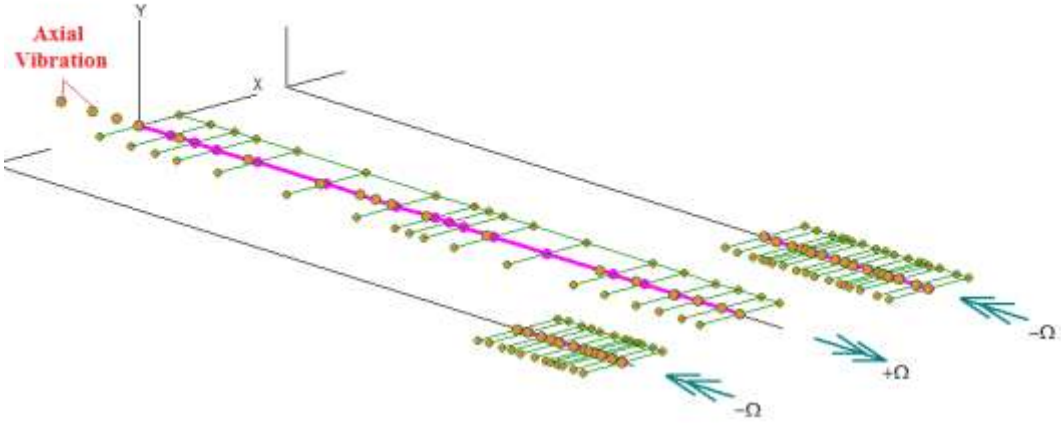

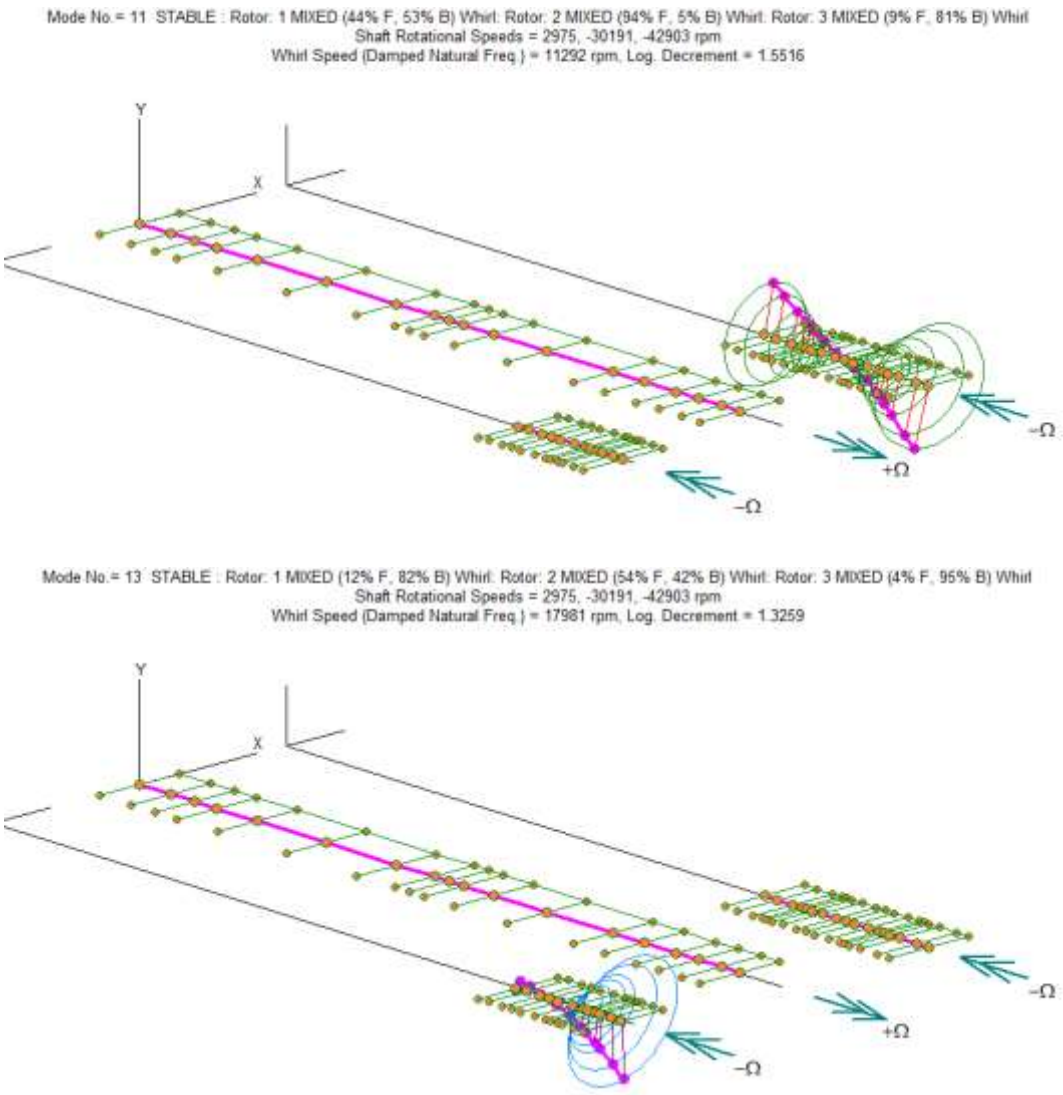

Figure 5-5 Selected mode shapes

Now, let us examine the steady state synchronous response and compare the results between the combined system and individual rotor. Figure 5-6 shows the steady state responses at stages 1 & 2 bearings from the individual rotor 2 (pinion 1) analysis. Note that since only single rotor is analyzed and the bearings are 4-pads tilting bearing bearings, the response orbit are circular and $|X|=|Y|$. If we analyze the entire 3-rotors system with only rotor 2 unbalance and neglect the gear mesh and rider ring effects, then the results will be identical and not repeated here.

However, the interest is to study the coupled effect through the gear mesh and rider ring. Figure 5-7 shows the steady state responses due to rotor 2 unbalance at the same stations from the entire train analysis with combined lateral-torsional-axial vibrations. With this lateral-torsional-and axial coupling, the system is no longer isotropic and the x and y amplitudes are quite different. As expected, when the rotor 2 goes through critical speed, it also excites rotor 1 and rotor 3 through the gear mesh and rider ring. Figure 5-8 shows the response at bull gear bearing and stage 3 bearing due to rotor 2 unbalance. Although the vibration is small, it does exist. Figures

5-9 and 5-10 show the gear dynamic force between bull gear and rotor 2 and the collar axial dynamic force due to vibration. It shows that the rider ring dynamic force is more than 10 times higher than the gear mesh dynamic force. It is evident in some integrally geared compressors with rider ring design, the vibration is strongly influenced by the rider ring effect.

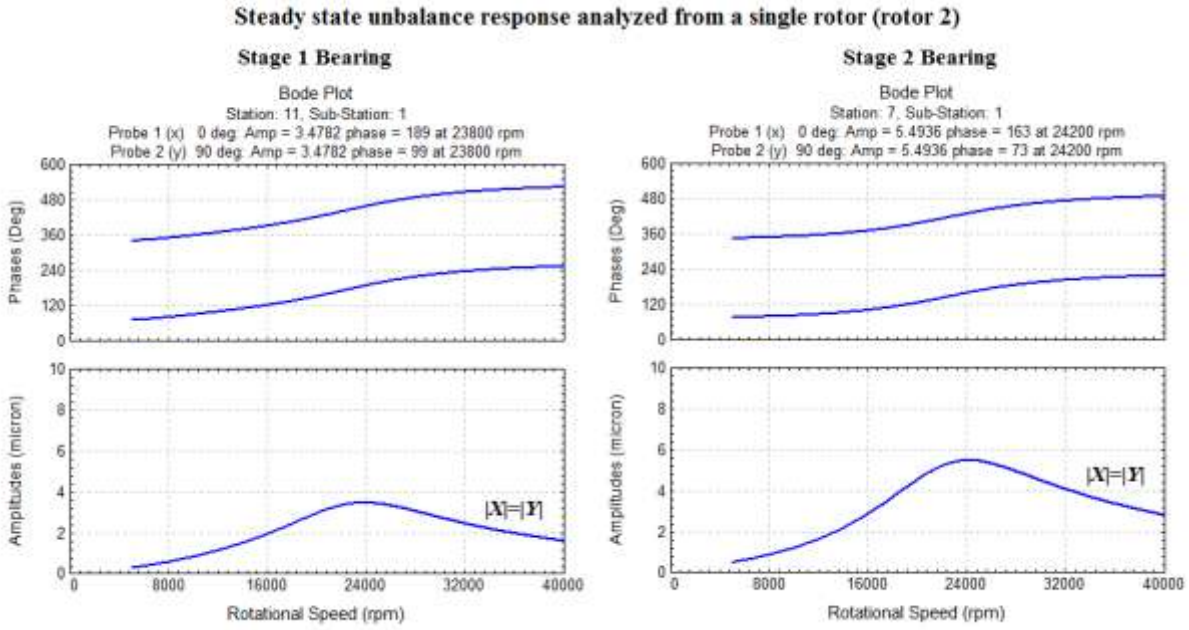

Figure 5-6 Responses at bearings obtained from the individual rotor analysis

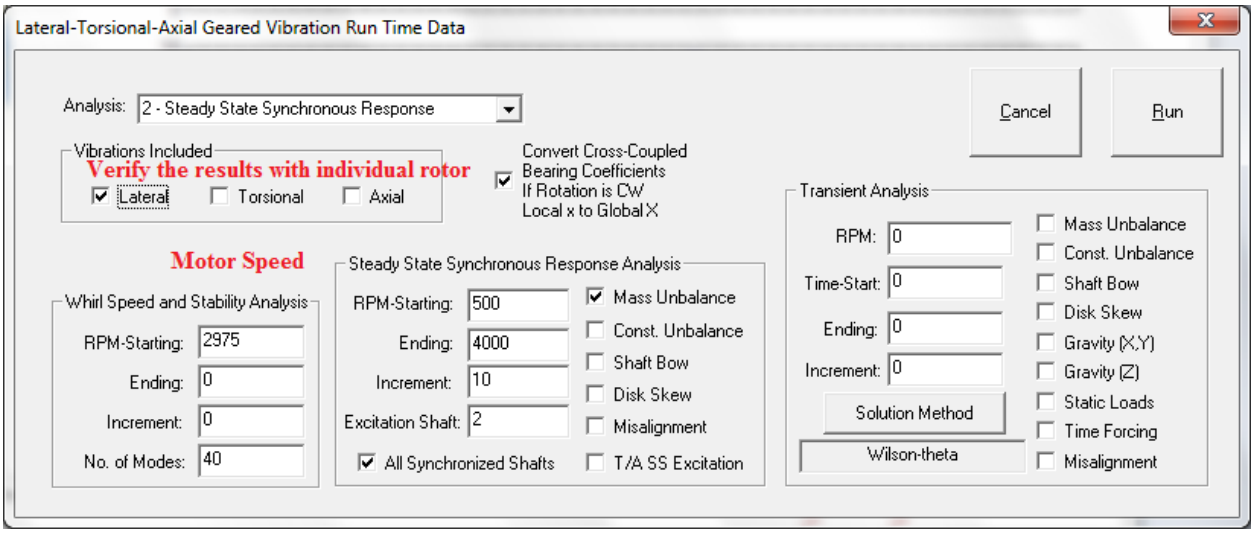

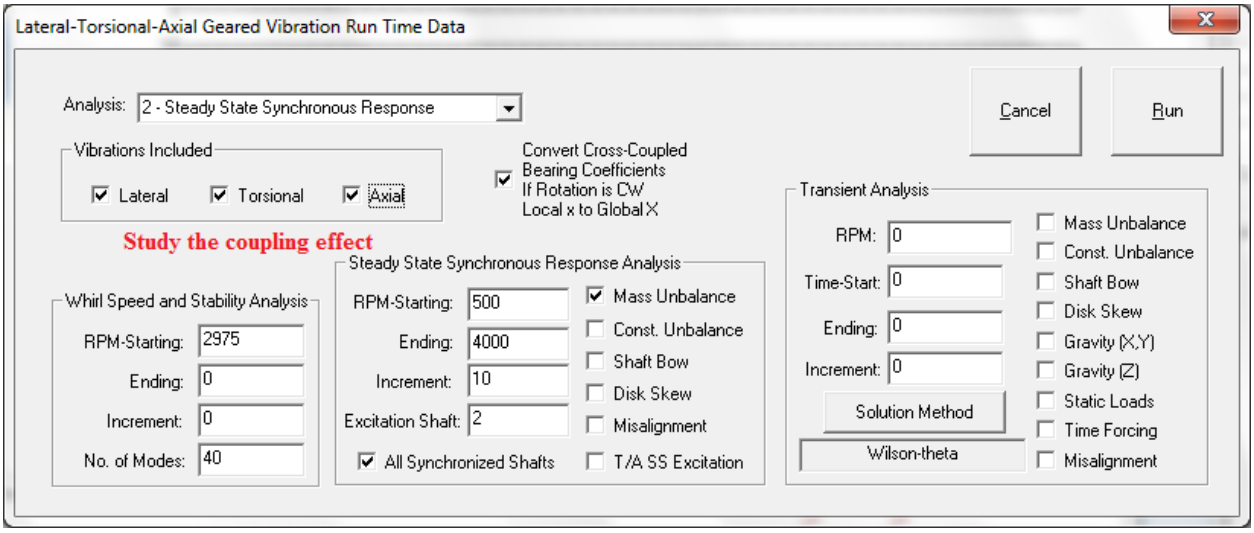

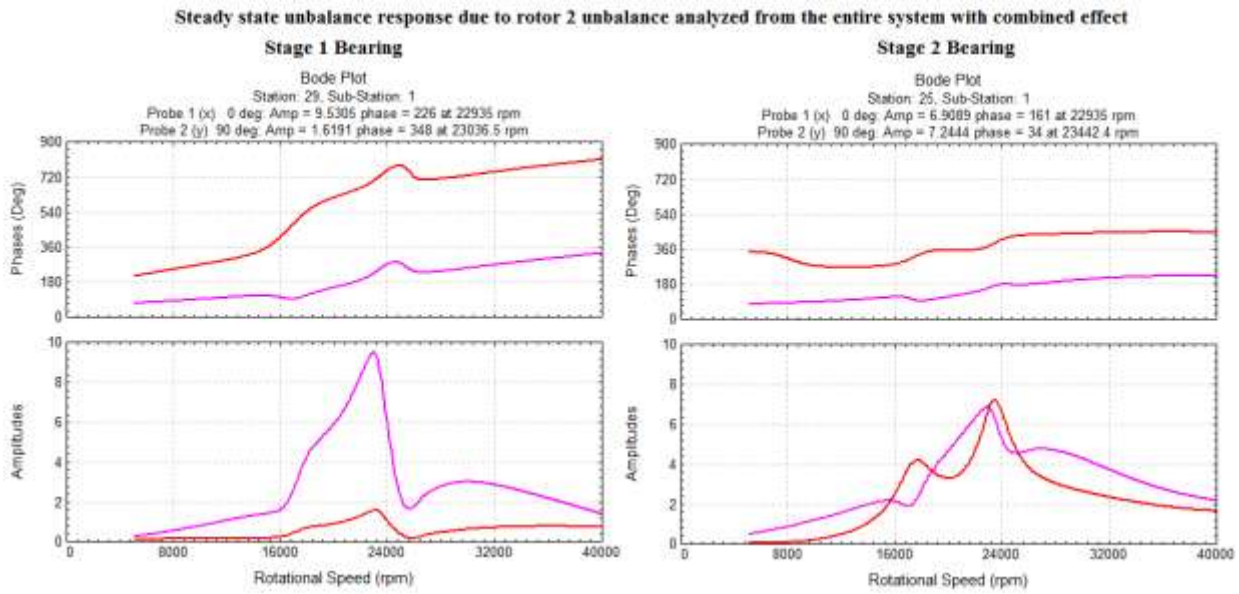

Figure 5-7 Responses at bearings due to rotor 2 unbalance obtained from the entire system with combined effect

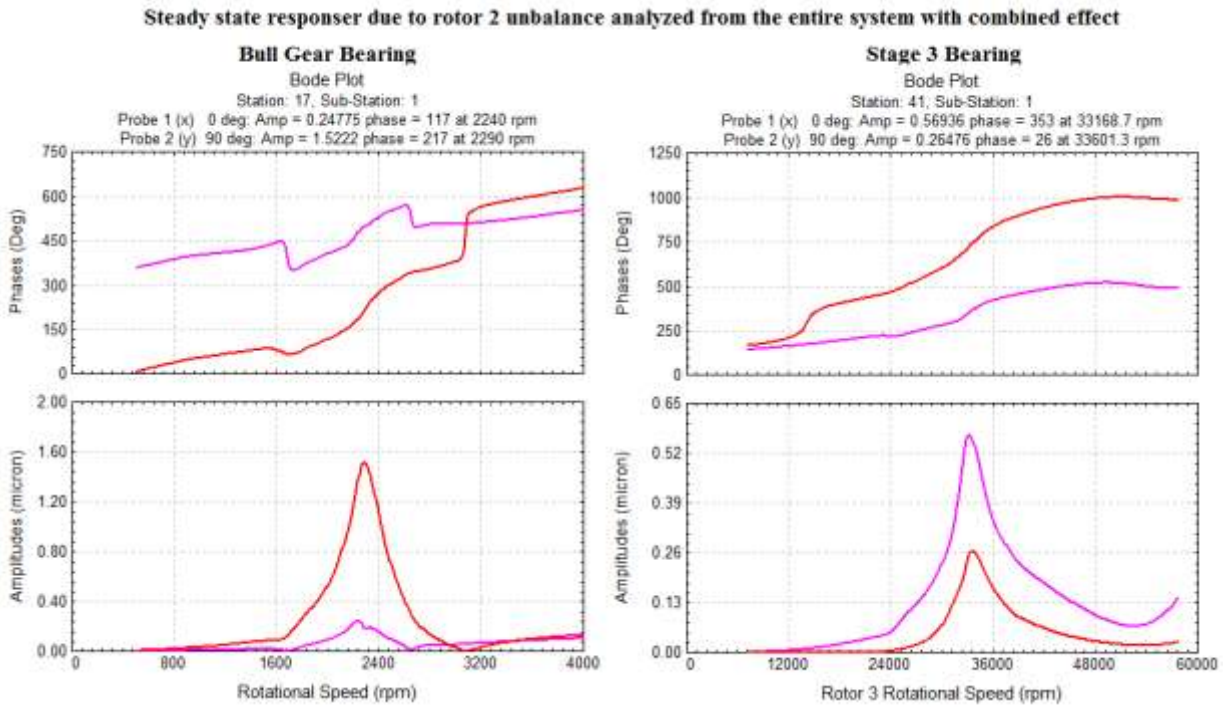

Figure 5-7 Responses at bull gear bearing and stage 3 bearing due to rotor 2 unbalance obtained from the entire system with combined effect

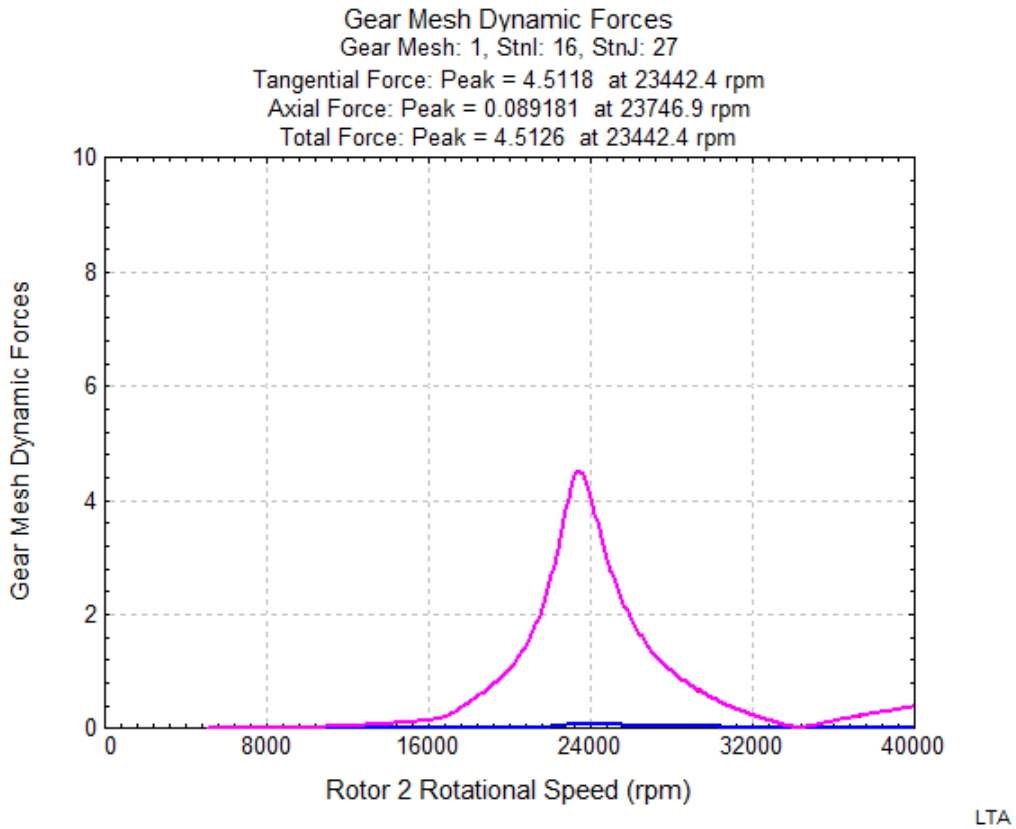

Figure 5-10 Gear mesh dynamic force between rotor 1 and rotor 2

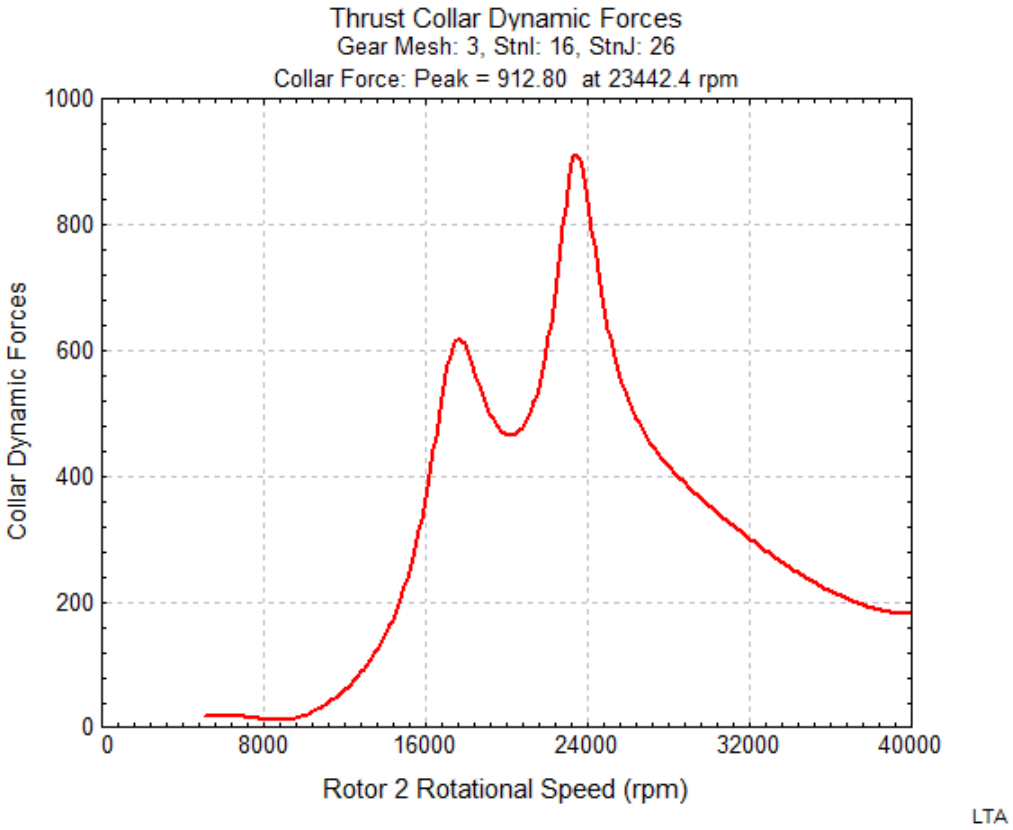

Figure 5-11 Thrust collar dynamic force between rotor 1 and rotor 2